Electrostatic Supramolecular Assembly of Charged Dendritic Polymers and Their Biological Application

Dissertation

zur Erlangung des Grades

„Doktor der Naturwissenschaften“

am Fachbereich Chemie, Pharmazie und Geowissenschaften

der Johannes Gutenberg-Universität Mainz

Yaming Yu

geb. in Liaoning, V. R. China

Mainz, 2010

Tag der mündlichen Prüfung: 29, Mar. 2010

Contents

List of Figures

List of Tables

Abbreviations

AAO	anodic aluminum oxide
AFM	atomic force microscopy; atomic force microscope
ATRP	atomic transformation radical polymerization
Au	gold
BSA	bovine serum albumin
Cr	Chromium
Cy5	cyanine
2-D	two-dimensional
3-D	three-dimensional
DB	degree of branching
DMF	N,N-dimethylformamide
DNA	oligonuleotides
DP_1^+	first generation of dendritic star polymer
DP_2^-	second generation of dendritic star polymer
EDC	1-ethyl-3-(3-dimethylaminopropyl) carbodiimide
FTIR	fourier transform infrared spectroscopy
$G_4(CH^-COO^-Na^+)_{96}$	anionic phosphorus dendrimer
$G_4(NH^+Et_2Cl^-)_{96}$	cationic phosphorus dendrimer
hbPG	hyperanched polyglycerol

LbL	layer by layer assembly
3-MPA	3-mercaptopropionic acid
MF	melamine formaldehyde
NaCl	sodium chloride
NaOH	sodium hydroxide
NBS	N-bromosuccinimide
NHS	N-hydroxysuccinimide
NMR	nuclear magnetic resonance
PAA	poly(acrylic acid)
PAMAM	polyamidoamine dendrimer
PBS	phosphate buffer solution
PDI	polydispersity index
PDMAEMA	poly[2-(dimethylamino)ethyl methacrylate]
PEG	polyethylene glycol
pK_a	acid dissociation constant
PNA	peptide nucleic acid
PS	polystyrene
RMS	root mean square
SPPs	surface plasmon polaritons
SAM	self-assembled monolayer

SPR, SPS or SPRS	surface plasmon resonance spectroscopy
SPFS	surface plasmon field enhanced fluorescence spectroscopy
SFM	scanning force microscope
ss-DNA	single strand DNA
TEA	triethylamine
THF	tetrahydrofuran
TMA	trimethylamine
UV-Vis	ultraviolet visible

Chapter 1

General Introduction

There is an ongoing challenge in nanotechnology: the construction of materials and devices that owe their valuable properties to nanoscale aspects of their structures. Generally speaking, there are two fundamental ways of fabricating nanostructures: top-down and bottom-up. The top-down technique is the most widely explored and utilized approach to achieve miniaturization of devices, which is usually based on photolithography.[1] However, precise nanostructures can hardly be achieved by conventional top-down approaches due to obvious limitations, for example the resolution of photolithography.[2] As an alternative strategy, nanofabrication via the bottom-up approach, in which functional nanostructures are formed by the self-assembly of molecular building blocks is considered to be a promising solution for the ultimate size reduction.[3]

Nature uses self assembly strategies based on non-covalent interactions, such as hydrogen bonds, salt bridges, electrostatic interaction and even metal coordination to organize biological systems.[4] Biological systems often provide us with perfect examples of dividing complex structures and functions into different levels of building blocks, through non-covalent (or supramolecular) chemistry.[5] By learning these lessons from biology, chemists are now starting to compose highly complex chemical systems from components that interact via non-covalent intermolecular forces.[4] Among the various molecular interactions commonly used in self assembly, electrostatic interactions possess the unique characteristics of a combination of high strength, long range and non-selective nature.[6]

Layer-by-layer (LbL) assembly, an important bottom-up strategy,[7] has been widely employed as a simple and versatile method in constructing

controlled nanostructures on a surface.[8] It allows the creation of highly tunable and functional thin films with nanometer-level control over the structure, composition, and properties. The most often used materials for LbL fabrication through electrostatic interaction are linear polyelectrolytes. Beyond the linear polymer systems, inorganic nanoparticles,[9] polymeric micelles,[10] carbon nanotubes,[11] and biological molecules[12] are employed as well. The incorporation of a broader range of materials based on the various intermolecular interactions has expanded the potential applications of LbL assembly, ranging from hydrogen storage[13] and electrochemical devices[14] to sensors or biosensors[15] and drug delivery[16]. Dendrimers, dendritic like polymers and hyperbranched polymers possessing a tree-like structure as a new class of materials have been developed with respect to their regular and highly branched three-dimensional architecture. Polyelectrolytes based on the dendritic like structures have recently been introduced and developed as new nanoscale materials in LbL assembly; therefore, it would be of great interest to investigate the effects on structures and morphology of LbL multilayer films that contain polymers with unusual architecture and functionalities compared to conventional polyelectrolytes as well as to study the potential applications based on such novel multilayer structures.

The aim of this thesis is to design the novel multilayer films based on the imperfect structure (hyperbranched polymers) and the perfect structure (phosphorus dendrimers and dendritic star polymers), explore the influence of the dendritic architecture on the multilayer films under various deposition conditions, create functionalities in the resulting multilayer films and apply them for a broad range of purposes, ranging from DNA biosensors to antifouling coatings. The surface properties of multilayers fabricated based on the phosphorus dendrimers and hyperbranched polyglycerols (hbPG) were examined and compared. The hyperbranched polyglycerol layers were investigated as antifouling coatings. The dendrimer and dendritic star

polymer multilayer films were systematically studied as DNA biosensors to detect DNA immobilization and hybridization.

Chapter 2 provides a brief review regarding recent developments of dendritic structures and the fundamentals of the electrostatic assembly technique. Apart from introduction on the substrate-assisted layer by layer assembly, examples on closely related issues of polyelectrolyte complex formation will also be covered.

Chapter 3 describes the experimental characterization methods used in this thesis and their principles.

Chapter 4 deals with the study of the effect of deposition conditions on the cationic phosphorus dendrimer/anionic hyperbranched polyglycerols multilayers. The structural properties of multilayers of cationic phosphorus dendrimers/anionic hbPG are systematically investigated, varying molecular weight, pH value and ionic strength and are also compared with the system of pure phosphorus-based dendrimer multilayers.

In Chapter 5, the resistance towards non specific protein adsorption of hyperbranched polyglycerol layers is studied. The cationic hbPG is used for the fabrication of hbPG bilayer with anionic hbPG. The parameters that affect the antifouling ability of hbPG layers are systematically discussed.

Chapter 6 describes the fabrication of phosphorus dendrimer multilayers and their application as DNA biosensor platforms. Optimized deposition conditions are discussed and the capability for DNA immobilization on the optimized multilayer surface is evaluated. Finally, DNA hybridization and limit of detection are detected and compared on various numbers of multilayer surfaces.

In the last experimental part (Chapter 7), dendritic star polymers based on a dendritic polyphenylene core will be studied. Firstly, the surface morphology of the dendritic star polymers is studied by atomic force microscopy (AFM). Subsequently, multilayers based on the oppositely

charged dendritic star polymers with different generation were fabricated and the multilayer properties were systematically studied by various methods. DNA immobilization and hybridization processes were carried out on these dendritic star multilayer surfaces and also compared with the phosphorus dendrimer multilayer system.

References

1 Geissler, M.; Xia, Y. N. *Adv. Mater.* **2004**, *16*, 1249.

2 (a) Niemeyer, C. M. *Science* **2002**, *297*, 62. (b) Ito, T.; Okazaki, S. *Nature* **2000**, *406*, 1027.

3 Whitesides, G. M.; Mathias, J. P.; Seto, C. T. *Science* **1991**, *254*, 1312.

4 Ballauf, M.; Bauer, R. E.; BalboBlock, M.A. et. al. (Eds.) *Functional Molecular Nanostructures,* Springer, Berlin Helderburg, Germany, **2005.**

5 Whitesides, G. M.; Crzybowski, B. *Science* **2002**, *295*, 2418.

6 Faul, C. F. J.; Antonietti, M. *Adv. Mater.* **2003**, *15*, 673.

7 Decher, G.; Schlenoff, J. B. (Eds.) *Multilayer Thin Films, Sequential Assembly of Nanocomposite Materials*, Wiley-VCH, Weinheim, Germany, **2003**.

8 (a) Decher, G. *Science* **1997**, *277*, 1232. (b) Caruso, F. *Adv. Mater.* **2001**, *13*, 11. (c) Peyratout, C. S.; Dahne, L. *Angew. Chem., Int. Ed.* **2004**, *43*, 3762. (d) Hammond, P. T. *Adv. Mater.* **2004**, *16*, 1271.

9 Lee, D.; Rubner, M. F.; Cohen, R. E. *Nano Lett.* **2006**, *6*, 2305.

10 Cho, J. H.; Hong, J. K.; Char, K.; Caruso, F. *J. Am. Chem. Soc.* **2006**, *128*, 9935.

11 Mamedov, A. A.; Kotov, N. A.; Prato, M.; Guldi, D. M.; Wicksted, J. P.; Hirsch, A. *Nat. Mater.* **2002**, *1*, 190.

12 Lvov, Y.; Ariga, K.; Ichinose, I.; Kunitake, T. *J. Am. Chem. Soc.* **1995**, *117*, 6117.

13 Borodina, T. N.; Grigoriev, D. O.; Andreeva, D. V.; Möhwald, H.; Shchukin, D. G. *ACS Appl. Mater. Interfaces* **2009**, *1*, 996.

14 (a) Hu, Y.; Hu, N. F. *J. Phys. Chem. B* **2008**, *112,* 9523. (b) Kim, J. Y.; Stickney, J. L. *J. Phys. Chem. C*, 2008, 112, 5966.

15 Shchukin, D. G.; Kommireddy, D. S.; Zhao, Y.; Cui, T.; Sukhorukov, G. B.; Lvov, Y. M. *Adv. Mater.* **2004**, *16*, 389.

16 (a) Sukhorukov, G. B.; Donath, E.; Lichtenfeld, H.; Knippel, E.; Knippel, M.; Budde, A.; Möhwald, H. *Colloids Surf., A* **1998**, *137*, 253. (b) Shchukin, D. G.; Patel, A. A.; Sukhorukov, G. B.; Lvov, Y. M. *J. Am. Chem. Soc.* **2004**, *126*, 3374. (c) Kuila, D.; Tien, M.; Krishna, G.; Lvov, Y.; McShane, M.; Singh, S.; Potluri, A.; Kaul, S. *Proc. SPIE—Int. Soc. Opt. Eng.* **2004**, *5593*, 267.

Chapter 2

Fundamentals

2.1 Dendritic Architectures

The dendritic architecture is perhaps one of the most pervasive topologies observed on our planet. Dendritic architectures can be found in our daily life and range from abiotic systems including lightning patterns, snow crystals, tributary/erosion fractals, as well as in the biological world for example, the branching of trees or roots, plant or animal vasculatory systems and neurons.[1] These topologies resulting from a long structural evolution are assumed to represent optimized structures to provide maximum interfaces for optimum energy extraction/distribution and information storage/retrieval. Apart from the above mentioned dendritic architectures in Nature, syntheses aiming at the deliberate construction of macromolecules possessing branched architectures have been reported since late 1970ies.[1]

Broadly speaking, dendritic architectures in chemistry encompass dendrimers, dendrimer like polymers and hyperbranched polymers. They exhibit unique properties compared with those of their linear analogues. Because of the high connectivity of their repeating units, which in turn shape them in globular structures, these highly branched macromolecules have been investigated as functional polymers for a wide range of potential applications, such as drug delivery, sensors and functional coatings.[2] Different types of dendritic architectures will be introduced below.

2.1.1 Dendrimers

Dendrimers are globular macromolecules with a peculiar architecture

constituted of three distinct domains: (1) a central core which is either a single atom or an atomic group having at least two identical chemical functions; (2) branches emanating from the core, constituted of repeat units having at least one branch junction, whose repetition is organized in a geometrical progression that results in a series of radially concentric layers called generations, and (3) many terminal functional groups, generally located in the exterior of the macromolecule, which play a key role for the properties.[3]

Dendrimers could be thought as unique nanoscale devices. Each architectural component manifests a specific function while at the same time defining properties for these nanostructures as they are grown generation by generation.[1] For example, the core may be thought of as the molecular information center from which size, shape, directionality and multiplicity are expressed via the covalent connectivity to the outer shells. Within the interior, one finds the branch cell amplification region, which defines the type and amount of interior void space that may be enclosed by the terminal groups as the dendrimer is grown. The interior composition and amount of solvent filled void space determines the extent and nature of guest-host properties that are possible with a particular dendrimer family and generation.[1]

From the synthesis point of view, two conceptually different synthetic approaches for the construction of high-generation dendrimers exist: the divergent approach and the convergent approach. Both approaches rely on a repetition and alternating series of reaction steps, each repetition accounting for the creation of an additional generation. The two methodologies have their own characteristics, and therefore, the perfection of the final product is related to its synthetic approach. The divergent approach generates dendrimers by successive addition of monomer layers, first to a central core molecule, then to the growing dendrimer proceeding radially in outwards fashion (Figure 2.1). Conversely, the convergent approach, which constructs

these macromolecules from the chain ends and proceeds toward the center, begins by adding the "peripheral" moieties to the monomer to generate a small dendritic fragment or dendron (Figure 2.1).

Compared with other classes of dendritic architecures, dendrimers have a well-controlled size and shape. However, they are usually prepared by multi-step reactions with tedious isolation and purification procedures.

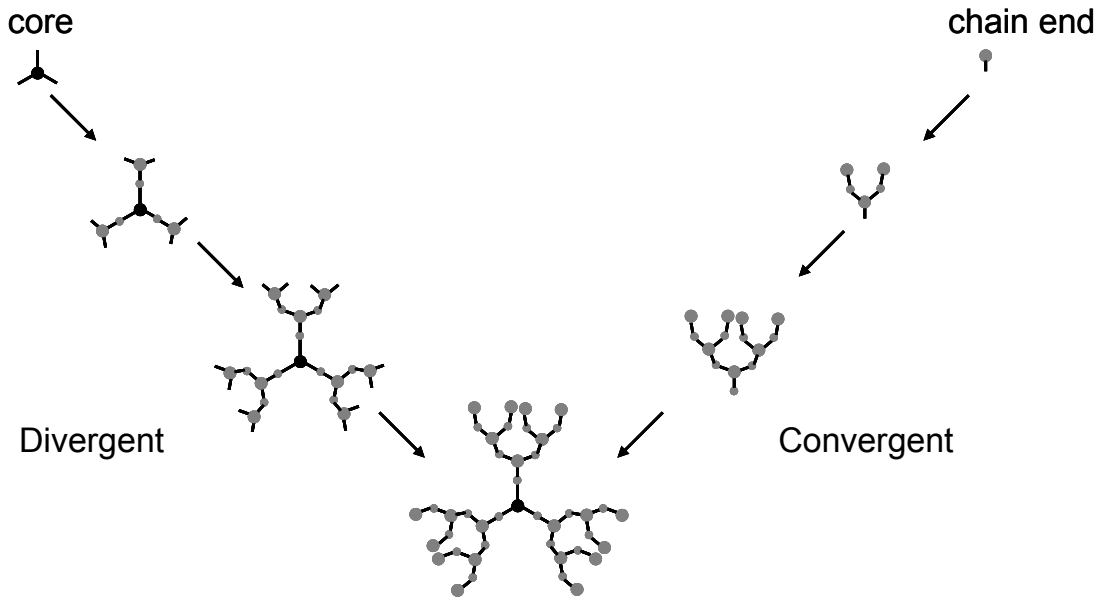

Figure 2.1 Schematic illustration of dendrimer formation by divergent and convergent methods, respectively.

2.1.2 Hyperbranched Polymers

Whereas the well-characterized, perfect structures of dendrimers constructed by discrete stepwise procedures have been illustrated in the above, this section describes the related, less-than-perfect hyperbranched polymers. Hyperbranched polymers are highly branched macromolecules. Normally, they are simply prepared by a one step polymerization, which differs strongly from the methods to prepare dendrimers. Various kinds of hyperbranched polymers have been prepared from AB_x type monomers, and the polymerization reactions can be classified into three categories: (1) step growth polycondensation of AB_x monomer; (2) self-condensing vinyl

polymerization of AB_x monomers; (3) multibranching ring-opening polymerization of latent AB_x monomers.[4] A typical branched polymer structure obtained from an AB_2 type monomer is shown schematically in Figure 2.2.

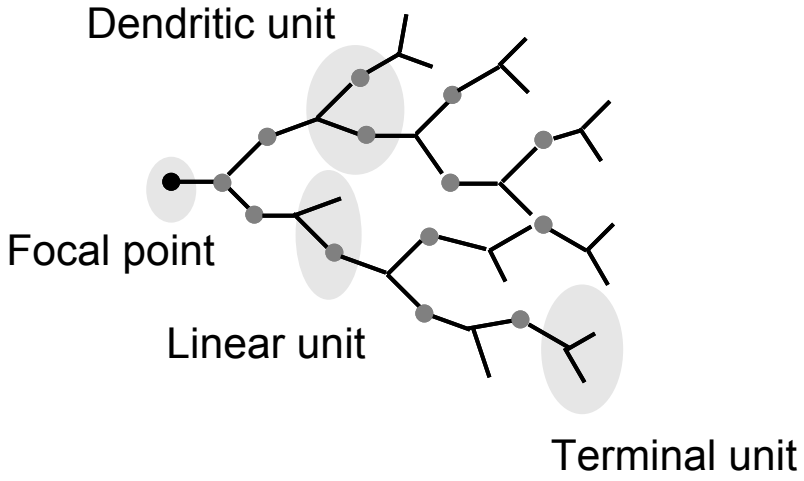

Figure 2.2 Schematic illustration of a hyperbranched polymer based on AB2 monomer units.

Since the formation of hyperbranched polymers is based on one synthetic step, hyperbranched polymers possess a randomly branched topology and are generally composed of dendritic, linear and terminal units. Normally, a degree of branching (DB) as a global parameter helps to describe their structures.[5] The DB can be calculated by the following equation:[6]

$$DB_{Frey} = \frac{2D}{2D + L} \qquad \textbf{Equation 2.1}$$

Here D is the fraction of dendritic units, while L represents fraction of linear units.

Figure 2.3 shows the comparison of the degree of branching among linear polymer, hyperbranched polymer and dendrimer. There is no dendritic unit in the linear polymer and hence, the DB of linear polymers is zero. Dendrimers do not possess linear units and therefore the DB is calculated to be 1 according to Equation 2.1. Accordingly, hyperbranched

polymers should constitute of an intermediate DB between 0 and 1. The DB of hyperbranched polyglycerols studied in this thesis is in the range of 0.5-0.66.

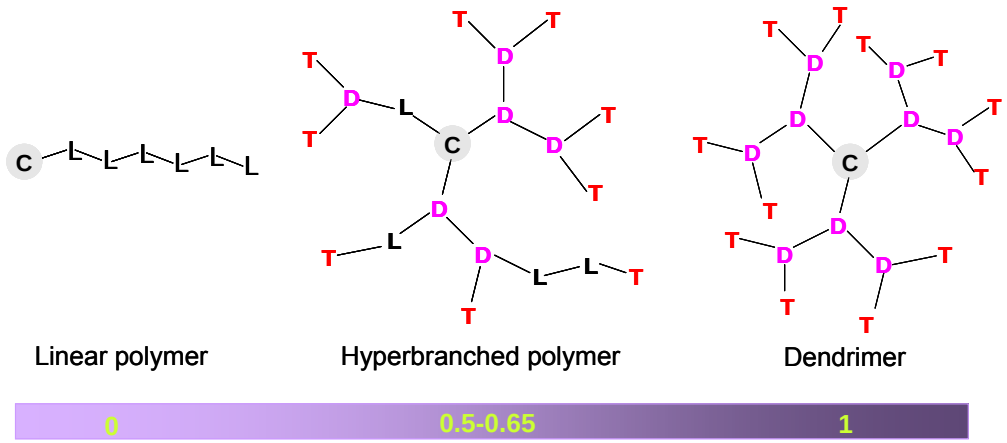

Figure 2.3 Comparison of linear polymer, hyperbranched polymer and dendrimer as a function of the degree of branching. (D: dendritic units; L: linear units; T: terminal units)

2.1.3 Other Dendritic Macromolecules

Besides dendrimers and hyperbranched polymers, a novel class of dendritic macromolecules whose branching points are linked to each other by true polymeric chains has emerged in the literature. Different names have been proposed to name them depending upon the architecture designed and the synthetic method used: comb-bursts polymers, dendrigrafts, polymers with dendritic branching, hyper-macs, and finally dendrimer-like (star) polymers to which this highlight is devoted. From a synthetic point of view, these materials are generally obtained by combination of ''controlled/living'' polymerization techniques with selective branching reactions. These types of dendritic macromolecules can thus be viewed as dendrimers comprising a central core, a precise number of branching points and outer terminal functions but whose generations are of macromolecular size (Figure 2.4).[7]

Unlike regular dendrimers, dendritic macromolecules are composed of macromolecular generations and as such they represent a new class of highly

branched polymeric architectures. They share, however, similar features with regular dendrimers such as a precise number of branching points and functions but differ from them by the possibility to entangle or crystallize. Advantages provided by the dendritic structure, in particular the multiplicity of reactive sites, can thus be combined with the properties of specific polymers.[7]

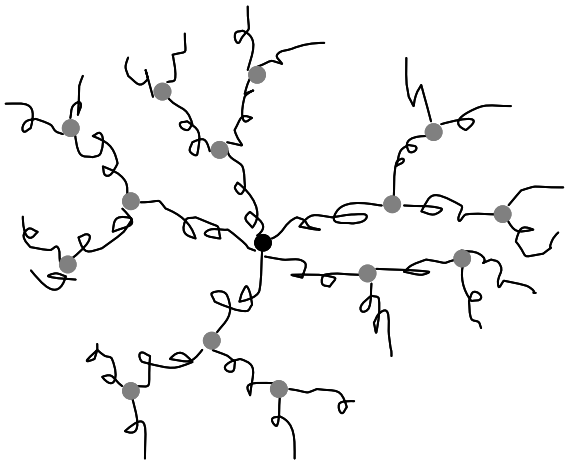

Figure 2.4 Schematic illustration of the structure of dendrimer like polymers.

These dendritic polymers can be further modified with charges and formed into the polyelectrolytes for fabrication dendritic multilayer films via the LbL assembly technique. Therefore, some fundamental behaviors of the polyelectrolyts in solution or interface, and polyelectrolyte complexes in solution will be introduced below.

2.2 Electrostatic Assembly with Polyelectrolytes

2.2.1 Polyelectrolytes in Solution

Polyelectrolytes combine the basic terms of polymers and electrolytes. The main difference to other polymeric systems is that a fraction or all of the monomeric units consists of ionized functional groups. When polyelectrolytes are dissolved in polar solvents like water, the ion-pairs dissociate, resulting in charges that are fixed to the polymeric backbone, and

small counter ions that are released into the solution. Depending on the ionic groups present in the macromolecule, it is possible to distinguish cationic and anionic polyelectrolytes, which carry positive and negative charges, respectively. Furthermore, if a polyelectrolyte can and will completely disassociate within a normal pH range, it is referred to as a "strong" polyelectrolyte. Conversely, if there are only partially dissociated ions from the polyelectrolyte in an aqueous solution, it is referred to as a "weak" polyelectrolyte.

The conformation of a polyelectrolyte in solution depends on the polymer concentration, the interactions with the solvent and the chain length. Furthermore, it depends on the acid or base strength of the ionic groups, the charge density, as well as the charge distribution along the chain and the nature of the counter ions. The importance of these parameters is given by the repulsive electrostatic interactions between the charges at the polymer backbone, which result in a stretched chain conformation in aqueous medium or in electrolyte solutions with low ionic strength.

First, we will discuss the solution properties of strong polyelectroytes. If the charge density in the polyelectrolyte chain is very low, the electrostatic interactions do not play any role and the chain is Gaussian, its end to end distance is $R_0=N^{1/2}a$. If the charge is higher, it is stretched by the repulsive electrostatic interactions between monomers. In the presence of a concentration n of added salt, the coulombic interaction between two charges at a distance r is given by the Debye-Hückel potential $v(r) = \frac{kTl_B}{r}\exp - kr$ where $l_B = \frac{q^2}{4\pi\varepsilon kT}$ is the so-called Bjerrum length (q is the elementary charge and ε the dielectric constant of water) and $k^{-1} = (8\pi n l_B)^{-1/2}$ is the Debye screening length. In the absence of added salt, the Debye-Hückel interaction reduces to the standard Coulomb interaction. In the absence of added salt, the interaction is long ranged and the chains are highly stretched;

their size R is given by

$$R \sim Na(f_B^2/a)^{1/3} \qquad \textbf{Equation 2.2}$$

A weakly charged polyelectrolyte chain is not fully stretched but it can be viewed as an elongated chain of Gaussian electrostatic blobs of size $\xi \sim a(\frac{f^2 l_B}{a})^{-1/3}$ containing each $g_{el} \sim (\frac{f^2 l_B}{a})^{-2/3}$ monomers as stretched. As salt is added to the local blob structure of the chain, the chain is no longer fully elongated and bends. It is general characterized by a persistence length l_p which is the length over which it remains stretched.[8]

When their concentrations are increased, polyelectrolyte chains interact strongly and eventually overlap. The electrostatic interaction between chains is much larger than the thermal excitation when the concentration is close to overlap (i.e. when the distance between the chains is of the order of their size). This could induce an ordering of the chains but there is no clear evidence for that experimentally.

2.2.2 Polyelectrolytes at Interfaces

The adsorption of polyelectrolytes onto a surface is governed by several parameters such as the charge density of the polyelectrolyte, charge density at the surface as well as the relative sign of the charges of both, the ionic strength and the pH of the solution for weak polyelectrolytes.

When polyelectrolytes are adsorbed from aqueous solution or an electrolyte solution of low ionic strength, a thin film is formed by the polyelectrolyte rods. In contrast, the adsorption from a solution with increased ionic strength results in a coiled structure of the polyelectrolytes on the surface. In the close proximity of the charged surface, the tightly bound surface charges constitute the Stern layer, which is covered by a diffuse layer composed of mobile ions. The surface potential created in this case, decreases with the distance from the surface (Figure 2.5). Similar to polyelectrolyte

solutions, the decay of the surface electrical potential also depends on solution ionic strength according to the Debye-Hückel approximation. Adsorption of polyelectrolytes will happen as long as the screening length κ^{-1} is smaller than the chain thickness.[8]

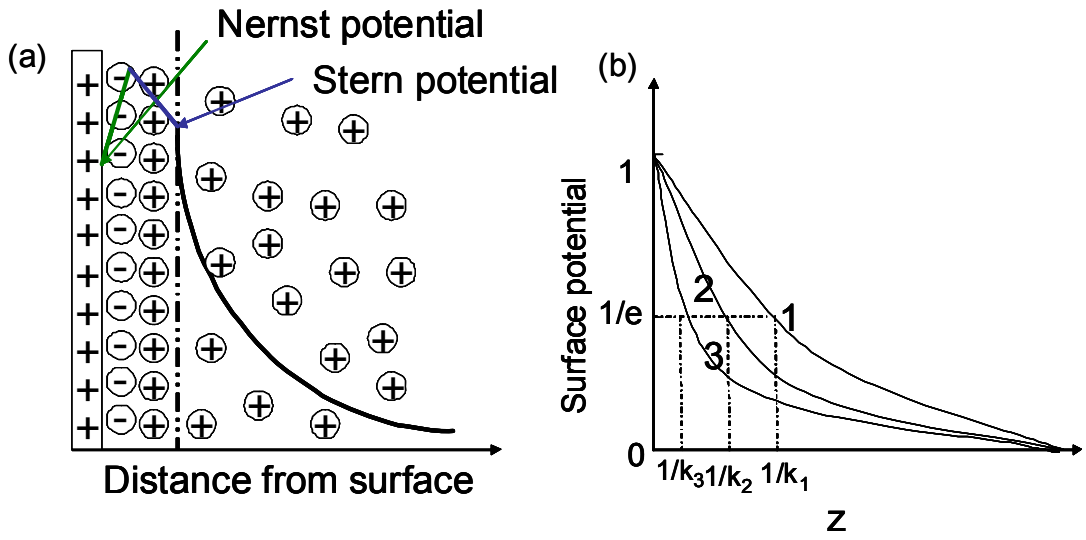

Figure 2.5 (a) Schematic representation of the electrical double layer of a charged surface in contact with an electrolyte solution. The tightly bound surface charges constitute the Stern layer, which is covered by the diffuse layer composed of mobile ions. The electrical potential decreases exponentially in the diffuse layer. (b) Schematic representation of the surface electrical potential dependence on solution ionic strength. The solution ionic strength increases in the sequence of 1-2-3. The Debye screening length κ-1 denotes the double layer thickness, which decreases with increasing solution ionic strength.

2.2.3 Polyelectrolyte Complexes

When two oppositely charged polyelectrolyte solutions are mixed, the polymers have a tendency to form a dense phase and to separate from the solvent. The dense phase is called a polyelectrolyte complex (PEC). The polyelectrolyte complex shows a wide range of behavior depending on stoichiometry (the relative molecular weights and charge contents of the two polymers), ionic strength and temperature etc. [9] The reaction of

polyelectrolyte complex formation can be described by the following equation:

$$(>\!\!-A^{-}c^{+})_n + (>\!\!-C^{+}a^{-})_m \;<=>\; (>\!\!-A^{-}C^{+})_x + (>\!\!-A^{-}c^{+})_{n-x} + (>\!\!-C^{+}a^{-})_{m-x} + xa^{-} + xc^{+}$$

Equation 2.3

where A^-, C^+ are the charged groups of the polyelectrolytes; a^-, c^+ are counterions; n, m are the number of the anionic and cationic groups in solution; n/m or m/n=X is the molar mixing ratio; $\theta=x/n$, $n<m$ or $\theta=x/m$, $m<n$ and θ is the degree of conversion. The degree of conversion determines whether the ionic sites of the components in efficiency are completely bound by the oppositely charged polyelectrolytes or whether low molecular counterions partly remain in the complex. Another characteristic quantity is the overall composition of the polyelectrolyte complex structures at any mixing ratio. Even if the stoichiometry of the ionic binding is 1:1, the major component may be bound in excess, leading to an overcharging of the PEC particles.[10]

The driving force of complex formation is mainly the gain in entropy due to the release of the low molecular counter ions. However, other interactions such as hydrogen bonding or hydrophobic ones may play an additional part. There are quite different structures formed due to polyelectrolyte formation, which depend on the characteristics of the components and the external conditions of the reaction. Generally, there are two complex models from the resulting structures. One is named a "ladder-like" structure, where complex formation takes place on a molecular level via conformational adaptation (zip mechanism). The other one is the "scrambled egg" model, where a high number of chains are incorporated into a particle.

The polyelectrolyte complex can not only be formed from the two oppositely charged species of polyelectrolytes in aqueous solution, but has also been developed by a number of alternative procedures. For example,

multilayer films of polyelectrolyte complexes were prepared by chemisorption from solution. This is well-known as the layer-by-layer technique and synonymously as electrostatic self-assembly.[11]

2.3 Driving Forces for the Fabrication of Multilayers

2.3.1 Electrostatic Interactions

Electrostatic interaction is one of the most often used forces to build up multilayer films via LbL assembly. Many publications have shown that there is a critical minimal charge density below which no LbL assembly is possible.[12] However, in some cases it was also shown that a multilayer can be formed when only a small fraction of charges is present.[13] Hence, it was proposed by Laschewsky et al. that the matching of charges is more important for a regular layer growth than a critical charge density of the polymers.[14] For combinations of strongly dissociating polyelectrolytes, charges between the polymers are generally well matched, excluding small salt ions from the bulk of the film.[15] Since electrostatic interactions are screened in solutions containing salt, the ionic strength has a strong influence on the assembly of multilayers as well as on the stability of preformed films. The screening effect of ions from the salt is used to change the polymer conformation and thus tunes the thickness of the assembled multilayer films.[16] However, a higher salt concentration can also promote the dissolution of the layers.[17] In addition to the adsorbed amount, the structure of the films also depends on the salt concentration, resulting in rougher surfaces when the ionic strength is increased.[18] Furthermore, there is an influence of increasing ionic strength on preformed multilayers. Without additional salt, charges within a multilayer are mainly compensated by polyelectrolytes of the opposite charge. When the ionic strength of the solution is increased, the amount of

segments that are charge-compensated by salt counterions increases and the amount of polyelectrolyte ion pairs decreases according to the following relation,[19]

$$Pol^+Pol^-(m) + Na^+(aq) + Cl^-(aq) \rightarrow Pol^+Cl^-(m) + Pol^-Na^+(m) \qquad \textbf{Equation 2.4}$$

with (m) denoting the multilayer and (aq) the surrounding solution. These results in a swelling and smoothing of polyelectrolyte multilayers adsorbed on flat substrates.[19] On the contrary, polyelectrolyte capsules show a pronounced shrinking effect upon addition of salt and they adopt a thermodynamically preferred conformation in order to enhance the mobility of charge-paired polyelectrolyte chains. It is assumed that the driving force of the shrinking of polyelectrolyte capsules is the reduction of the surface energy.[20]

2.3.2 Hydrogen Bonding Interactions

In addition to electrostatic interactions, hydrogen bonds can also play an important role in the formation of multilayers. Intermolecular hydrogen-bonds occur between hydrogen atoms, which are covalently bound to electronegative atoms like oxygen or nitrogen, and free electron pairs of other strongly electronegative atoms of a neighboring molecule. The hydrogen bonding interactions employed for the LbL assembly were first demonstrated by Stockton and Rubner in 1997[21] and have been successfully used in the self-assembly process.[22] Hydrogen bonded multilayers were also assembled by the use of weak polyelectrolytes at low pH, followed by pH changes to induce charges within the layers. Moreover, it was recently reported that hollow capsules made from hydrogen bonding multilayers can be obtained.[23]

2.3.3 Other Interactions for Multilayer Fabrication

Multilayers cannot only be formed by the interactions mentioned above,

but it is also possible to employ specific recognition and noncovalent interaction between molecules for the assembly of multilayers. This can be obtained by means of biological affinity including biotin-avidin, sugar-lectin and avidin-streptavidin interactions.[24] In addition, the binding of carbohydrates by lectins, e.g. concanavalin A (Con A) was also used for the assembly of multilayers that were not stabilized by electrostatic interactions. Con A possesses four binding sites for its ligand D-glucose and allows for the binding of glycogen (branched polyglucose).[25]

2.4 Layer by Layer Assembly via Electrostatic Interaction

2.4.1 Multilayer Assembly on Planar Substrates

The layer by layer deposition technique can be viewed as "template assisted assembly". Template assisted assembly is much faster than self-assembly or chemical modification cycles, whose outcome is often uncertain or difficult to predict. The electrostatic layer-by-layer (LbL) technique is based on the sequential adsorption of cationic and anionic species onto charged surfaces. In 1966, Iler firstly showed that it was possible to fabricate particles onto solid substrates in the LbL manner.[26] However, it was Decher who reported pioneering work involving the LbL assembly of a combination of linear, oppositely charged polyelectrolytes in the early 1990ies that an explosive growth occurred in the use of the LbL technology.[27] The general process to fabricate multilayer films via oppositely charged polyelectrolytes is shown in Figure 2.6. In the LbL assembly, a positively charged substrate is first exposed to a solution of polyanions, which adsorb on the positively charged surface. After several minutes, the excess of polymer is removed by washing steps. The adsorption of the polyanions results in an overcompensation of the surface charge, leading to charge reversal. After the washing step, the negatively charged substrate is

immersed into a solution of polycations, which adsorb onto the surface, resulting in substrate with positive charges. Again the physical adsorption of excess polymer is eliminated with a washing step. This procedure can be followed by consecutive circles until the designed number of multilayers is reached.

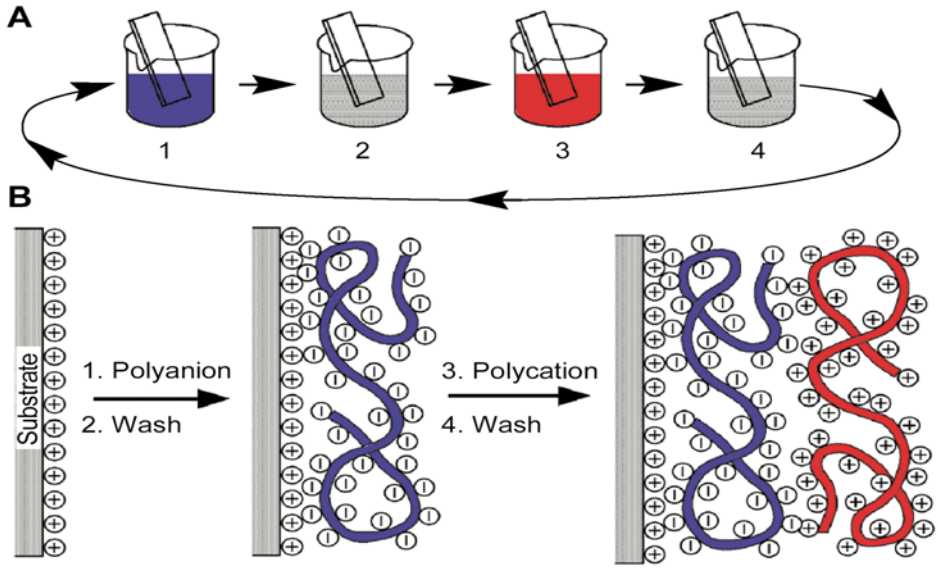

Figure 2.6 Schematic illustration for the construction of a multilayer of polyelectrolytes by the successive adsorption of a polyanion and a polycation by the repetition of the cycle. Steps 1 and 3 represent the adsorption of a polyanion and polycation, respectively, whereas steps 2 and 4 are washing processes.[28]

In contrast to polyelectrolyte complexes, the stepwise LbL process provides control over the structure, thickness, composition and interdigitation of different polyelectrolyte layers. There are nearly no restrictions concerning the materials in such films, as long as it is possible to adsorb them onto a surface and the new surface that results during the adsorption step bears functionalities that allow for the adsorption of the next layer. Meanwhile, the LbL technique has been developed far beyond polyelectrolyte systems and a wide range of applications has been found in

the assembly of synthetic functional polymers with conductive, photo-reactive, light emitting and redox active functionalities, as well as liquid crystalline polyelectrolytes and polymers that allow for molecular recognition. Furthermore, different functional organic pigments as well as dendrimers were used for the self-assembly. Charged nano-objects based on metal oxides, polyoxometalates, nanoparticles, fullerenes and metal colloids were also applied. In addition to synthetic polymers and colloidal particles many biological macromolecules such as proteins, enzymes, DNA and charged polysaccharides, lipids as well as viruses were assembled by the LbL technique to produce multicomposite materials.[29]

It is difficult to obtain a consistent picture of multilayer growth and structure. The combination of various characterization methods, such as X-ray and neutron reflectivity, x-ray photoelectron spectroscopy,[30] zeta potential measurements,[31] ellipsometry,[32] quartz crystal microbalance and surface plasmon resonance spectroscopy[30] have been employed. Basically, the research integrates the observations of layer interpenetration, individual layer profiles, charge stoichiometry, surface charge, and counterion content in a consistent way.[8]

The growth of the layer thickness is not always linear with the number of cycles. It is possible to distinguish films with linear and with exponential growth. Films that show linear increase in thickness are constructed under conditions in which the polyelectrolyte solution only interacts with the polyelectrolytes of opposite charge at the external surface of the film. Normally, the linear growth is observed for strong polyelectrolyte systems, however, there are several reports showing that the film thickness can increase more than linearly with the number of deposited layers. Exponential growth was reported for several weak polyelectrolytes, particularly for multilayers that consisted of biopolymers[33], and it was associated with an assembly process involving the diffusion of at least one of the

polyelectrolytes through the whole film at each bilayer deposition step.[34]

2.4.2 Multilayer Assembly on Curved Substrates

Another important feature of the LbL strategy is that multilayers can readily be transferred from planar surfaces to three dimensional substrates. In 1998, Möhwald's group reported the fabrication, structure and properties of polyelectrolyte multilayer capsules.[35] The preparation method is similar to those for flat substrates, involves consecutive polyelectrolyte adsorption steps, followed by the decomposition of the template.[36] After each layer deposition, centrifugation is used. The supernatant is removed and the colloidal particles are redispersed in a washing solution for next layer deposition. This washing step is repeated several times before the next layer is adsorbed. Additionally, it was shown that it is also possible to assemble a multilayer by adding just the amount of polymer that is required to observe a surface charge reversal, thus allowing the assembly of multilayers without intermediate washing steps. Various templates have been used for the fabrication of microcapsules such as weakly crosslinked melamine formaldehyde (MF) particles, [37] polystyrene (PS),[38] inorganic core materials including SiO_2, [39] and carbonates. [40] The multilayer deposition and the core dissolution process are schematically described in Figure 2.7.

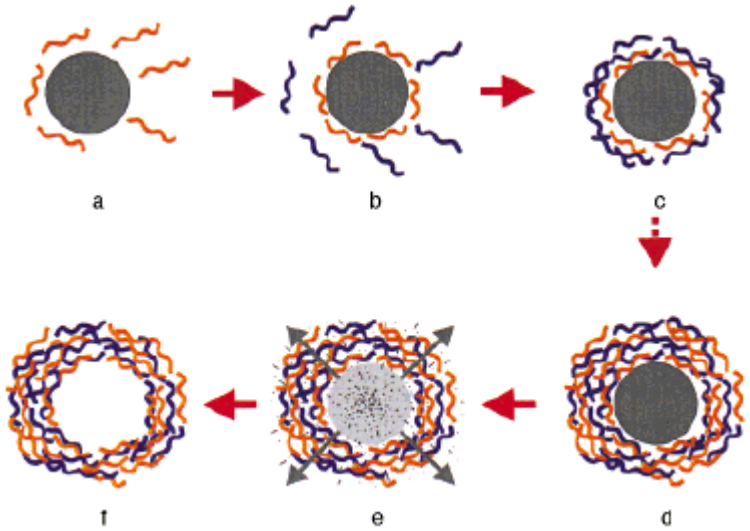

Figure 2.7 Scheme of the LbL deposition process on colloidal particles followed by core removal. The stepwise film formation by repeated exposure of the template to differently charged polyelectrolytes is illustrated in (a-d), and (e) shows the core dissolution, resulting in hollow polyelectrolyte capsules (f). (Ref. 20 (a))

1.5 Reference

1 Fréchet, J. M. J.; Tomalia D. A. *Dendrimers and other dendritic polymers.* Wiley Series in polymer science. John Wiley & Sons, West Sussex, UK, **2001**.

2 Taton, D.; Feng, X.; Gnanou, Y. *New J. Chem.* **2007,** *31,* 1097.

3 Caminade, A.-M.; Laurent, R.; Majoral, J.-P. *Advanced Drug Delivery Reviews* **2005**, *57,* 2130.

4 Jikei, M.; Kakimoto, M. *Prog. Polym. Sci.* **2001,** *26,* 1233.

5 Sunder, A.; Heinemann, J.; Frey, H. *Chem. Eur. J.* **2000,** *6,* 2499.

6 Hölter, H.; Burgath, A.; Frey, H. *Acta Polym.* **1997,** *48,* 30.

7 Taton, D.; Feng, X.; Gnanou, Y. *New J. Chem.* **2007,** *31,* 1097.

8 Decher, G.; Schlenoff, J. B. (Eds.) *Multilayer Thin Films, Sequential Assembly of Nanocomposite Materials*, Wiley-VCH, Weinheim, Germany, **2003**.

9 Philipp, B.; Dautzenberg, H.; Dautzenberg, H.; Linow, K.; Kötz, J.; Dawydoff, W. *Prog. Polym. Sci.* **1998,** *14,* 823.

10 Thünemann, A. F.; Müller, M.; Dautzenberg, H.; Joanny, J. F.; Löwen, H. *Adv. Polym. Sci.* **2004,** *166,* 113.

11 Bertrand, P.; Jonas, A.; Laschewsky, A.; Legras, R. *Macrom, Rapid. Comm.* **2000,** *21,* 319.

12 (a) Steitz, R.; Jaeger, W.; von Klitzing, R. *Langmuir* **2001,** *17,* 4471. (b)Schöler, B.; Kumaraswamy, G.; Caruso, F. *Macromolecules* **2002,** *35,* 889. (c) Glinel, K.; Moussa, A.; Jonas, A. M.; Laschewsky, A. *Langmuir* **2002,** *18,* 1408. (d) Voigt, U.; Jaeger, W.; Findenegg, G. H.; von Klitzing, R. *J. Phys. Chem. B.* **2003,** *107,* 5273.

13 Schöler, B.; Poptoschev, E.; Caruso, F. *Macromolecules* **2003,** *36,* 5258.

14 (a) Fischer, P.; Laschewsky, A.; Wischerhoff, E.; Arys, X.; Jonas, A.; Legras, R. *Macromol. Symp.* **1999,** *137,* 1. (b) Bertrand, P.; Jonas, A.; Laschewsky, A.; Legras, R. *Macromol. Rapid Commun.* **2000,** *21,* 319.

15 (a) Korneev, D.; Lvov, Y.; Decher, G.; Schmitt, J.; Yaradaikin, S. *Physica B* **1995,** *213-214,* 954. (b) Schlenoff, J.B.; Ly, H.; Li, M. *J. Am. Chem. Soc.* **1998,** *120,* 7626.

16 (a) Decher, G.; Schmitt, J. *Progr. Colloid Polymer Sci.* **1992,** *89,* 160. (b) Dubas, S. T.; Schlenoff, J. B. *Macromolecules* **1999,** *32,* 8153.

17 Sui, Z.; Salloum, D.; Schlenoff, J. *Langmuir* **2003,** *19,* 2491.

18 McAloney, R.A.; Sinyor, M.; Dudnik, V.; Goh, M.C. *Langmuir* **2001,** *17,* 6655.

19 Dubas, S. T.; Schlenoff, J. B. *Langmuir* **2001,** *17,* 7725.

20 (a) Georgieva, R.; Dimova, R.; Sukhorukov, G. B.; Ibarz, G.; Möhwald, H. *J. Mater. Chem.* **2005,** *15,* 4301. (b) Heuvingh, J.; Zappa, M.; Fery, A. *Langmuir* **2005,** *21,* 3165.

21 Stockton, W. B.; Rubner, M. F. *Macromolecules* **1997**, *30,* 2717.

22 (a) Wang, L. Y.; Wang, Z. Q.; Zhang, X.; Shen, J. C.; Chi, L.; Fuchs, H. *Macromol. RapidCommun.* **1997,** *18,* 509. (b) Pontes, R. S.; Raposo, M.; Camilo, C. S.; Dhanabalan, A.; Ferreira, M.; Oliveira, O. N., *Physica Status Solidi A* **1999,** *173,* 41.

23 Zhang, Y.; Guan, Y.; Yang, S.; Xu, J.; Han, C. C. *Adv. Mater.* **2003,** *15,* 832.

24 (a) Hong, J. D.; Lowack, K.; Schmitt, J.; Decher, G. *Progr. Colloid Polymer Sci.* **1993,** *93,* 98. (b) He, P.-G.; Takahashi, T.; Hoshi, T. ; Anzai, J.-I.; Suzuki, Y. ; Osa, T. *Mater. Sci. Eng. C* **1994,** *2,* 103. (c) Anzai, J.-I.; Kobayashi, Y.; Nakamura, N.; Nishimura, M.; Hoshi, T. *Langmuir* **1999,** *15,* 221.

25 Lvov, Y.; Ariga, K.; Ichinose, I.; Kunitake, T. *J. Chem. Soc., Chem. Commun.* **1995,** *22,* 2313.

26 Iler, R. K. *J. Colloid Interface Sci.* **1966,** *21,* 569.

27 (a) Decher, G.; Hong, J.D.; Schmitt, J. *Thin Solid Films* **1992,** *210-211,* 831. (b) Decher, G.; Hong, J. D.; Bunsen-Ges. Ber. *Phys. Chem.* **1991,** *95,* 1430. (c) Decher, G.; Hong, J. D. *Makromol. Chem., Macromol. Symp.* **1991**, *46,* 321.

28 Decher, G. *Science* **1997,** *277,* 1232.

29 Bertrand, P.; Jonas, A.; Laschewsky, A.; Legras, R. *Macromol. Rapid Commun.* **2000** *21,* 319.

30 (a) Laurent, D.; Schlenoff, J. B. *Langmuir* **1997,** *13,* 1552. (b) Caruso, F.; Niikura, K.; Furlong, D. N. Okahata,Y. *Langmuir* **1997,** *13,* 3422.

31 Hoogeveen, N. G.; Stuart, M. A. C.; Fleer, G.; Boehmer, M. R. *Langmuir* **1996,** *12,* 3675.

32 Ruths, J.; Essler, F.; Decher, G.; Riegler, H. *Langmuir* **2000,** *16,* 8871.

33 (a) Picart, C.; Lavalle, P.; Hubert, P.; Cuisinier, F. J. G.; Decher, G.; Schaaf, P.; Voegel, J.-C. *Langmuir* **2001**, *17,* 7414. (b)Boulmedais, F.; Ball, V.; Schwinte, P.; Frisch, B.; Schaaf, P.; Voegel, J.-C. *Langmuir* **2003,** *19,* 440.

34 Lavalle, P.; Picart, C.; Mutterer, J.; Gergely, C.; Reiss, H.; Voegel, J.-C.; Senger, B.; Schaaf, P. *J. Phys. Chem. B* **2004,** *108,* 635.

35 (a) Donath, E.; Sukhorukov, G. B.; Caruso, F.; Davis, S. A.; Möhwald, H. *Angew. Chem. Int. Ed.* **1998**, *37*, 2201. (b) Peyratout, C. S.; Dähne, L. *Angew. Chem. Int. Ed.* **2004**, *43*, 3762.

36 Voigt, A.; Lichtenfeld, H.; Sukhorukov, G. B.; Zastrow, H.; Donath, E.; Bäumler, H.; Möhwald, H. *Ind. Eng. Chem. Res.* **1999,** *38,* 4037.

37 Gao, C.; Moya, S.; Donath, E.; Möhwald, H. *Macromol. Chem. Phys.* **2002,** *203,* 953.

38 Déjugnat, C.; Sukhorukov, G. B. *Langmuir* **2004,** *20,* 7265.

39 (a) Adalsteinsson, T.; Dong, W.-F.; Schöhoff, M. *J. Phys. Chem. B* **2004,** ***108****,* 20056. (b) Itoh, Y.; Matsusaki, M.; Kida, T.; Akashi, M. *Chem. Lett.* **2004,** *33,* 1552. (c) Köhler, K.; Shchukin,D. G.; Möhwald, H.; Sukhorukov, G. B. *J. Phys. Chem. B* **2005** *109,* 18250. (d) Yang, S.; Zhang, Y.; Yuan, G.; Zhang, X.; Xu, J. *Macromolecules* **2004,** *37,* 10059. (e) Zhang, Y.; Guan, Y.; Yang, S.; Xu, J.; Han, C.C. *Adv. Mater.* **2003,** *15,* 832.

40 Antipov, A. A.; Shchukin, D.; Fedutik, Y.; Petrov, A. I.; Sukhorukov, G. B.; Möhwald, H. *Colloids Surfaces A* **2003,** *224,* 175.

Chapter 3

Characterization Methods

3.1 Surface Plasmon Resonance

Surface plasmon resonance spectroscopy (SPR, SPS or SPRS) is a more than century old technique, which can be referred to the findings of Wood's anomaly seen in the reflected light from diffraction gratings.[1] The underlying principles and theories of SPR are well understood, and numerous publications have reported on the method in detail.[2] In this section, the basis of SPR technique will be briefly described.

Surface plasmons are electromagnetic waves which can be excited at the interface between a noble metal (e.g. Au, Ag, Pt) and a dielectric material. The exact excitation conditions strongly depend on the optical properties of the system. The changes in these properties will lead to altered experimental excitation conditions. This measurable response of the system permits the sensitive monitoring of processes near this interface. Plasmons are basically light waves that are bound to the surface by the interaction with free electrons of the conductor, as illustrated in Figure 3.1. As a result, the free electrons respond collectively by oscillating in resonance with the light wave. The resonant interaction between the surface charge oscillation and the electromagnetic field of the light constitutes the SPs and strongly depends on the optical properties of the system.

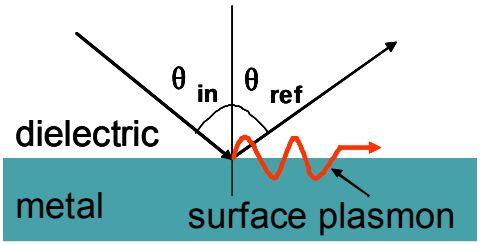

Figure 3.1 Schematic illustration of surface plasmon excited at the interface due to reflection of light wave at an interface of a metal and a dielectric.

An interface is considered to exist in the xy-plane between two half-infinite spaces, 1 and 2. The relationship that expresses the dispersion of the plasmon along this interface between the x-component of the wave vector of the plasmon K_{photon}, and both dielectric materials functions, ε_M (metal), ε_D (medium: air or aqueous solution) has been derived for a homogeneous dielectric (ε_1) as follows:

$$K_{photon} = \frac{\omega}{c}\sqrt{\varepsilon_1} \qquad \textbf{Equation 3.1}$$

Where, ω is the frequency of light and *c* is the speed of light.

The electron charges propagate along an interface between two media and whose amplitudes decrease exponentially normal to the surface on a metal boundary can perform coherent oscillations, termed surface plasmon polaritons (SPPs). Surface plasmon polaritons involve photons coupled to surface electric-dipole and/or magnetic-dipole excitations.

S-polarized light (transversal electric TE) propagating along the x-direction possesses only electric field component parallel to the surface (y-direction), and hence is unable to induce a surface charge density and excite surface polaritons. Only p-polarized light (transversal magnetic TM) modes with components along x and z can result in a periodic surface charge density and induce this interface electromagnetic wave. Of such an electrostatic field is coupled to "surface photons" a so-called surface polariton is created, the total electric field of which consists of a superposition of the constituting electrostatic and electromagnetic fields.

3.1.1 The Reflection Measurement Mode of SPR

For a thin, non-adsorbing layer defined by a thickness d and a refractive index n, the resonant angle displacement Δθ is proportional to the optical thickness, n·d of the layer.

$$\Delta\theta = n \cdot d$$
$$n = (n_{film} - n_{dielectric}) \qquad \textbf{Equation 3.2}$$

The relationship between the refractive index and the dielectric constant, ε is expressed in the complex form as follows;

$$\varepsilon = n^2 = (n + ik)^2 = n^2 + 2ikn - k^2 = \varepsilon' + \varepsilon'' \qquad \textbf{Equation3.3}$$

where, n = real part of the refractive index; *i*k = imaginary part of the refractive index (corresponds to the absorption); ε′= real part of the dielectric constant, ($\varepsilon' = n^2 - k^2$) ; ε′′= imaginary part of the dielectric constant, ($\varepsilon'' = 2kn$) .

The imaginary part of the Equation of 3.3 is equal to zero, if the film is non-adsorbing, then the dielectric constant would be $\varepsilon = n^2$. A limitation to this method is that the refractive index and thickness cannot be determined simultaneously. The refractive index need to be determined from another measurement technique, e.g. ellipsometry, then the Fresnel's equation can be used to convert the shift in incidence angle to film thickness. In this thesis, the refractive indices of all the films, the prism and Au film used were referred to the relating literatures. The reflection curves were fitted by the Winspall software, developed by A. Scheller at the Max Planck Institute for Polymer Research. The software calculates the Fresnel coefficients of each film/layer with recursion formalism.[3]

3.1.2 SPR with Prism Coupling

A direct coupling of incident light is not possible on a smooth surface, since the impulse of light in a dielectric is too small to couple to a surface. This can be improved, by passing the photons through a medium with a higher refractive index than the dielectric. There are two kinds of prism

arrangements, i.e., the Otto configuration and the Kretschmann configuration that had been developed until now.

Figure 3.2(a) shows the schematic illustration of the Otto configuration. A prism is positioned very close to a metal, and the evanescent field couples across the small air gap onto the metal surface. The Otto configuration is based on the total internal reflection of a plane wave incident at an angle θ at the base of a prism. The evanescent tail of this inhomogeneous wave can excite surface plasmons at the metal/dielectric interface provided that the coupling gap is sufficiently narrow. The major technical drawback of the Otto configuration is that it is difficult to get the metal surface close enough to the prism base, typically within 200 nm. Furthermore, a few dust particles may prevent efficient coupling.[4]

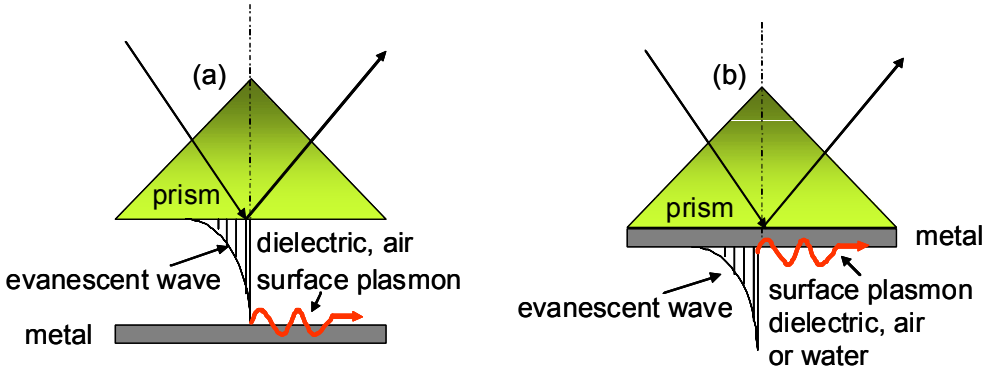

Figure 3.2 (a) Otto configuration (b) Kretschmann configuration of SPR excitation by prism coupling. In both cases, the surface plasmon propagates along the metal/dielectric interface.

Compared to the Otto configuration, the Kretschmann configuration (Figure 3.2(b))[5] is currently the most widespread version for practical surface plasmon resonance spectroscopy, because it is easier to build in than create an air gap between the prism and the metal. In this configuration, a thin metal layer is evaporated directly onto the base of the prism or a glass slide, which is then refractive index-matched to the base of the prism. In this case, photons in the prism couple through the thin layer metal to the surface plasmons on the other side, which is in contact with the dielectric medium.

The thickness of the metal film should be sufficiently thin for the evanescent wave to penetrate into the opposite surface, but still thick enough to avoid undue reradiation back into the prism. Experimentally, a thin metal film, Au is evaporated directly onto a glass substrate. The glass substrate is coupled to the base of the prism, with the refractive index-matching oil for optical reasons, thus both materials have the same refractive index.

In both configurations, resonance coupling is observed by monitoring the reflected light intensity as a function of the incident angle (Figure 3.3). The reflected intensity increases at low angle, as described by the Fresnel expressions. Then, from a certain angle, the angle of total reflection (critical angle θ_c), onwards it reaches a plateau. It is worthy to note, firstly, that the reflectivity before θ_c is rather high, which is due to the evaporated metal film that acts as a mirror reflecting most of the incident light. Secondly, the maximum reflected intensity never reaches unity since the photon energy is partly dissipated in the metal layer. The light energy is coupled to the SPR and hence the reflected light intensity reaches a minimum. Finally, the position of the critical angle only depends on the substrate and superstrate, i.e. prism and water, and is not influenced by any of the intermediate layers.

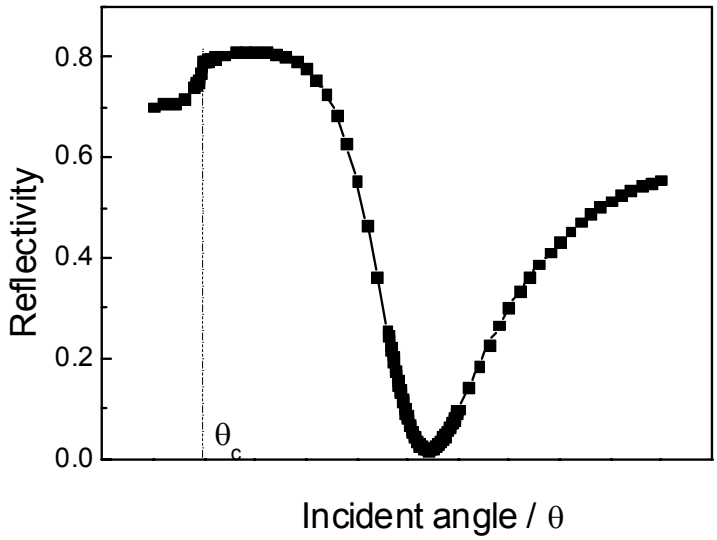

Figure 3.3 A typical angle scan SPR curve, i.e., reflectivity as a function of incident angle.

When adding a layer to the existing system, it is equivalent to an increase of the overall effective refractive index integrated over the evanescent field of a surface plasmon mode. The net effect is a slight shift of the dispersion curve corresponding to the increase of the wave vector of the surface plasmon (k_{sp}) for any given energy. As a consequence, the incident angle that determines the photon wave vector along the surface plasmon propagation direction has to be slightly increased in order to couple resonantly to the surface plasmon mode again (Figure 3.4). The critical angle is unaffected by the presence of a thin dielectric layer.

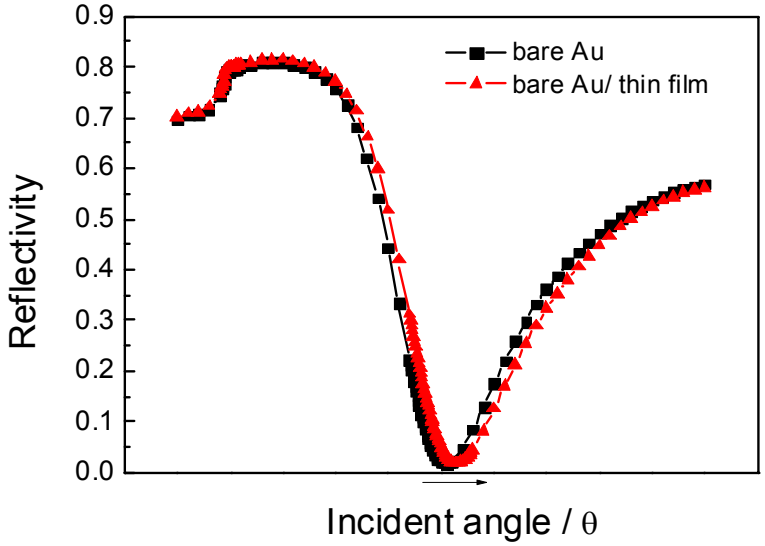

Figure 3.4 Angle scan curves of before and after deposition of a thin film on the gold substrate.

If light passes through a high refractive index prism, the dispersion of the free photons changes. This implies changing the dielectric constant of one of the media would also influence the wave vector of the surface plasmon resonance along the x-axis of the prism. Based on this theory, the deposition of a thin and non-adsorbing film, (thickness less than the decay length along the z-axis), with a different dielectric constant, would also affect the total dielectric constant over the evanescent field. This will cause the SPR angle to shift to the right, as shown in Figure 3.4. It is possible to obtain resonance of

the system by changing the incidence angle θ (of the incoming laser beam), until the wave vector of the photons in the x-axis is equal to product of the photons wave vector and sin θ, (i.e. $k_{ph,x} = k_{ph,}\sin\theta$). The system is in resonance, when the surface plasmons have been excited by the energy of the incident light and the intensity of the reflected light decreases.

Upon increasing the refractive index n or the thickness d of the dielectric layer, the resonance angle shifts toward higher values. The angular shift θ is a function of d and the optical contrast to the surrounding medium, which is given by:

$$\theta = f\left(d_{layer}, (\varepsilon_{layer} - \varepsilon_d)\right) \qquad \textbf{Equation 3.4}$$

This indicates that d and n cannot be determined independently by SPR with one angle shift only. However, if the refractive index of the material is known, the geometrical thickness can be obtained, and vice versa.

3.1.3 The Combined SPR and SPFS Setup

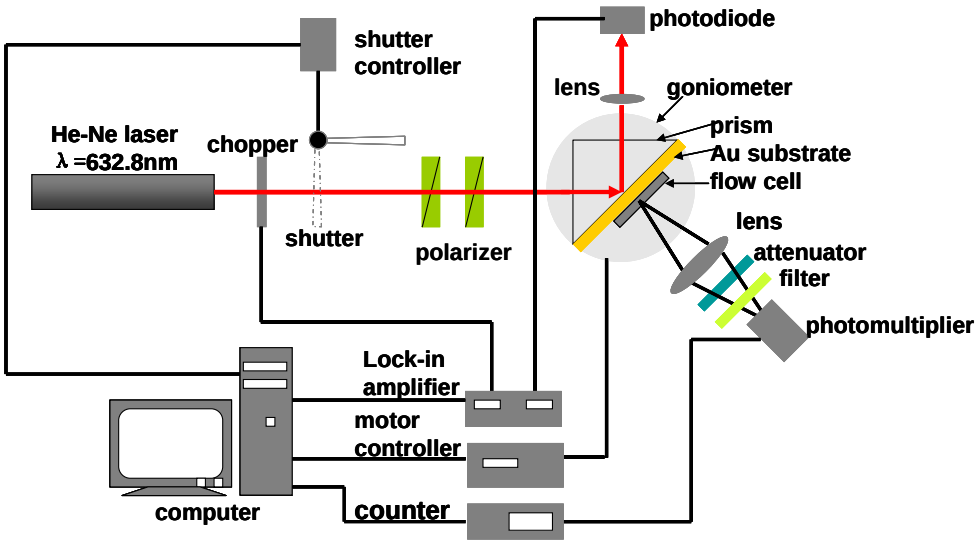

Figure 3.5 Schematic illustrations of the combined SPR setup and SPFS setup.

Figure 3.5 shows a tailor-made SPR setup and SPR combined

fluorescence spectroscopy setup (SPFS setup). This setup is based on the Kretschmann configuration mentioned in the section of 3.1.2. In brief, a HeNe laser beam (λ = 633 nm, JDS Uniphase, Model 1125p) is mechanically chopped at a frequency of 1150 H_z (PerkinElmer, Model 197) and then passes though two polarizers (Owis). The second polarizer generates a plane wave with the desired polarization, whereas, the first one is used for the attenuation of the laser. The reflected beam is collected and focused onto a photodiode (Spindler). The incident angle (θ) is varied by rotating the prism sample on a fine goniometer (Humber, 414a-10162) with an angle resolution of 0.001 degrees. The collection lens and the detector are rotated by an angle of 2θ in order to catch the reflected light. The output of the photodiode circuit is sent to a lock-in amplifier (PerkinElmer, Model 7265) to demodulate the signal voltage. In this manner, reflectivity versus incident angle curve is obtained.

3.1.4 Flow Cell and Sample Handling

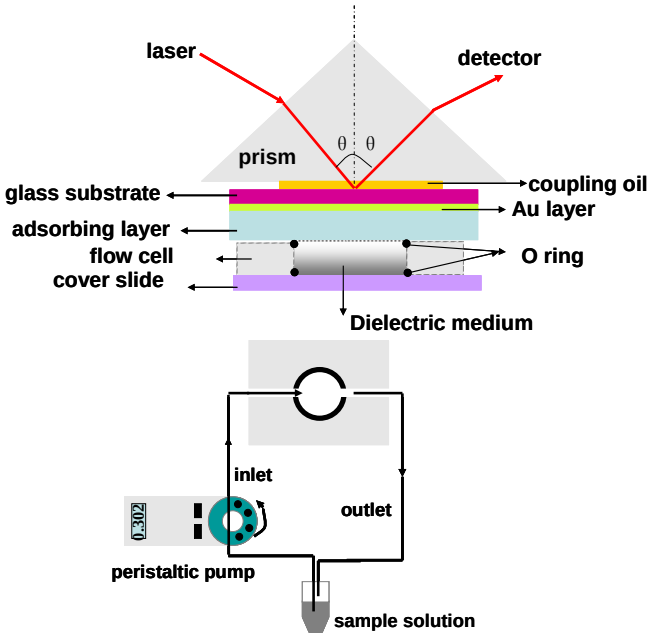

Figure 3.6 Schematic presentation of set up of flow cell which is sealed in prism and o ring and the cycling system with pump.

Some details of the design of flow cell used for measurement are shown in Figure 3.6. A reaction region for the thin film adsorption is created by a cover quartz glass on the bottom, sealed by a Viton O-ring and the sample substrate on the top and the whole body is amounted on the sample holder. The flow cell is also equipped with an inlet and outlet, which can hold a volume of about 200 μL, pumped by a peristaltic pump over the sample surface. It is important to avoid air bubbles in the flow cell, which might leads to a different refractive index as a wrong measurement result. The air bubbles were avoided by gradually increasing the liquid circulation flow rate, until the cell volume was filled without any air bubbles. The circulation flow rate was 0.8 mL/min^{-1} for optimized analyte delivery, minimizing mass transport effects, the prevention of backward flow and disruption in the reaction volume.

3.2 Surface Plasmon Field Enhanced Fluorescence Spectroscopy

Apart from the evanescent field excitation mechanism used in this work, it is very important to examine the behavior of fluorophores in the vicinity of metals. When a fluorophore close to a surface is excited by the evanescent wave, a strong fluorescent signal could be achieved. This phenomenon is termed as surface plasmon field enhanced fluorescence spectroscopy (SPFS).[6] The SPR evanescent field decays exponentially into the dielectric medium with a penetration depth of approximately hundreds of nanometers, which provides the surface sensitivity of SPFS. However, only fluorophores adsorbed, adhered, or bound to the surface can be excited, while the fluorophores in the bulk solution could not be excited.

On the other hand, there is an important factor needs to be taken into account when using SPFS technique. The metal employed in this system is a very efficient quencher for chromophores in the immediate proximity of the metal surface.

As schematically depicted in Figure 3.7, when the separation distance between fluorophores and metal is in the range of 5-10 nm, which is a typical distance for Förster energy transfer processes, all excitation energy is dissipated into the metal so that the dye molecules can not emit fluorescence photons.

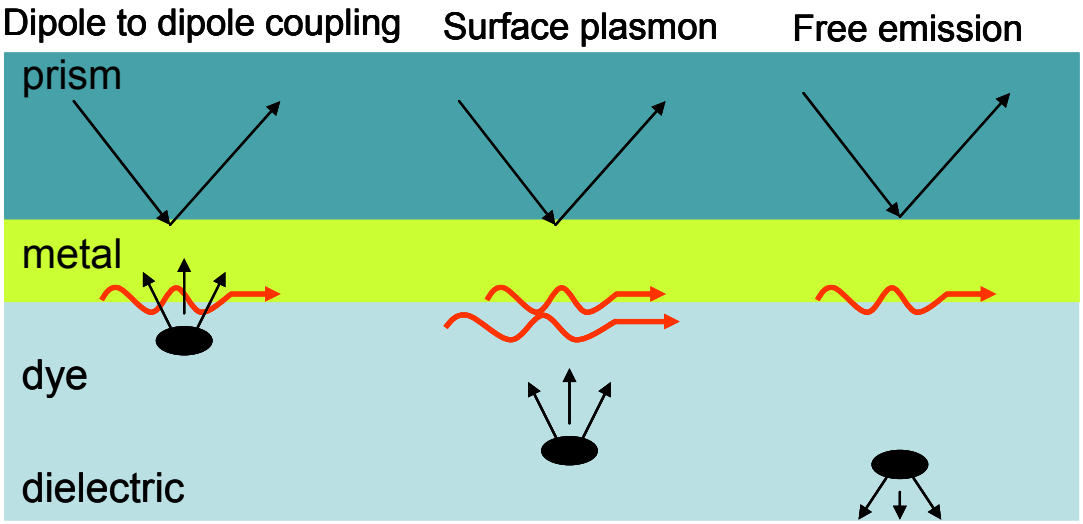

Figure 3.7 Schematic illustration of a fluorophore (dye) positioned close to a metal/dielectric interface. Different fluorescence decay channels take place at various fluorophore/metal separation distances.

When the separation distance is increased to the range of 10-20 nm, complex interaction channels can be observed: the SPR excited chromophores can vibronically relax some of the electronic excitation, resulting in a red-shifted surface plasmon in the metal, upon the de-excitation of the dye. The red-shifted SPR mode can then reradiate, according to the dispersion curve of surface plasmons (at an emission angle slightly different from the resonant excitation angle) via the prism.

At sufficient separation distances (>20 nm), free emission of the dyes dominates. As a consequence, there is no loss in fluorescence intensity due to the quenching process in the metal, while at the same time the dyes are located close enough to the metal to be excited by the enhanced PSP field.

3.3 Fourier Transform Infrared Spectroscopy

Fourier transform infrared spectroscopy (FTIR) is the study of the interaction of infrared light with matter. FTIR spectroscopy is based on the measurement of vibrational transitions between the ground state and an excited state in a molecule and is used for material characterization because of the fact that the chemical bonds in a material have specific frequencies at which they vibrate corresponding to their energy levels. The resonance or vibrational frequencies are determined by the shape of the molecular potential energy surfaces, the masses of the atoms and eventually by the associated vibronic coupling. The changes in vibrational energy are due to radiation in the spectral region of mid infrared (400-4000 cm^{-1}). The absorption or emission of an infrared wave changes the vibrational energy of a molecule,

$$\Delta E = E_2 - E_1 = h\nu = hc\tilde{\nu} \qquad \textbf{Equation 3.5}$$

with the initial and final energy E_1 and E_2, the Planck constant h, the velocity of light c, the frequency of the vibration ν (s^{-1}) and the wave number $\tilde{\nu}$ (cm^{-1}). A polyatomic molecule with N atoms has 3N−6 normal modes of vibration (3N−5 for a linear molecule), each mode of vibration having a defined vibrational frequency. In order for a vibrational mode in a molecule to be IR active, it must be associated with changes in the dipole moment. The vibrations can be understood with the model of the harmonic oscillator, in which the covalent bond is represented by a spring binding two masses. For a diatomic molecule the frequency of the vibration of such an oscillator depends on the mass of the atoms and the force of the binding, which is represented by the force constant k,

$$\nu = \frac{1}{2\pi}\sqrt{\frac{k}{\mu}} \qquad \textbf{Equation 3.6}$$

where ν is the fundamental frequency and $\mu = \frac{m_1 m_2}{m_1 + m_2}$ is the reduced mass of the oscillator between the masses m_1 and m_2. One consequence of this relation is that the vibration of heavy atoms in comparison to light atoms occurs at smaller wave numbers.

The most important component of a FTIR spectrometer is an interferometer based on the original design by Albert Michelson1 in 1880, as shown in Figure 3.8. Light from the source is split into two beams by a half-silvered mirror and make one of the light beams travel a different distance than the other (one is reflected off a fixed mirror and one off a moving mirror which introduces a time delay). The difference in distance travelled by these two light beams is called optical path difference, λ (or optical retardation). The Fourier transform spectrometer is just a Michelson interferometer with a movable mirror. Constructive or destructive interference can occur depending upon the light wavelength δ factor. A combination of both interferences can occur and the light beam intensity would be somewhere between very bright and very weak. A plot of the light intensity versus optical path difference or a large number of sinusoidal signals added together is called an interferogram. The variation of the light intensity with optical path difference is measured by the detector as sinusoidal wave. This is the fundamental measurement obtained by FTIR, which is Fourier transformed to give a spectrum.

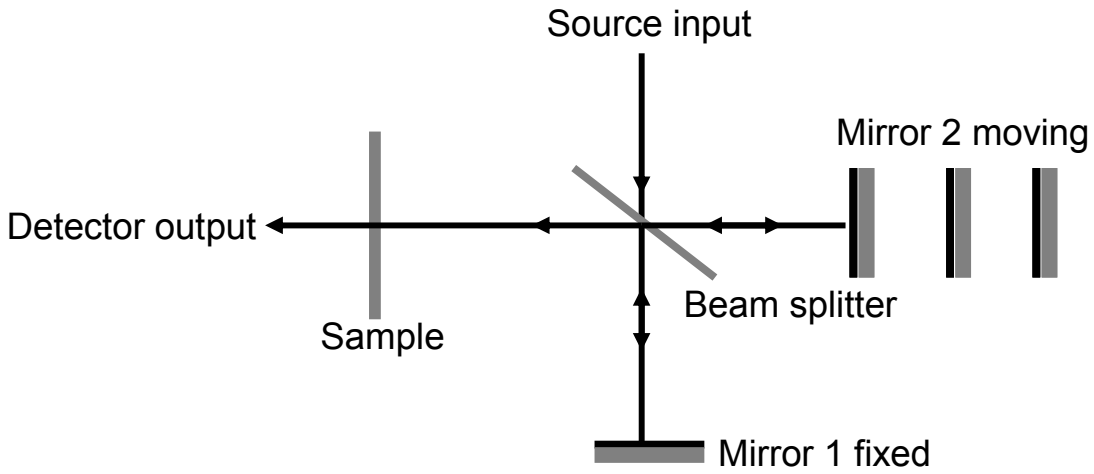

Figure 3.8 Schematic illustration of a generic Michelson interferometer.

The characteristic vibrations of covalent bonds can be classified in two distinct groups:

1. stretching vibrations, which change the bond length:
   (a) symmetric stretching
   (b) asymmetric stretching
2. bending vibrations, which change the angle between two bonds:
   (a) wagging vibrations
   (b) scissoring vibrations
   (c) rocking vibrations
   (d) twisting vibrations

The vibrational spectrum of a molecule is a fingerprint of this substance. In addition, different functional groups of a molecule have characteristic vibrational frequencies, which can be assigned to absorption bands in the IR spectrum[7].

3.4 Atomic Force Microscope

The atomic force microscope (AFM) or scanning force microscope (SFM) is one of the foremost tools for imaging, measuring and manipulating matter at the nanoscale. Binning, Quate, and Gerber invented the first AFM in 1986.

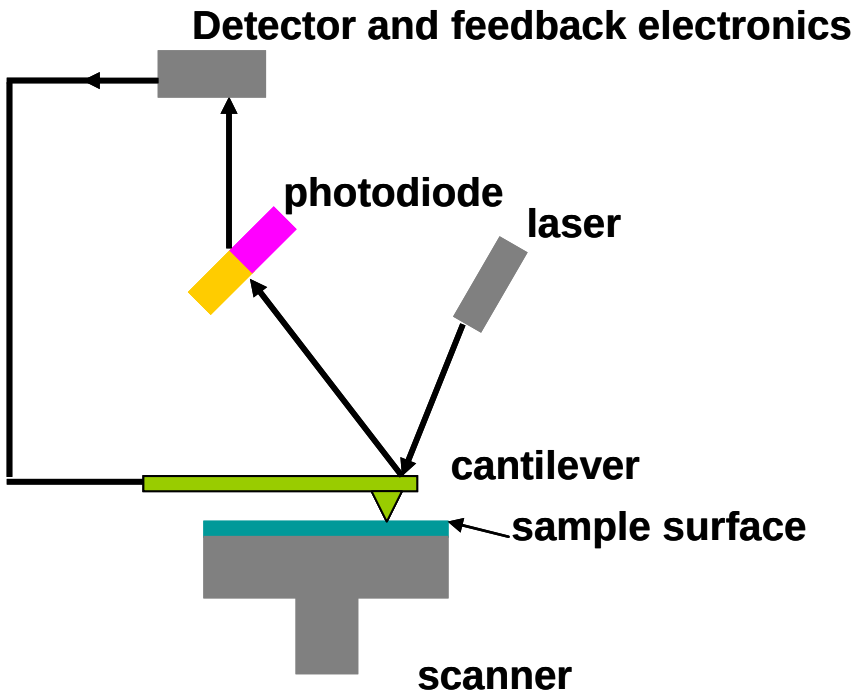

Figure 3.9 Schematic representation of an atomic force spectroscope.

The interactions between the tip and the sample include attractive Van der Waals interactions, capillary forces, repulsive steric forces and Coulomb interactions that can be either attractive or repulsive. A combination of these different interactions is observed with AFM. The AFM consists of a cantilever with a sharp tip (probe) at its end that is used to scan the sample surface (Figure 3.9). During an AFM measurement, the sample surface is scanned with a sharp tip that is mounted on the end of a cantilever. The force on the tip can be measured as a deflection of the cantilever, which is optically detected by the movement of a focused laser beam on the back of the cantilever. The sample is placed on a piezo-element and approaches the tip until there is an interaction between the tip and the surface that results in a deflection of the cantilever. Due to the horizontal movements of the piezo-elements the sample surface is scanned, and the force between the tip and the surface is kept constant with a feedback mechanism and converted in a height profile of the sample.

The AFM can be operated in a number of modes, depending on the

application. In general, it can be divided into contact mode, tapping mode, and non contact mode.

In contact mode, the force between the tip and the surface is kept constant during scanning by maintaining a constant deflection. The contact mode is also called the static mode. The static tip deflection is used as a feedback signal. Because the measurement of a static signal is prone to noise and drift, low stiffness cantilevers are used to boost the deflection signal. However, close to the surface of the sample, attractive forces can be quite strong, causing the tip to "snap-in" to the surface.

In tapping mode, the cantilever is driven to oscillate up and down at near its resonance frequency by a small piezoelectric element mounted in the AFM tip holder. The amplitude of this oscillation is greater than 10 nm, typically 100 to 200 nm. Due to the interaction of forces acting on the cantilever when the tip comes close to the surface, Van der Waals force or dipole-dipole interaction, electrostatic forces, etc cause the amplitude of this oscillation to decrease as the tip gets closer to the sample.

In non-contact mode, the tip of the cantilever does not contact the sample surface. The cantilever is instead oscillated at a frequency slightly above its resonance frequency where the amplitude of oscillation is typically a few nanometers (<10 nm). The Van der Waals forces, which are strongest from 1 nm to 10 nm above the surface, or any other long range force which extends above the surface acts to decrease the resonance frequency of the cantilever. This decrease in resonance frequency combined with the feedback loop system maintains a constant oscillation amplitude or frequency by adjusting the average tip-to-sample distance. Measuring the tip-to-sample distance at each (x, y) data point allows the scanning software to construct a topographic image of the sample surface.[8]

3.5 References

1 Wood, R. W. *Philosophical Magazine* **1902,** *4,* 396.

2 (a) Raether, H., *Surface Plasmon on Smooth and Rough Surfaces and on Gratings*. Springer: Berlin, **1988.** (b) Yeh, P., *Optical Waves in Layered Media* John Wiley & Sons: New York, **1988.** (c) Agranovich, V. M., *Surface Polaritons*. North Holland, Amsterdam, **1982.** (d) Knoll, W., *MRS Bulletin* **1991,** XVI, (7).

3 Kovacs, G., *Electromagnetic Surfaces Modes*. John Wiley & Sons: New York, **1982.**

4 Otto, A. *Z. Phys.* **1968,** *216,* 398.

5 Kretschmann, C.; Raether, H. *Z. Naturforsch.* **1968**, 2135.

6 (a) Liebermann, T.; Knoll, W. *Colloid. Surface. A* **2000,** *171,* 115. (b) Liebermann, T.; Knoll, W.; Sluka, P.; Herrmann, R. *Colloid. Surface. A* **2000,** *169,* 337. (c) Neumann, T.; Johansson, M. L.; Kambhampati, D.; Knoll, W. *Adv. Func. Mater.* **2002,** *12,* 575.

7 (a) Hesse, M.; Meier, H.; Zeeh, B. *Spektroskopische Methoden in der organischen Chemie* Georg Thieme Verlag, Stuttgart, **1995.** (b) Atkins, P.W. *Physikalische Chemie* VCH, Weinheim, **1996.**

8 Giessibl, F. J. *Reviews of Modern Physics* **2003,** *75,* 949.

Chapter 4

Hyperbranched Polyglycerol / Phosphorus Dendrimer Multilayers as a Function of Molecular Weight, Ionic Strength and pH

This chapter describes the assembly of dendrimer/hyperbranched polymer multilayers from cationic phosphorus dendrimers, deposited in alternation with anionic hyperbranched polyglycerols (hbPGs). The functionalized hyperbranched polyglycerols with carboxylic acid groups containing elevated molecular weights were obtained by succinate functionalization. The influence of assembly conditions, such as molecular weight, ionic strength and pH of anionic hyperbranched polyglycerol solutions on the growth of multilayer thin films was studied. Surface plasmon resonance spectroscopy (SPR) was employed for in situ detecting the multilayer deposition. The results show that the thicknesses of multilayer films unexpectedly increase with decreasing the molecular weight of anionic hbPGs and the multilayer films fabricated by low molecular weight of anionic hyperbranched polyglycerols grow less regularly. By varying the pH of anionic hbPG solutions from 4.5 to 9, the thickness of multilayer films is reduced with increasing pH. Changing the concentration of NaCl from 0.025 M to 0.1 M leads to an increase of film thickness. However, a further increase of the concentration of NaCl up to 0.5 M results in a drop of film thickness. Surface morphology of multilayers fabricated at various pH values was imaged by atomic force microscopy (AFM). The observed changes of multilayer thickness and surface morphology can be interpreted with the aid of theories regarding the charge density and conformation of the anionic hbPG chains in solution. Fourier transform infrared spectroscopy (FTIR) measurements further confirm that structural changes of the multilayer films are induced by pH adjustments.

4.1 Introduction

During the past decades, layer by layer (LbL) assembly deposition has been demonstrated to be a versatile technique that permits the construction of multilayer thin films with accurate control of film thickness, composition, morphology, and chemical functionality.[1] Fabrication of these films originally involved alternating immersions of oppositely charged species via electrostatic interaction. With each adsorption step, the surface charge is reversed, allowing fabrication of the next species. The materials for the LbL assembly deposition range from linear polymers, polymeric microgels,[2] biomacromolecules[3] and inorganic particles[4] to dendritic macromolecules.[5] The driving force for LbL film fabrication is diverse, including electrostatic interaction, hydrogen-bond,[6] halogen-bond,[7] coordination bond,[8] charge-transfer interactions,[9] biospecific interaction (e.g., sugar-lectin interactions)[10] and guest-host interaction[11] etc. An essential advantage of the LbL strategy is that it is readily transferred from planar surface to the three dimensional substrates such as anodic aluminum oxide (AAO)[12] and colloidal particles[13]. The nanotubes and hollow capsules are achieved by subsequent removal of the AAO and colloidal particle templates. These nano- or microstructures have the potential for controlled delivery applications if the prepared multilayers are equipped with active functional groups which are responsive to various external stimuli such as pH,[14] ionic strength,[15] and light.[16]

Dendrimers differ from other polymer classes such as linear and branched polymers since they are globular-shaped and well defined macromolecules with a high degree of molecular uniformity and large number of functionalities.[17] Cationic phosphorus dendrimers represent a new class of branched polyamines with protonated tertiary amine end-groups, possessing a hydrophilic surface and a hydrophobic core.[18]

Based on these phosphorus dendrimers, microcapsules and nanotubes with potential for application in biosensensors[19] were produced. Besides the structural difference, dendrimers are distinguished from classical polymers by another important difference: they usually have to be prepared by a tedious and time-consuming sequential ("generation-wise") synthesis protocol.

Hyperbranched polymers are associated with fast and convenient preparative accessibility.[20] Most synthetic approaches are based on one-pot syntheses via polymerization of AB_m-type monomers that lead to the formation of randomly branched structures. Hyperbranched polyglycerol, due to its dendritic architecture, high end-group functionality, thermal stability and a fully biocompatible[21] polyether scaffold, is currently being used for various biomedical purposes.[22] Hyperbranched polyglycerols employed were synthesized based on the ring-opening polymerization of glycidol under slow monomer addition technique (Figure 4.1).[23] The obtained hbPGs process relatively narrow molecular weight distribution (M_w/M_n is about 1.5, determined by size exclusion chromatography vs. poly (propylene oxide) standards, compared this polydispersity index (PDI) with the normal range 3-5), and the molecular weight can range from 1000 to 24000 g/mol. Recently, our group introduced a facile two-step strategy that relied on the use of a low molecular weight hbPG (M_n = 500 and 1,000 g/mol) as a macroinitiator for the slow addition of glycidol, permitting to overcome previous limitations concerning molecular weights and molecular weight control. Based on this method, a series of hbPGs with molecular weights up to M_n = 24,000 g/mol were obtained under fully controlled conditions.[24]

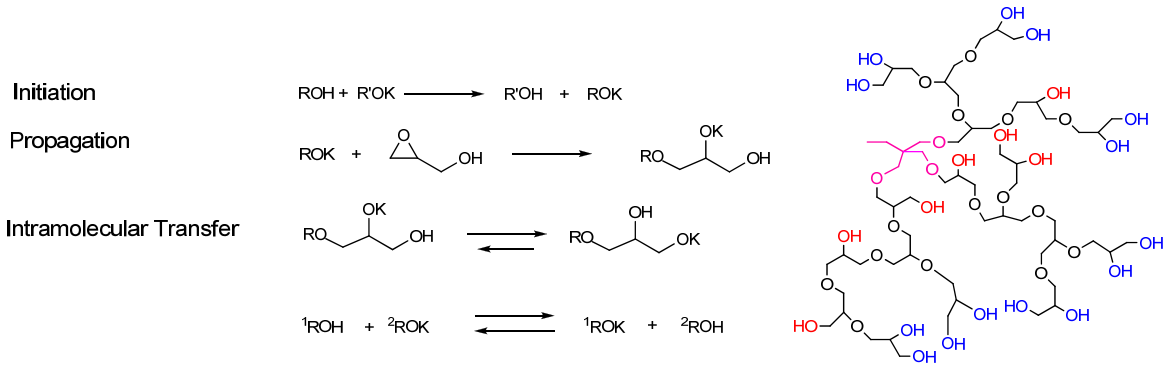

Figure 4.1 Mechanism of the anionic ring-opening polymerization of glycidol, employing a partially deprotonated alcohol as initiator. A proton exchange equilibrium affords primary and secondary alkoxide sites and thus leads to a hyperbranched polyether scaffold with multiple hydroxyl groups.

We reported in a previous Communication on a combination of these two classes of dendritic materials, oppositely charged phosphorus dendrimers and hyperbranched polyglycerols by fabricating hybrid organic/TiO_2 nanostructures via an electrostatic LbL approach. This nanostructure could potentially be applied in catalysis, sensors, optics and optoelectronics.[25] However, no systematic investigation of the characteristic changes of multilayers under various deposition conditions has been reported yet. Hence, it is critical to exploit factors that can be varied to tune the structural changes on the nanometer length scale.

In this study, we report on the fabrication of dendrimer/hyperbranched polymer multilayers by employing cationic phosphorus dendrimers and anionic hbPGs. The effect of deposition conditions on thickness and morphology of the resulting multilayers was investigated. Multilayers of cationic phosphorus dendrimers and anionic hbPGs were prepared by sequential electrostatic adsorption onto a modified 3-mercaptopropionic acid (3-MPA) self-assembled gold substrate and in situ detected via surface plasmon resonance spectroscopy (SPR). Surface properties and composition of multilayers based on anionic hbPGs were systematically compared by varying the molecular weights of hbPGs, pH, and ionic strength, respectively.

Surface morphology of the multilayers deposited with varying pH was visualized by atomic force microscopy (AFM) and the chemical nature of the multilayers was further confirmed by FTIR.

4.2 Experimental Section

Materials

The cationic phosphorus dendrimer ($G_4(NH^+Et_2Cl^-)_{96}$) and anionic phosphorus dendrimer ($G_4(CH\text{-}COO^-Na^+)_{96}$) employed are the 4th generation of N, N-disubstituted hydrazine phosphorus dendrimers containing 96 positive and negative functional groups, respectively, on the edge of the structure and the process of synthesis has been described in the paper previously published.[26] The structures of oppositely charged phosphorus dendrimers have been shown in Figure 4.2.

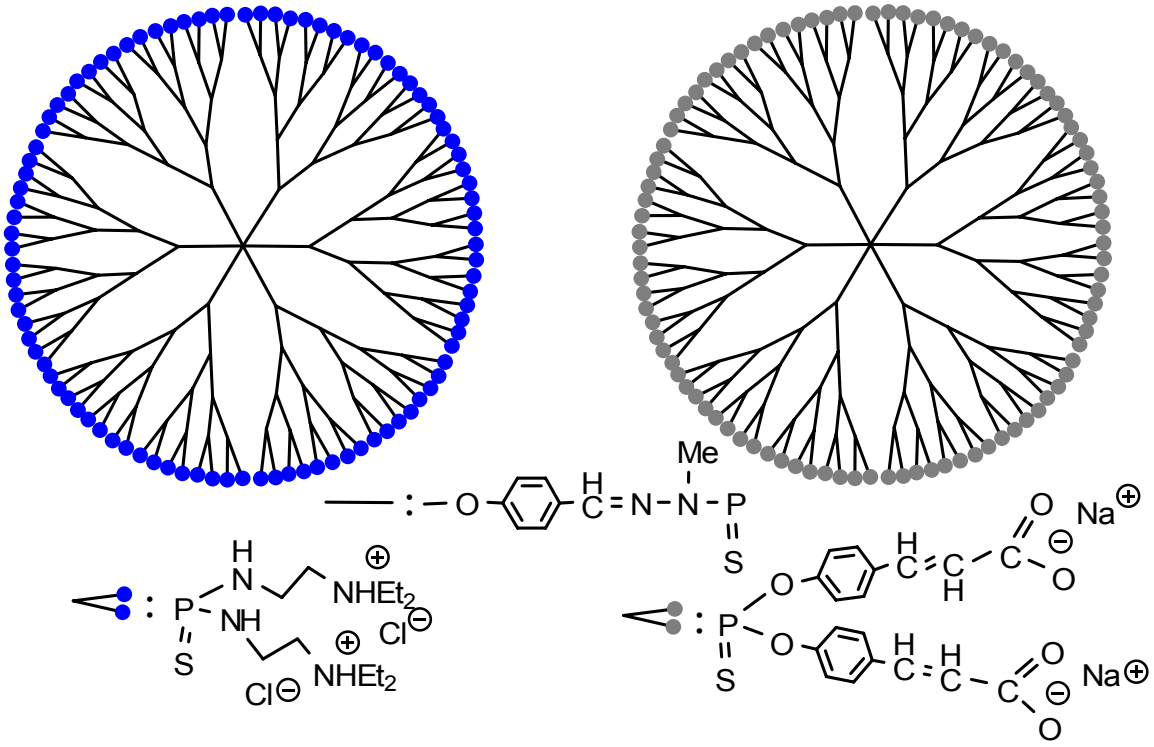

Figure 4.2 Schematic illustration of cationic phosphorus dendrimers and anionic phosphorus dendrimers.

All chemicals for the synthesis were purchased from Aldrich or Acros Organics or Fluka. Acetone p.a., methanol p.a., isopropanol p.a., Dowex® 50WX8, 200-400 mesh, ion exchange resin, sodium hydroxide, 30 weight-% H_2O_2 and 1m potassium tert-butylate solution in THF were used as received. THF was distilled over sodium prior to use. Acrylonitrile and DMF were purified by distillation prior to use. Acteone-d6, Methanol-d4 and D_2O were purchased from Deutero GmbH.

3-mercaptopropionic acid (3-MPA) was used and purchased from Aldrich (Germany). LaSFN9 glass slides were purchased from Hellma Optik. (Jena, Germany). A millipore water purification unit was used to obtain 18.2 MΩcm water，which was employed to prepare the aqueous solutions for the experiments.

Synthesis of anionic hbPG with carboxylic acid groups

(1) Synthesis of anionic hbPG by Michael addition reaction followed by hydrolysis

Preparation of hbPG with nitrile groups.

4 g (1.33 mmol, 0.048 mmol –OH groups) hyperbranched polyglycerol was placed in a reactor and dissolved in 15 ml absolute DMF under argon atmosphere. 0.27 g (2.4 mmol) potassium tert-butoxide was added to the polymer solution to achieve 5% deprotonation of the hydroxyl groups. The reaction mixture was stirred and heated up to 80 °C for 4 hours and then cooled down to 0°C. Distilled acrylonitrile (5.4g, 0.1 mmol) was slowly added via a syringe to the reactor and the temperature was kept at 0°C. After 6 hours the reactor was heated up to 5°C and the solution became slightly red. The reaction mixture was kept for another 20 hours at 5 °C and finally 48 hours at room temperature. Then 1 g of a cationic exchange resin was added to the reactor and that was stirred for 24 hours. After filtration, DMF and the rest of acrylonitrile were distilled off. The modified polyglycerol was firstly dissolved in acetone and then precipitated in methanol. Both fractions were

analyzed. Both fractions are brown. The acetone fraction is a solid and the methanol fraction is high viscous oil. The nitrile functionalized hbPG was dried in vacuum at 50°C for two days.

^{1}H NMR (d6-acetone, 300 MHz):

δ=3.9-3.4 ppm (m, CH_3-CH_2-C(CH_2-O)$_3$-[***hbPG***-C***H*****$_2$**-CH_2-CN]$_x$, 2H), δ=2.7 ppm (s, CH_3- CH_2-C(CH_2-O)$_3$-[hbPG-CH_2-C***H*****$_2$**-CN]$_x$, 2H), δ=1.4 ppm (CH_3-C***H*****$_2$**-C(CH_2-O)$_3$-[hbPGCH_2- CH_2-CN]$_x$, 2H), δ=0.89 ppm (m, C***H*****$_3$**-CH_2-C(CH_2-O)$_3$-[hbPG-CH_2-CH_2-CN]$_x$, 3H)

Preparation of anionic hbPG with carboxylic acid groups.

hbPG with nitrile groups (2g) was placed in 120 ml 6 N sodium hydroxide solution. A 30% weight H_2O_2 solution (10 ml) was carefully added and the mixture was stirred for 1 hour at 50°C, then for 1 day at 60°C and finally cooled down to room temperature for 2 days. A 2 M sodium sulfite solution was added and the reaction mixture was dialyzed for 2 days in water. The reaction mixture solutions were precipitated in ethanol. The product is a slightly yellow solid.

^{1}H NMR (D_2O, 300 MHz):

δ = 4.0-3.4 ppm (m, CH_3-CH_2-C(CH_2-O)$_3$-[***hbPG***-C***H*****$_2$**-CH_2-COOH]$_x$, 2H), δ = 2.4 ppm (s, CH_3-CH_2-C(CH_2-O)$_3$-[hbPG-CH_2-C***H*****$_2$**-COOH]$_x$, 2H), δ=1.3 ppm (m, CH_3-C***H*****$_2$**-C(CH_2-O)$_3$-[hbPG-CH_2-CH_2-COOH]$_x$, 2H), δ=0.8 ppm (m, C***H*****$_3$**-CH_2-C(CH_2-O)$_3$-[hbPG-CH_2-CH_2-COOH]$_x$, 3H).

(2) Synthesis of anionic hbPG by succinate functionalization

Anionic hbPG with carboxylic acid groups was obtained by succinate functionalization of hbPG according to a previously published strategy[27]. Hyperbranched polyglycerol (DP=39 (degree of polymerization), 2.31g, 0.032mol) was treated with succinic anhydride (1.92g, 0.019mol) at 40^{o}C in the presence of triethylamine (TEA, 0.1ml), in anhydrous N, N-dimethylformamide (DMF; 20 ml). After evaporation of the solvent under vacuum line, the residue was dissolved in distilled water, dialyzed by

employing a 1200 cut-off membrane, and dried in vacuum oven at 40°C for 2 days as a colorless paste.

^{1}H NMR (D_2O, 300 MHz):

δ = 5.1 ppm (s, C***H***OCO, 1 H), δ = 4.26–3.88 (m, C***H*****$_2$**OCO, 2 H), δ = 3.61-3.49 ppm (m, hbPG backbone), δ =2.59 ppm (s, OCOC***H*****$_2$C*H*$_2$**COOH, 4 H), δ =1.27 ppm (s, CH_3C***H*****$_2$**$C(CH_2O)_3$, 2 H), δ =0.75 ppm (s, C***H*****$_3$**$CH_2C(CH_2O)_3$, 3 H).

^{13}C NMR (D_2O, 75 MHz):

δ = 176.7 ppm (***C***OOH), δ =173.7 ppm (O***C***O), δ =78.1–62.8 ppm (hbPG-***C***), δ = 46.4 ppm (CH_3CH_2***C***$(CH_2O)_3$), δ = 29.0 ppm (COO***C***H_2***C***H_2COOH), δ = 8.0 ppm (***C***$H_3CH_2C(CH_2O)_3$).

Substrate Preparation

All LaSFN9 glass slides were covered with a 2 nm chromium adhesion layer by evaporation, followed by 50 nm gold. Chromium and gold coating were accomplished using an Edwards Auto 305 vacuum evaporator. The gold substrate was modified with a self assembled monolayer (3-MPA) by immersing into a 1 mM of 3-MPA ethanol solution for at least 6 hours, followed by a brief ethanol rinse and drying with a gentle stream of N_2.

Preparation of Cationic Phosphorus Dendrimer and Anionic Hyperbranched Polyglycerol Solution

Solutions of $G_4(NH^+Et_2Cl^-)_{96}$ and $hbPG_m(COO^-H^+)_n$ were prepared with a concentration of 0.03 mM in water and further pH adjusted with either HCl or NaOH. No additional salt (NaCl) was added to the $G_4(NH^+Et_2Cl^-)_{96}$, $hbPG_m(COO^-H^+)_n$ and rinse solutions except specially mentioned.

LbL Multilayer Assembly and in situ Surface Plasmon Resonance Spectroscopy

The principles of SPR and the experimental setup have been described in previous publications.[28] Surface plasmons are collective oscillations of the

electron gas in a metal film that results from incident electromagnetic excitation at certain frequencies. In the Kretschmann configuration, monochromatic p-polarized light (λ= 632 nm) is directed through a prism to excite surface plasmons at the gold/dielectric interface at a certain angle of incidence, resulting in a sharp minimum in the intensity of the reflected light. Adsorption processes occurring at the interface are followed up in real time by selecting an appropriate incident angle and recorded by monitoring the reflected intensity as a function of time.

MPA modified gold substrates were exposed to a rinse solution before multilayers were produced by alternately exposing the substrates to the respective solutions of $G_4(NH^+Et_2Cl^-)_{96}$ and $hbPG_m(COO^-H^+)_n$ for 15 min. The substrates were rinsed for 2 min between each adsorption step in order to remove the physical adsorption. The multilayers with 4 bilayers were assembled at each combination of pH value and ionic strength.

Atomic Force Microscopy (AFM) Imaging

AFM images were taken on air-dried multilayer films with a Veeco Dimension 3100 setup in tapping mode. Image processing was obtained using the Nanoscope 5.12r5 software.

Fourier Transform Infrared (FTIR) Spectroscopy Measurements

The chemical structure of the multilayer films was analyzed using a Nicolet Magna-IR 850 spectrometer in the reflection mode using glass substrates coated with 2 nm chromium and 50 nm of gold deposited by thermal evaporation. Omnic series software was utilized for data acquisition. For each sample, 1000 scans were taken at a resolution of 4 cm^{-1} with 30 min induction time for N_2 exposure to eliminate noise from atmospheric water.

Titration of Anionic Hyperbranched Polyelectrolytes

To determine the pKa values of $hbPG_m(COO^-H^+)_n$ at ambient temperature, the potentiometric titrations at mass concentrations of 0.5

mg/ml were carried out by the use of a Mettler Toledo MP225 pH meter. Solutions of $hbPG_m(COO^-H^+)_n$ were titrated with 0.1 M NaOH. The pKa value was determined from the titration curve at the point where half of the amount of base necessary for reaching the equivalence point was added.

4.3 Results and Discussion

4.3.1 Characterization of Anionic Hyperbranched Polyglycerols

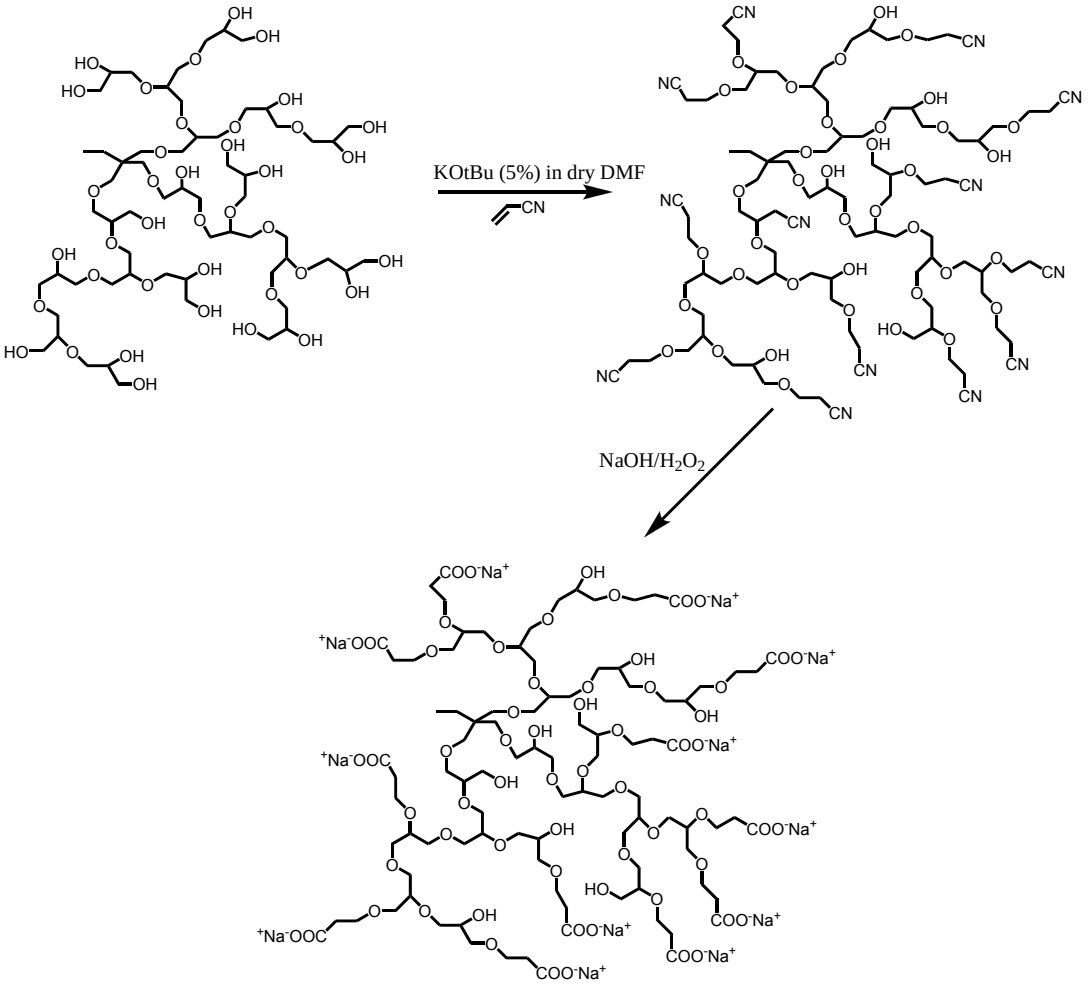

Figure 4.3 Synthesis of carboxylated hyperbranched polyglycerol via Michael addition followed by hydrolysis.

Hyperbranched polyglycerols were modified via the hydroxyl end groups by two strategies. The first method was achieved via Michael addition reaction followed by hydrolysis, as shown in Figure 4.3. Firstly, the

hydroxyl groups are converted into nitrile groups, and the obtained hbPG with nitrile groups are hydrophobic. hbPG was dried and dissolved in DMF and partially deprotonated (5% mol. of the hydroxyl groups). During addition of acrylonitrile the temperature was kept under 0°C in order to control the reaction. The reaction mixture solutions were precipitated twice from acetone solution into methanol. The products are viscous and brown.

Secondly, the nitrile groups are hydrolyzed with hydrogen peroxide in the presence of sodium hydroxide (NaOH) and the materials become soluble in aqueous solution. The hbPG with carboxylic acid groups are then precipitated in diethyl ether. The anionic hbPG with carboxylic acid groups are viscous, yellow materials. They were purified by dialysis against water.

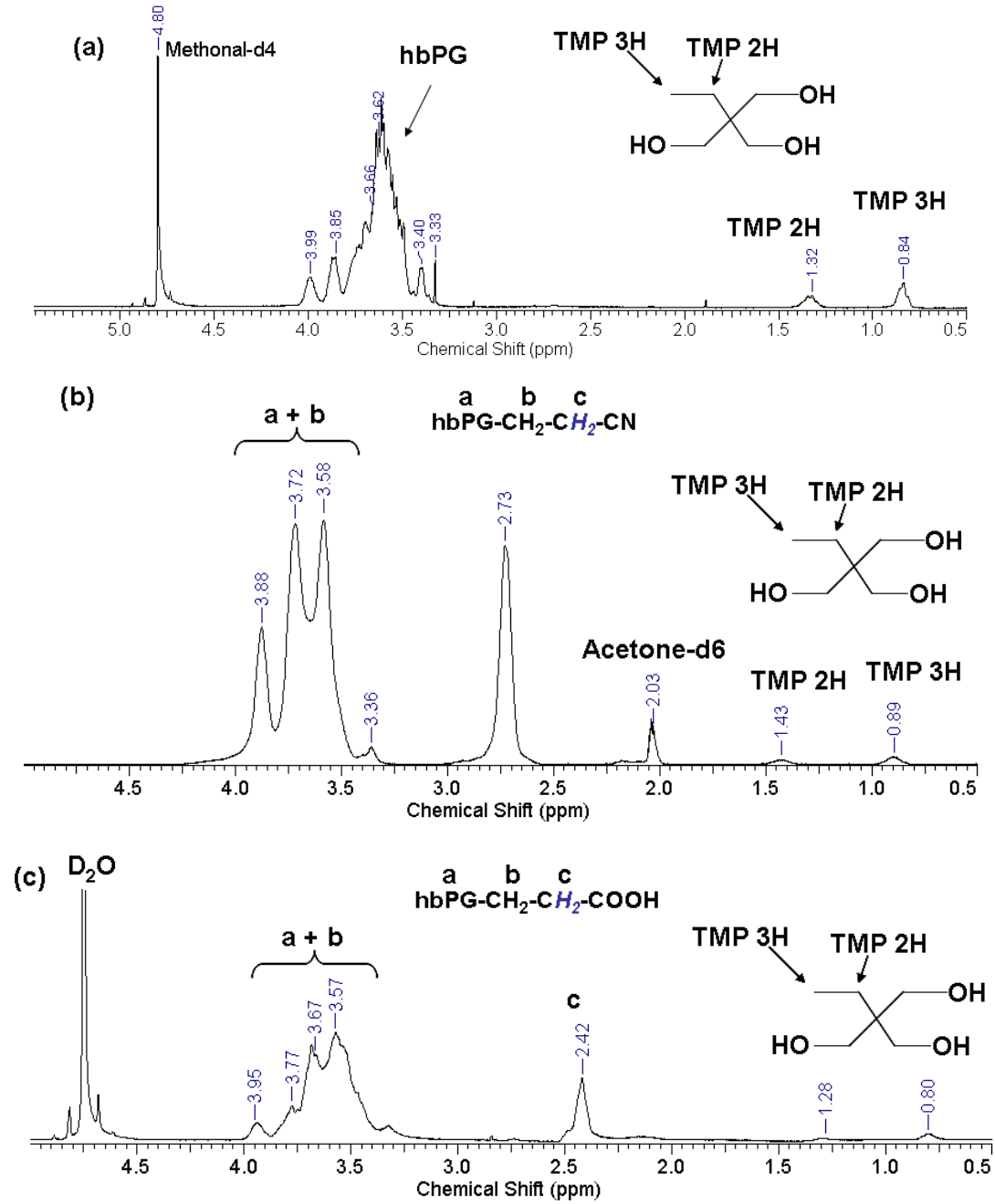

Figure 4.4 ^{1}H NMR spectra of (a) hbPG in d4-methanol; (b) hbPG-CH_2-CH_2-CN in d6-acetone; (c) hbPG-CH_2-CH_2-COOH in D_2O.

Figure 4.4 shows the ^{1}H NMR spectra of original hyperbranched polyglycerol ($hbPG_{39}$) and modified $hbPG_{39}$ with carboxylic acid groups. The signals between 3.3 and 3.9 ppm are assigned to the protons from the backbone of hbPG. The resonances at 0.8 ppm and 1.3 ppm are due to the protons from the methyl group, the methylene group of the initiator-core

TMP (1,1,1-tris(hydroxymethylpropane). After the Michael addition reaction the two protons next to the nitrile group are visible at 2.7 ppm (Figure 4.4 (b)). This signal is shifted to 2.4 ppm after hydrolysis (Figure 4.4 (c)).

Table 4.1 Characterization data of hbPG with carboxylic acid groups via Michael addition reaction followed by hydrolysis. The values have been obtained from ^{1}H NMR spectra.

Samples		hbPG		hbPG-CN		hbPG-COOH	
		Mn g/mol	OH groups	-CN groups	% Modif. of –CN	-COOH groups	% Modif. of –CN
1	$hbPG_{42}$	3000	39	37	95	20	54
2	$hbPG_{74}$	5400	74	68	92	34	50
3	$hbPG_{90}$	6600	90	76	84	38	35

A series of hbPGs with different molecular weights were functionalized by the first strategy (Table 4.1). For the sample 1 and 2, the degree of modification with nitrile groups is 95% and 92% and around 84% for the sample 3 (higher molecular weights). As expected, the degree of conversion is high and decreases as the molecular weight increases. However, the degree of modification of nitrile groups into carboxylic acid groups is low. For the sample 1 and 2, the degree of modification is 54% and 50% and about 35% for the sample 3. The reaction of the nitrile groups from the interior of the hyperbranched architecture is more difficult than of the ones present at the periphery. They are less accessible and this phenomenon is affected by the molecular weight. This modification conversion is difficult to control and require two steps to obtain the targeted products. The number of carboxylic acid groups from hbPGs is less and it might be hard for preparation of hbPG multilayers via the layer by layer deposition by electrostatic interaction. Therefore, it is necessary find an alternative way to realize the designed

degree of modification of the anionic hbPGs with elevated molecular weight for further characterization and applications.

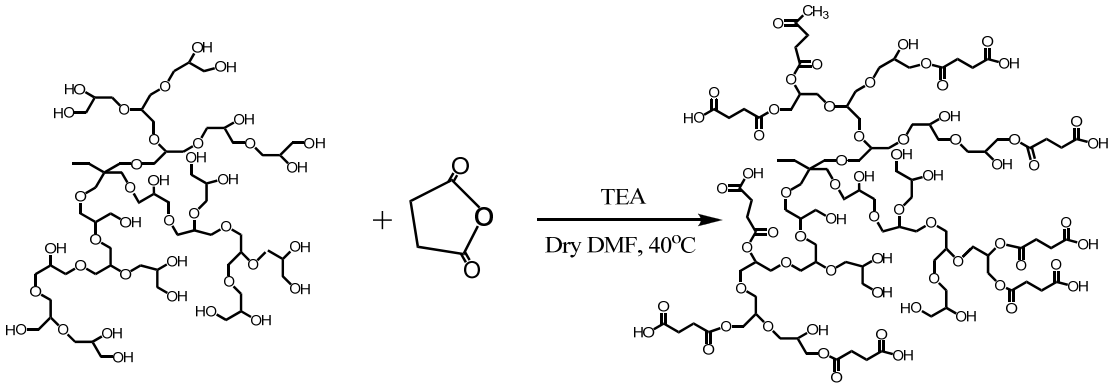

Figure 4.5 Succinate functionalization of hyperbranched polyglycerols into anionic hyperbranched polyglycerols with carboxylic acid groups.

The second strategy employed to convert hydroxyl groups into carboxylic acid groups is based on the succinate functionalization and the reaction process is shown in Figure 4.5. Hydroxyl groups in hbPG were reacted with succinic anhydride together with TEA in anhydrous DMF. After the reaction was carried out for 12h, the reaction mixture was evaporated. The residue was dissolved in distilled water and dialyzed against water for 2 days. The products are colorless paste.

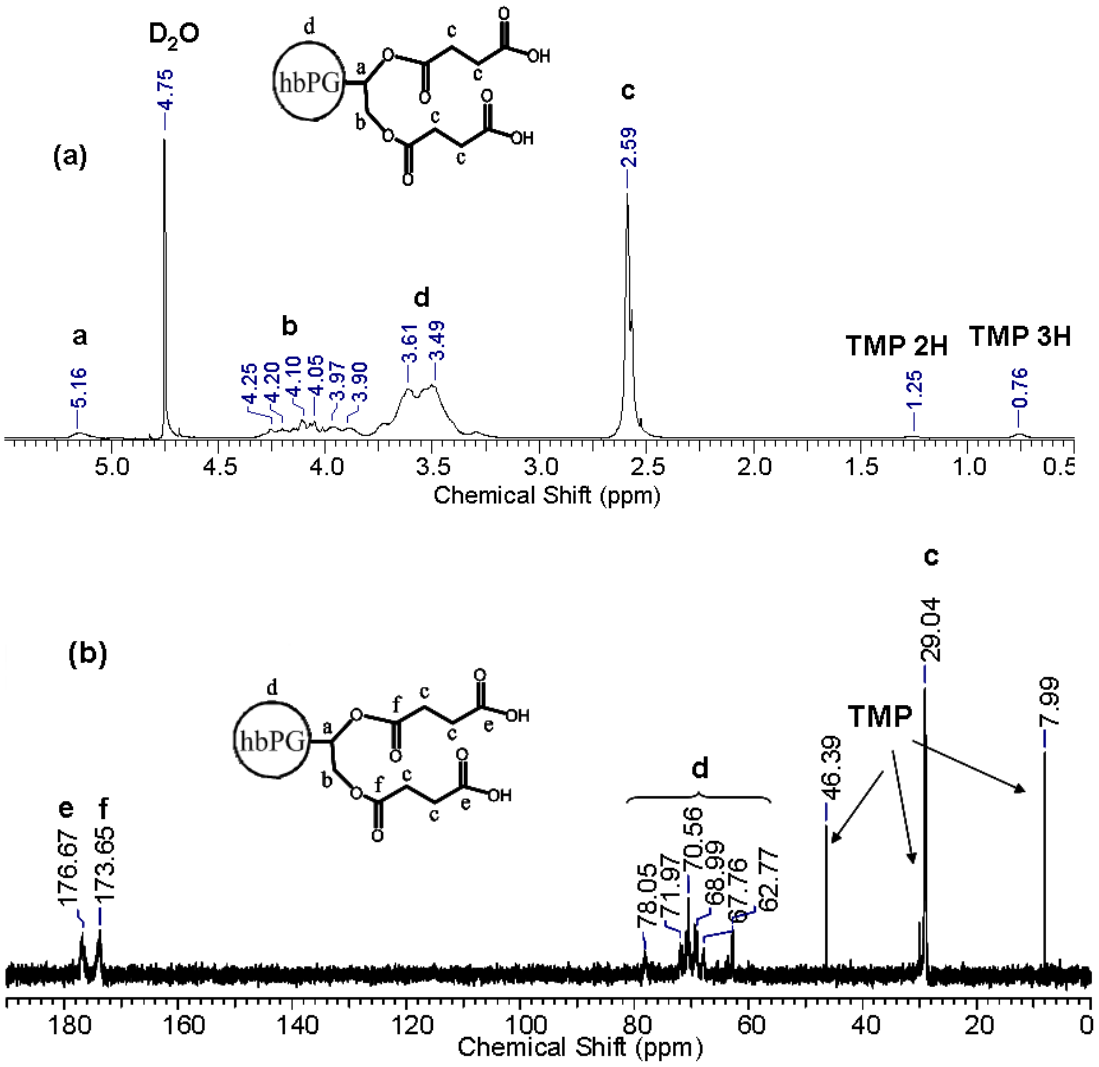

Figure 4.6 ^{1}H NMR (a) and ^{13}C NMR (b) of the modified hbPG into anionic hbPG with carboxylic acid groups via succinate functionalization.

Figure 4.6 (a) shows the ^{1}H NMR and ^{13}C NMR spectra of the modification of hbPG with DP of 39 into the carboxylic groups via succinate functionalization. Resonances at 0.76 ppm and 1.25 ppm are due to protons from the methyl group and the methylene group of the initiator-core TMP (1,1,1-tris(hydroxymethylpropane), respectively. The signals between 3.49 and 3.61 ppm are assigned to the protons from the backbone of hbPG. After the succinate functionalization, two methylene groups with four protons next to carboxylic acid groups are visible at 2.59 ppm. Meanwhile, the protons

from the methylene and methine groups next to the modified carboxylic acid chains are also visible at 3.90-4.25 ppm and 5.16 ppm, respectively.

The ^{13}C NMR spectrum of the hbPG with carboxylic acid groups (Figure 4.6 (b)) also shows the expected signals. The chemical shift at 176.67 ppm is due to the carbons from achieved carboxylic acid groups. The signal at 173.65 ppm is assigned to the carbons from the ester groups in the modified chains. Resonance at 29.04 ppm is due to the two carbons next to the carboxylic acid groups.

Table 4.2 Fundamental characterization data for the anionic hyperbranched polyglycerols.

Samples	Hyperbranched polyglycerols	Anionic hyperbranched polyglycerols			
	M_n[a],SEC (g/ mol)	M_n[b],NMR (g/mol)	M_n[c],SEC (g/mol)	M_w/M_n [a]	% Modif.
1 $hbPG_{42}(COO^-H^+)_{28}$	3000	7500	17000	1.3	66
2 $hbPG_{90}(COO^-H^+)_{52}$	6600	21000	20000	1.4	58
3 $hbPG_{433}(COO^-H^+)_{288}$	32000	62000	80000	2.0	66

[a] Determined via SEC-RI in DMF using linear PS standards. [b] Calculated from ^1H NMR spectra by comparison of repeat unit signal intensity to core signal intensity. [c] Determined via SEC-RI in $NaNO_3$ solution using pullulan standards.

A serious of hbPG with carboxylic acid groups via one–step succinate functionalization method were achieved and summarized in Table 4.2. The conversion of degree of carboxylic acid groups can achieve up to 90% (data is not shown here) and could be precisely controlled. The conversion of degree of carboxylic acid groups were designed at about 60% in order to carry out the layer by layer deposition.

4.3.2 Determination of pKa of Anionic Hyperbranched Polyglycerol Solutions

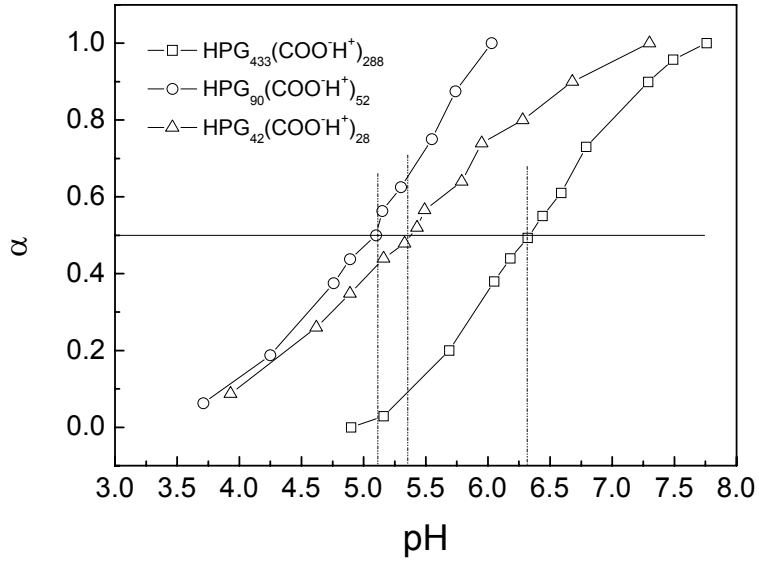

Figure 4.7 Potentiometric titration curves for anionic hyperbranched polyglycerols: $hbPG_{42}(COO^-H^+)_{28}$, $hbPG_{90}(COO^-H^+)_{52}$ and $hbPG_{433}(COO^-H^+)_{288}$.

Potentiometric titrations were carried out to determine the pKa of $hbPG_m(COO^-H^+)_n$. In all cases, the $hbPG_m(COO^-H^+)_n$s were purified by ultra filtration before titration. The pH dependence on the degree of ionization or the activity coefficient, $\alpha = C_b / C_c$, where C_b is the concentration of NaOH added to the solution and C_c is the concentration of carboxylic acid groups in solution, is depicted in Figure 4.7. The shape of the potentiometric curves does not change significantly with increasing number of carboxylic acid groups. However, such an increase results in a shift of the titration curves to higher pH values and thus to higher apparent values of pKa=6.2 for $hbPG_{433}(COO^-H^+)_{288}$, which is used as the pH at α=0.5. Since the number of carboxylic acid groups in $hbPG_{433}(COO^-H^+)_{288}$ is higher than in lower $hbPG_m(COO^-H^+)_n$s, the carboxylic acid groups are packed in close proximity

and high densities. This results in higher osmotic pressure inside the $hbPG_{433}(COO^-H^+)_{288}$ molecules and the pKa values achieved higher than others.[29]

4.3.3 Cationic Phosphorus Dendrimer/Anionic Hyperbranched Polyglycerol Multilayer Assembly

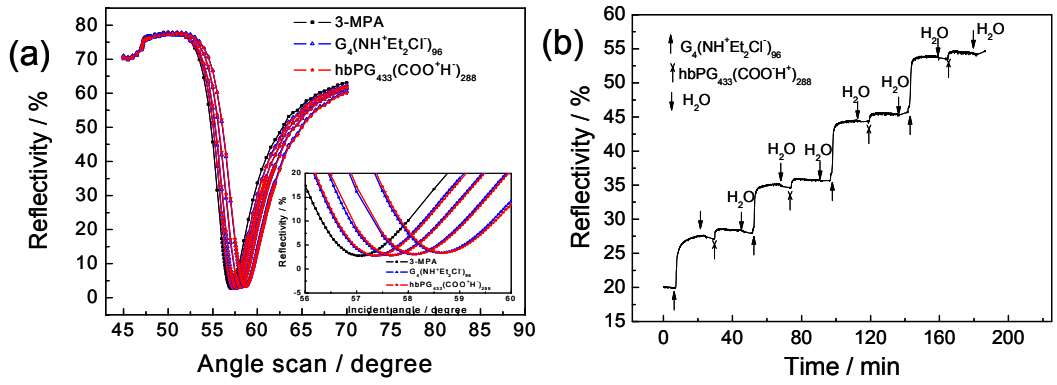

Figure 4.8 (a) Scan mode of SPR curves for the $G_4(NH^+Et_2Cl^-)_{96}$/ $hbPG_{433}(COO^-H^+)_{288}$ multilayer assembled up to 4 bilayers. pH of $G_4(NH^+Et_2Cl^-)_{96}$ solution is at 5.5 and $hbPG_{433}(COO^-H^+)_{288}$ solution is at 6.5. (b) Kinetic mode of SPR curve of reflectivity as a function of time during multilayer assembly showing 5 min rinse and 15 min adsorption intervals.

Multilayer films prepared from $G_4(NH^+Et_2Cl^-)_{96}$ / $hbPG_m(COO^-H^+)_n$ under various deposition conditions were in situ measured by SPR. Figure 4.8 is one of the examples of LbL assembly deposition which shows the 4 bilayers assembled at pH= 5.5 of $G_4(NH^+Et_2Cl^-)_{96}$ and pH= 6.5 of $hbPG_{433}(COO^-H^+)_{288}$. The incident angle of the laser light was fixed at the initial position where the reflectivity was 20%. In Figure 4.8(a), the curves represent the SPR scan mode during the rinse, following each adsorption process. During the first 5 min, the MPA gold substrate coating was exposed to the rinse solution. This is followed by a 15 min $G_4(NH^+Et_2Cl^-)_{96}$ adsorption step. A significant reflectivity shift occurs during $G_4(NH^+Et_2Cl^-)_{96}$ adsorption (from 6 to 24 min in Figure 4.8(b)), caused both by a change in refractive

index of the adsorption solution, as well as $G_4(NH^+Et_2Cl^-)_{96}$ adsorption on the surface. During the subsequent 5 min rinse step, the reflectivity decreases to a value smaller than the one obtained during the curve leveling off stage. This rinse was followed by a 15 min $hbPG_{433}(COO^-H^+)_{288}$ adsorption step and another 5 min rinse to complete the fabrication of the first bilayer. Subsequent bilayers were fabricated by iteration of this procedure. $G_4(NH^+Et_2Cl^-)_{96}$ / $hbPG_{433}(COO^-H^+)_{288}$ multilayer assembly was continued for a total of 8 layers (4 bilayers) with a 5 min rinse following each adsorption step. The following LbL multilayer depositions were carried out in analogous procedures.

4.3.4 Effect of Molecular Weight of Anionic Hyperbranched Polyglycerols on the Thicknesses of Multilayers

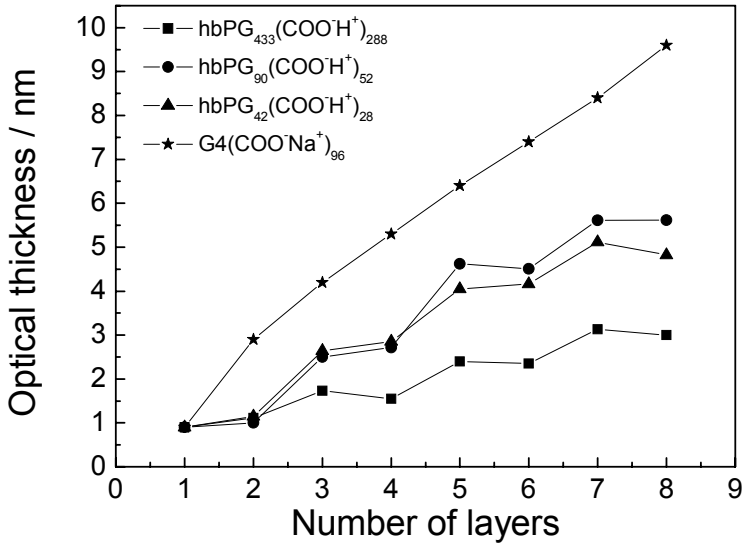

Figure 4.9 Multilayer thickness from various molecular weights of $hbPG_m(COO^-H^+)_n$ and $G_4(CH\text{-}COO^-Na^+)_{96}$ measured by SPR as a function of number of layers.

The refractive indices of the phosphorus dendrimer and $hbPG_m(COO^-H^+)_n$ of 1.5[30] are used to determine the optical multilayer thickness from the resonance angle shift data. Figure 4.9 depicts the optical

film thickness measured by SPR from $hbPG_m(COO^-H^+)_n$ ($hbPG_{42}(COO^-H^+)_{28}$, $hbPG_{90}(COO^-H^+)_{52}$ and $hbPG_{433}(COO^-H^+)_{288}$) alternating adsorption with $G_4(NH^+Et_2Cl^-)_{96}$ as a function of the number of layers. In order to compare the multilayers deposited from $G_4(NH^+Et_2Cl^-)_{96}/hbPG_m(COO^-H^+)_n$, the multilayers fabricated by the $G_4(NH^+Et_2Cl^-)_{96}/G_4(COO^-Na^+)_{96}$ was also prepared. At first glimpse, the results are surprising, since the growth of multilayers from $G_4(NH^+Et_2Cl^-)_{96}/hbPG_m(COO^-H^+)_n$ is not linear and the film thickness of each single hbPG layer is thin. Compared with the hbPG multilalyers, the growth of $G_4(NH^+Et_2Cl^-)_{96}/G_4(COO^-Na^+)_{96}$ is linear and regular. The pH of $hbPG_m(COO^-H^+)_n$ solutions is adjusted to 6.5. Under these conditions, the carboxylic groups are ionized. The pH of the $G_4(NH^+Et_2Cl^-)_{96}$ solution is fixed at 5.5. In each curve, odd numbered layers represent the thickness obtained from $G_4(NH^+Et_2Cl^-)_{96}$ adsorption while even numbered layers refer to the thickness obtained after $hbPG_m(COO^-H^+)_n$ adsorption steps. The increase of 4 bilayers of multilayer thickness is more pronounced for $hbPG_m(COO^-H^+)_n$ with low molecular weight than for the corresponding high molecular weight species. When pH is maintained at 6.5, there are more ionized carboxylate groups in $hbPG_{433}(COO^-H^+)_{288}$ molecules than in the case of the low molecular weight hbPG, which increases repulsive forces among the carboxylate groups stronger, inducing a more extended structure as a result of low film thickness. The second reason might be due to the mobility of the molecule. It was reported by Lynn et al.[31] that because the mobility of low molecular weight poly (acrylic acid) (PAA) is greater than that of higher molecular weight PAA, the thicknesses of films fabricated using lower molecular weight polymer are significantly greater than those fabricated using polymer. On the other hand, the film thickness increases more regularly in the case of $hbPG_{433}(COO^-H^+)_{288}$ compared to $hbPG_{42}(COO^-H^+)_{28}$ and $hbPG_{90}(COO^-H^+)_{52}$. The significant desorption or slow conformational rearrangement of the adsorption of low molecular of $hbPG_m(COO^-H^+)_n$

probably leads to the irregular growth of multilayers. From the curve plotted for the oppositely charged phosphorus dendrimers, it can be seen that, the thickness of a single $G_4(COO^-Na^+)_{96}$ layer is larger than that of any other molecular weight of hbPG, although the molecular weight of phosphorus dendrimer[32] is about 30,000 g/mol (smaller than that of $hbPG_{433}(COO^-H^+)_{288}$). These results demonstrates the unexpected finding that $hbPG_{433}(COO^-H^+)_{288}$ is considerably more flexible and can easily change shape during deposition and become more oblate and flattened on the surface. In addition, the growth profiles of hbPG multilayers are nonlinear as compared to the linear growth of phosphorus dendrimer multilayer. The potential influence of polydispersity of PAA on the nonlinear growth of PAH/PAA film was reported by Lynn.[31] They demonstrated that the slight but notable nonlinear increase in the growth of films fabricated using the higher polydispersity polymers. hbPGs employed in this chapter have certain polydispersity (PDI) arranged from 1.3 to 2.0. However, dendrimers are monodispersity (PDI=1.005 or 1.01). This might be the reason of the nonlinear deposition from hbPG multilayers.

4.3.5 Effect of Ionic Strength on the Thicknesses of Multilayers

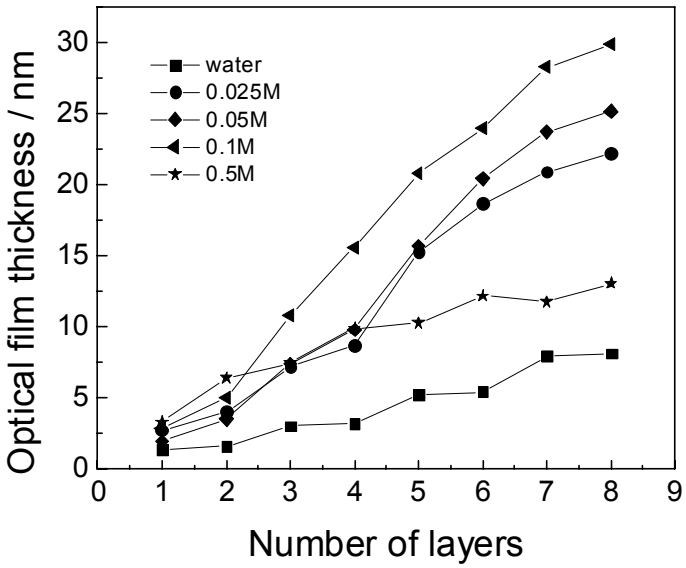

Figure 4.10 Multilayer thickness obtained from SPR data as a function of the number of layers and ionic strength of $hbPG_{433}(COO^-H^+)_{288}$.

Film thickness is subject to change when the multilayer is deposited in the presence of low NaCl concentrations due to the change of charge density of the polyelectrolyte chains.[33] The multilayers were prepared and studied by the use of a serious of molecular weights of hbPGs in the absence of NaCl. There is desorption when multilayers deposited from the small molecular weights of anioic hbPGs were rinsed. Since the charge density from the modified hbPG with carboxylic acid groups might affect the deposition of multilayers in the presence of NaCl, we employed the anionic hbPG with highest molecular weight and studied how the concentration of NaCl affected the properties of multilayer films. In this study, both $G_4(NH^+Et_2Cl^-)_{96}$ and $hbPG_{433}(COO^-H^+)_{288}$ as the adsorption pair solution were prepared at the same NaCl concentration with pH of 5.5 and 6.5, respectively. Multilayers of $G_4(NH^+Et_2Cl^-)_{96}$ / $hbPG_{433}(COO^-H^+)_{288}$ were fabricated in NaCl solutions of various concentrations from 0.025 M to 0.1 M. Thicknesses of multilayers

increased with increasing NaCl concentration which could be attributed to the screening of electrostatic charges among $G_4(NH^+Et_2Cl^-)_{96}$ and $hbPG_{433}(COO^-H^+)_{288}$ (Figure 4.10). However, a further increase of the salt concentration to 0.5 M resulted in a reduction of the film thickness. Sui et al. proposed that at high ionic strength, the thickness of polyelectrolyte multilayers can be decreased by "stripping" when one or both of the polyelectrolytes have a relatively low molecular weight (e.g. $G_4(NH^+Et_2Cl^-)_{96}$ in this case). In this process, soluble complexes of the polyanion or polycation are formed during the adsorption of the higher molecular weight component and are carried into solutions.[6 (c)(d)]

4.3.6 pH Effect on the Properties of Multilayers

The charge density of the weak polyanion is expected to be affected by changes in pH or ionic strength.[8] Here, $hbPG_{433}(COO^-H^+)_{288}$ with the highest molecular weight was studied with respect to the effects of pH and ionic strength on thickness. It was observed that the thickness of the adsorbed $hbPG_{433}(COO^-H^+)_{288}$ layer increased with lowering the pH (Figure 4.11). A decrease of the pH from 9 to 6 resulted in a 1.5 fold-increase of the film thickness (from 3 to 5 nm) for $hbPG_{433}(COO^-H^+)_{288}$. The highest multilayer thickness (9 nm) was detected at a pH of 4.5. At a pH of 9, the carboxyl groups of the dissolved $hbPG_{433}(COO^-H^+)_{288}$ are ionized. This induces an increase of repulsive forces between the charged groups along the branches of $hbPG_{433}(COO^-H^+)_{288}$ and causes the polymer to adopt a more extended conformation and to adsorb as a thinner layer. Conversely, the protonated carboxyl groups of $hbPG_{433}(COO^-H^+)_{288}$ along the polymer branches adsorb in a compact conformation at a pH of 4.5, resulting in significantly thicker multilayers.

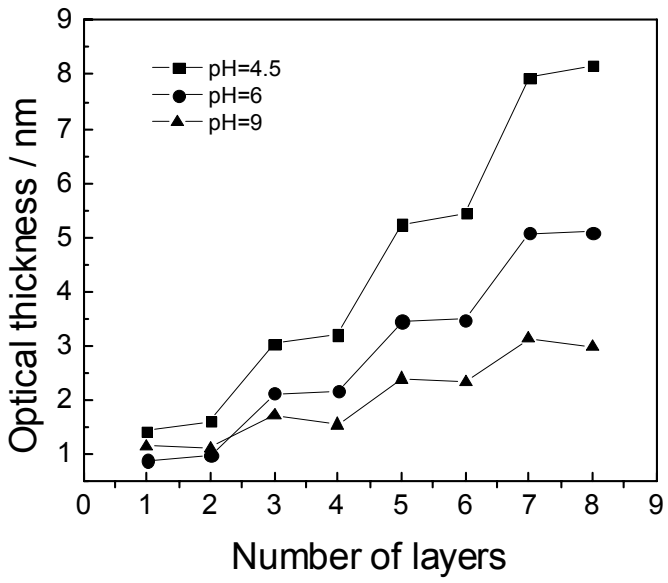

Figure 4.11 Multilayer thickness obtained from SPR data as a function of number of layers and pH of $hbPG_{433}(COO^{-}H^{+})_{288}$.

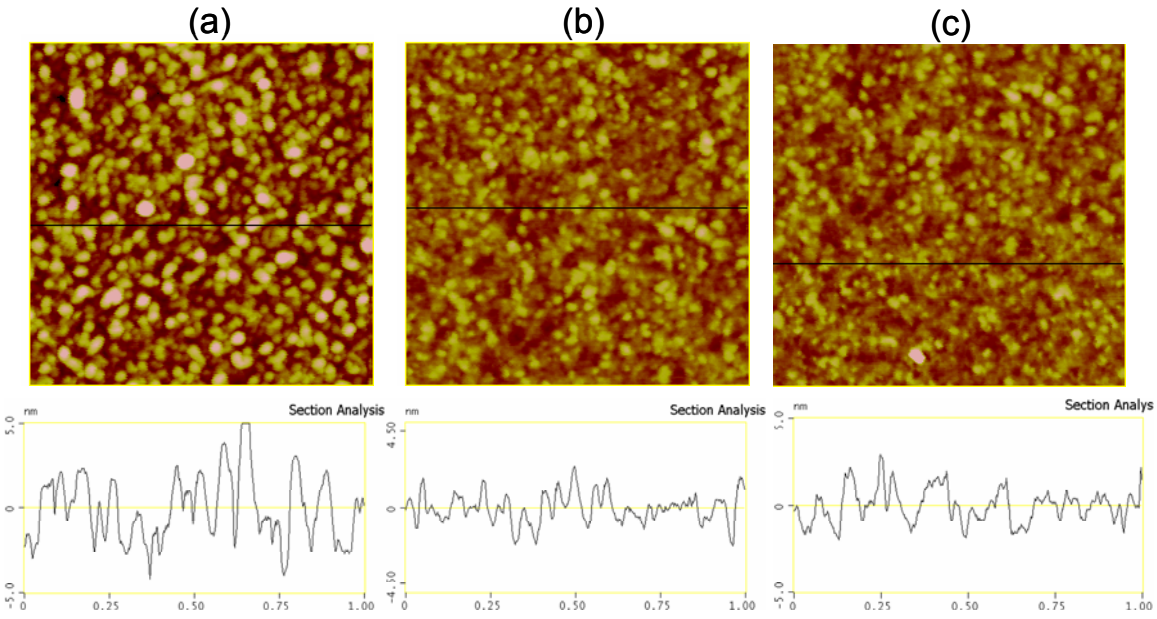

Figure 4.12 AFM images of 8- layer $G_4(NH^{+}Et_2Cl^{-})_{96}$ / $hbPG_{433}(COO^{-}H^{+})_{288}$ films deposited from $hbPG_{433}(COO^{-}H^{+})_{288}$ solutions with pH at 4.5, 6 and 9, respectively. Scan size: 1μm×1μm for all images.

Table 4.3 Roughness of air dried 8-layer films prepared from various $hbPG_{433}(COO^-H^+)_{288}$ in pH solutions, as measured by AFM.

$hbPG_{433}(COO^-H^+)_{288}$ pH	rms (nm)
4.5	2.0
6	1.0
9	1.2

It is well-known that the pH of the deposition solution is critical for a determination of the ionization degree of weak polyelectrolytes. It has been discussed above that an increase of the charge density of anionic hbPGs results in the deposition of thinner layers due to the stretched chain conformation during deposition. However, the pH of the polyelectrolyte solution not only affects the ionization of polyelectrolytes in solution but also changes the ionization of the polyelectrolyte multilayer surface onto which adsorption occurs.[34] In order to further explore the morphology effect by varying the deposition conditions, tapping mode AFM was performed on air-dried 4 bilayer films assembled from $hbPG_{433}(COO^-H^+)_{288}$ solutions with various pH values (see Figure 4.12). From the section analysis, it can be observed that the peaks on the surface at pH values of 4.5 are larger than in the case of pH= 6 and 9. It was also observed that the surface roughness takes a maximum value for the multilayer deposited at pH= 4.5 (Table 4.3) This can possibly be attributed to a more extended and thus less compact conformation due to the ionization of $hbPG_{433}(COO^-H^+)_{288}$ at pH= 6 and 9. The surface roughness from pH=9 is slightly higher than that from pH 6. However, the difference between them is not significant. We might conclude that when the multilayer surfaces are deposited from $hbPG_{433}(COO^-H^+)_{288}$ at pH value higher than its pKa, changes of surface roughness can not be

precisely differentiated by AFM. The FTIR spectra of the dendrimer/hyperbranched polymer films illustrate the molecular basis of the structural changes associated with the pH treatment (Figure 4.10). The peaks at 1740 cm^{-1} are generated by the C=O stretching of carbonyl groups both from carboxylic acid groups and ester groups from the $hbPG_{433}(COO^-H^+)_{288}$. Peaks at 1500 and 1443 cm^{-1} are generated by the asymmetric and symmetric stretching of carboxylate groups, respectively. Furthermore, an amide peak is visible at 1600 cm^{-1}, which can be attributed to the cationic phosphorus dendrimers on the multilayer films. Most of the carboxylic acid groups are protonated at pH= 4.5, as indicated by the weak COO^- peaks. As the pH increases, the intensity of C=O stretch at 1740 cm^{-1} decreases, while the intensities of the COO^- bands at approximately 1500 and 1443 cm^{-1} increase. This indicates an increase in the number of ionized COO^- groups. The transition from pH= 4.5 to 9 suggests a considerable structural change occurring at this pH range. This result corroborates the data obtained from the AFM experiments with respect to the relative changes in rms roughness under pH adjustment (Figure 4.13).

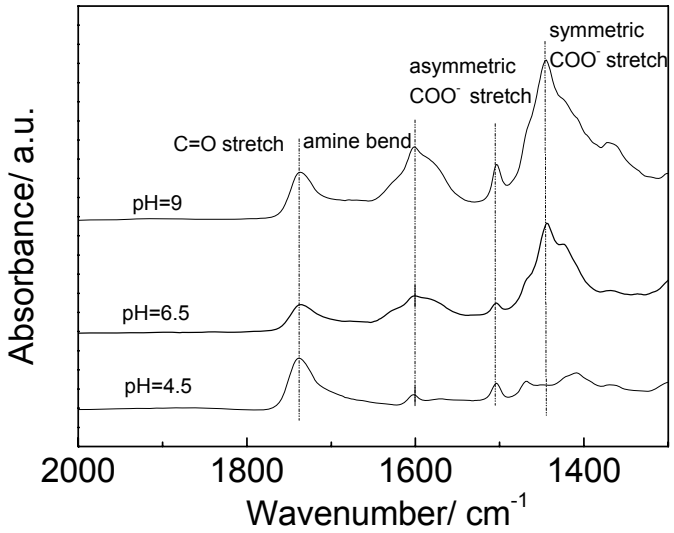

Figure 4.13 FTIR spectra of cast films multilayers of $G_4(NH^+Et_2Cl^-)_{96}$ / $hbPG_{433}(COO^-H^+)_{288}$ deposited at various pH values and FTIR band assignments are listed in Table 4.4.

Table 4.4 FTIR assignments for the multilayers

Wavenumber/ cm^{-1}	1740	1500	1443	1600
Assignment	C=O stretch	Asymmetric COO^-	Symmetric COO^-	amide

4.4 Conclusion

Multilayers of cationic phosphorus dendrimers/anionic hyperbranched polyglycerols were assembled at various deposition conditions (anionic hbPGs with different molecular weights, pH and ionic strength) and characterized using SPR, FTIR and AFM. We have demonstrated that the LbL technique can be used to tune the nanoscale structure of cationic phosphorus dendrimer/anionic hbPG surface coating by modulating simple processing conditions. Systematic investigations have shown distinct trends for the multilayer thicknesses at various deposition conditions. The multilayer thickness slightly increases with decreasing the molecular weight of the anionic hbPGs as well as with decreasing pH from 9 to 4.5. The film thickness of each single layer is thinner than expectation. Especially, the molecular weight of $hbPG_{433}(COO^-H^+)_{288}$ is larger than $G_4(COO^-Na^+)_{96}$. However, the film thickness of $hbPG_{433}(COO^-H^+)_{288}$ is even thinner than $G_4(COO^-Na^+)_{96}$. The growth of hbPG multilayer films is not linear as phosphorus dendrimer multilayer films. This might be due to the higher polydispersity from hbPG than dendrimer structures. It can be attributed from the flexible branches which make the hbPG molecules extending on the surface after the deposition. Ionic strength also affected the accessible thickness range. In the lower regime of ionic strength from 0.025 M to 0.1 M, the film thickness became higher with increasing ionic strength. Ionic strength up to 0.5 M results in thinner films. The surface morphology and structural changes of multilayer films deposited under pH treatment were

detected and confirmed by AFM and FTIR. The obtained results provide an insight to the influence of the molecular weight of anionic hbPGs, pH and ionic strength on the assembly and structure of multilayer films fabricated from different polymers with perfectly and imperfectly branched structures. Meanwhile, the pH responsively of the dendrimer-hyperbranced polymer multilayers renders these systems promising for application as pH-sensitive organic coatings in the development of biosensors and drug delivery systems.

4.5 References

1 (a) Decher, G.; Hong, J. D.; Schmitt, J. *Thin Solid Films* **1992,** *210*, 831. (b) Decher, G. *Science* **1997,** *277,* 1232.

2 (a) Nolan, C. M.; Serp, M. J.; Lyon, L. A. *Biomacromolecules* **2004,** *5,* 1940. (b) Serizawa, T.; Matsukuma, D.; Nanameki, K.; Uemura, M.; Kurusu, F.; Akashi, M. *Macromolecules* **2004,** *37,* 6531. (c) Kharlampieva, E.; Erel-Unal, I.; Sukhishvili, S. A. *Langmuir* **2007,** *23,* 175. (d) Wang, L.; Wang, X.; Xu, M. F.; Chen, D. D.; Sun, J. Q. *Langmuir* **2008,** *24,* 1902.

3 (a) Kong, W.; Zhang, X.; Gao, M. L.; Zhou, H.; Li, W.; Shen, J. C. Macromol. *Rapid Commun.* **1994,** *15,* 405. (b) Lvov, Y.; Ariga, K.; Ichinose, I.; Kunitake, T. *J. Am. Chem. Soc.* **1995,** *117,* 6117. (c) Lvov, Y.; Lu, Z.; Schenkman, J. B.; Zu, X.; Rusling, J. F. *J. Am. Chem. Soc.* **1998,** *120,* 4073. (d) Serizawa, T.; Yamaguchi, M.; Akashi, M. *Macromolecules* **2002,** *35,* 8656. (e) Johnston, A. P. R.; Read, E. S.; Caruso, F. *Nano Lett.* **2005,** *5,* 953. (f) Haynie, D. T.; Zhang, L.; Rudra, J. S.; Zhao, W.; Zhong, Y.; Palath, N. *Biomacromolecules* **2005,** *6,* 2895.

4 (a) Gao, M. Y.; Gao, M. L.; Zhang, X.; Yang, Y.; Yang, B.; Shen, J. C. *Chem. Commun.* **1994**, 2777. (b) Schmitt, J.; Decher, G. *Adv. Mater.* **1997**, *9*, 61. (c) Mamedov, A. A.; Belov, A.; Giersig, M.; Mamedova, N. N.; Kotov, N. A. *J.*

Am. Chem. Soc. **2001**, *123,* 7738.

5 (a) He, J.-A.; Valluzzi, R.; Yang, K.; Dolukhanyan, T.; Sung, C.; Kumar, J.; Tripathy, S. K.; Samuelson, L.; Balogh, L.; Tomalia, D. A. *Chem. Mater.* **1999**, *11*, 3268. (b) Huo, F. W.; Xu, H. P.; Zhang, L.; Fu, Y.; Wang, Z. Q.; Zhang, X. *Chem. Commun.* **2003**, 874.

6 (a) Wang, L. Y.; Wang, Z. Q.; Zhang, X.; Shen, J. C.; Chi, L. F.; Fuchs, H. *Macromol. Rapid Commun.* **1997**, *18*, 509. (b) Stockton, W. B.; Rubner, M. F. *Macromolecules* **1997**, *30*, 2717.

7 Wang, F.; Ma, N.; Chen, Q.; Wang, W.; Wang, L. *Langmuir* **2007**, *23*, 9540.

8 (a) Lee, H.; Kepley, L. J.; Hong, H. G.; Mallouk, T. E. *J. Am. Chem. Soc.* **1988**, *110*, 618. (b) Xiong, H. M.; Cheng, M. H.; Zhou, Z.; Zhang, X.; Shen, J. C. *Ad*V. *Mater.* **1998**, *10*, 529.

9 Shimazaki, Y.; Mitsuishi, M.; Ito, S.; Yamamoto, M. *Langmuir* **1997**, *13*, 1385.

10 (a) Anzai, J.; Kobayashi, Y.; Nakamura, N.; Nishimura, M.; Hoshi, T. *Langmuir* **1999**, *15*, 221. (b) Anzai, J.; Kobayashi, Y. *Langmuir* **2000**, *16*, 2851.

11 (a) Suzuki, I.; Egawa, Y.; Mizukawa, Y.; Hoshi, T.; Anzai, J. *Chem. Commun.* **2002**, 164. (b) Crespo-Biel, O.; Dordi, B.; Reinhoudt, D. N.; Huskens, J. *J. Am. Chem. Soc.* **2005**, *127,* 7594.

12 (a) Cai, Z.; Martin, C. R. *J. Am. Chem. Soc.* **1989**, *111*, 4138. (b) Liang, W.; Martin, C. R. *J. Am. Chem. Soc.* **1990**, *112*, 9666.

13 (a) Quinn, J. F.; Caruso, F. *Langmuir* **2004,** *20,* 20. (b) Quinn, J. F.; Caruso, F. *Macromolecules* **2005,** *38,* 3414. (c) Jaber, J. A.; Schlenoff, J. B. *Macromolecules* **2005,** *38,* 1300.

14 (a) Kharlampieva, E.; Sukhishvili, S. A. *Langmuir* **2003,** *19,* 1235. (b) Hiller, J.; Rubner, M. F. *Macromolecules* **2003,** *36,* 4078. (c) Cho, J.; Caruso, F. *Macromolecules* **2003,** *36,* 2845.

15 Antipov, A. A.; Sukhorukov, G. B.;Möhwald, H. *Langmuir* **2003,** *19,* 2444.

16 (a) Angelatos, A. S.; Radt, B.; Caruso, F. J. *Phys. Chem. B* **2005,** *109,* 3071. (b) Haynie, D. T.; Palath, N.; Liu, Y.; Li, B. Y.; Pargaonkar, N. *Langmuir* **2005,** *21,* 1136.

17 (a) Naylor, A. M.; Goddard, W. A.; Kiefer, G. E.; Tomalia, D. A. *J. Am. Chem. Soc.* **1989,** *111,* 2339. (b) Tomalia, D. A.; Naylor, A. M.; Goddard, W. A. *Angew. Chem., Int. Ed. Engl.* **1990,** *29,* 138. (c) Matthews, O. A.; Shipway, A. N.; Stoddart, J. F. *Prog. Poly. Sci.* **1998,** *23,* 1.

18 (a) Loup, C., Zanta, M. A., Caminade, A. M., Majoral, J. P.; Meunier, B. *Chem. Eur. J.* **1999,** *5,* 3644. (b) Solassol, J. ; Crozet, C. ; Perrier, V. ; Leclaire, J. ; Beranger, F. ; Caminade, A. M.; Meunier, B. ; Dormont, D.; Majoral, J. P. ; Lehmann, S. *J. Gen. Virol.* **2004,** *85,* 1791.

19 (a) Kim, D. H.; Karan, P. ; Göing, P.; Leclaire, J.; Caminade, A. M.; Majoral, J. P.; Göele, U.; Steinhart, M.; Knoll, W. *Small* **2005,** *1,* 99. (b) Feng, C.; Zhong, X.; Steinhart, M.; Caminade, A. M., Majoral, J. P.; Knoll, W. *Adv. Mater.* **2007,** *19,* 1933. (c) Hernandez-Lopez, J.; Khor, H.; Caminade, A. M.; Majoral, J. P.; Mittler, S.; Knoll, W.; Kim, D. *Thin Solid Films* **2008,** *516,* 1256. (d) Feng, C. L.; Zhong, X. H.; Steinhart, M.; Caminade, A. M.; Majoral, J. P.; Knoll, W. *Small* **2008,** *4,* 566.

20 (a) Kim, Y. H. *J. Polym. Sci. Part A: Polym. Chem.* **1998,** *36,* 1685. (b) Voit, B. *J. Polym. Sci. Part A: Polym. Chem.* **2000,** *38,* 2505. (c) Jikei, M.; Kakimoto, M. *Prog. Polym. Sci.* **2001,** *26,* 1233. (d) Yan, D.; Gao, C. *Prog. Polym. Sci.* **2004,** *29,* 183.

21 Kainthan, R. K.; Janzen, J.; Levin, E.; Devine, D. V.; Brooks, D. E. *Biomacromolecules* **2006,** *7,* 703.

22 (a) Türk, H.; Haag, R.; Alban, S. *Bioconjugate Chem.* **2004,** *15,* 162. (b) Kainthan, R. K.; Mugabe, C.; Burt, H.; Brooks, D. E. *Biomacromolecules* **2008,** *9,* 886. (c) Oudshoorn, M. H. M.; Penterman, R.; Rissmann, R.;

Bouwstra, J. A.; Broer, D. J.; Hennink, W. E. *Langmuir* **2007,** *23,* 11819.

23 Sunder, A. ; Hanselmann, R.; Frey, H.; Mülhaupt, R. *Macromolecules* **1999,** *32,* 4240.

24 Wilms, D.; Wurm, F.; Nieberle, J.; Böhm, P.; Kemmer-Jonas, U.; Frey, H. *Macromolecules*, **2009**, *42*, 3230.

25 Kim, D.; Lee, O.; Barriau, E.; Li, X.; Caminade, A. M.; Majoral, J. P.; Frey, H.; Knoll, W. *J. Nanosci. Nanotechnol.* **2006,** *6,* 3871.

26 (a) Loup, C.; Zanta, M. A.; Caminade, A. M.; Majoral, J. P.; Meunier, B. *Chem. Eur. J.* **1999**, *5,* 3644. (b) Boggiano, M. K.; Soler-Illia, G.; Rozes, L.; Sanchez, C.; Turrin, C. O. ; Caminade, A. M; Majoral, J. P. *Angew. Chem. Int. Ed.* **2000**, *39,* 4249.

27 Tziveleka, L.; Kontoyianni, C.; Sideratou, Z.; Tsiourvas, D. Paleo, C. *Macromol. Biosci.* **2006,** *6,* 161.

28 (a) Knoll, W. *Handbook of Optical Properties*; R. E. H. P. Wißmann, Ed.; CRC Press: London, New York, Tokyo **1997.** (b) Knoll, W. *Annu. Rev. Phy. Chem.* **1998,** *49,* 569.

29 (a) Connal, L. A.; Li, Q.; Quinn, J. F.; Tjipto, E.; Caruso, F.; Qiao, G. G. *Macromolecules* **2008**, *41*, 2620. (b) Plamper, F. A.; Becker, H.; Lanzendorfer, M.; Patel, M.; Wittemann, A.; Ballauf, M.; Muller, A. H. E. *Macromol. Chem. Phys.* **2005**, *206*, 1813.

30 Knoll, W.; Hick, W.; Sawodny, M.; Stumpe, J. *Makromol. Chem., Macromol. Symp.* **1991,** *48/49,* 363.

31 Sun, B.; Jewell, C. M.; Fredin, N. J.; Lynn, D. M. *Langmuir* **2007,** *23,* 8452.

32 Maszewska, M.; Leclaire, J.; Cieslak, M.; Nawrot, B.; Okruszek, A. ; Caminade, A. M.; Majoral, J. P. *Oligonucleotides* **2003**, 13, 193.

33 (a) Miller, M. D.; Bruening, M. L. *Chem. Mater.* **2005,** *17,* 5375. (b) Poptoshev, E.; Schoeler, B.; Caruso, F. *Langmuir* **2004,** *20,* 829. (c) Sui, Z. J.; Salloum, D.; Schlenoff, J. B. *Langmuir* **2003,** *19,* 2491.

34 Kim, B. S.; Gao, H.; Argun, A. A; Matyjaszewski, K.; Hammond, P. T.

Macromolecules **2009,** *42,* 368.

Chapter 5

Hyperbranched Polyglycerol Layers to Control the Non-specific Protein Adsorption

In this chapter, antifouling thin films derived from anionic hyperbranched polyglycerol (hbPG) single layers and cationic hbPG/anionic hbPG bilayers were investigated. The preparations of anionic hbPG single layers and cationic hbPG /anionic hbPG bilayers were based on the underlying self assembled monolayer (SAM) of cysteamine or 3-mercaptopropionic acid (MPA), which was deposited on gold substrates. The fabrication processes of anionic hbPG single layers or cationic hbPG/anionic hbPG bilayers were characterized by surface plasmon resonance spectroscopy (SPR). The adsorption of bovine serum albumin (BSA) and fibrinogen on a series of hbPG layers was measured and the ability to resist non specific protein adsorption was evaluated by SPR. It was demonstrated that the anionic hbPG single layer with the highest molecular weight can reduce non specific protein adsorption compared to that with lower molecular weights. All the cationic hbPG/anionic hbPG bilayers possessed excellent antifouling property. The antifouling properties of anionic hbPG single layers and the cationic hbPG/anionic hbPG bilayers were found to correlate with parameters of the molecular weight of anionic hbPG and the film thickness. The experimental results show that charged hyperbranched polyglycerol layers can strongly reduce the non specific protein adsorption and are a good alternative for the commonly used antifouling coatings.

5.1 Introduction

The design of surface coatings to prevent non specific protein adsorption is a challenge in numerous applications such as blood compatible materials, biomembranes, biosensors, and drug delivery systems.[1] Nonspecific protein adsorption degrades the performance of surfaces based diagnostic devices,

implants, catheters, or artificial organs and may have an adverse effect on the healing process for implanted biomaterials.[2] Therefore, it exists an increasing necessity to develop new materials with protein resistant properties especially in the field of biocompatible medical devices.

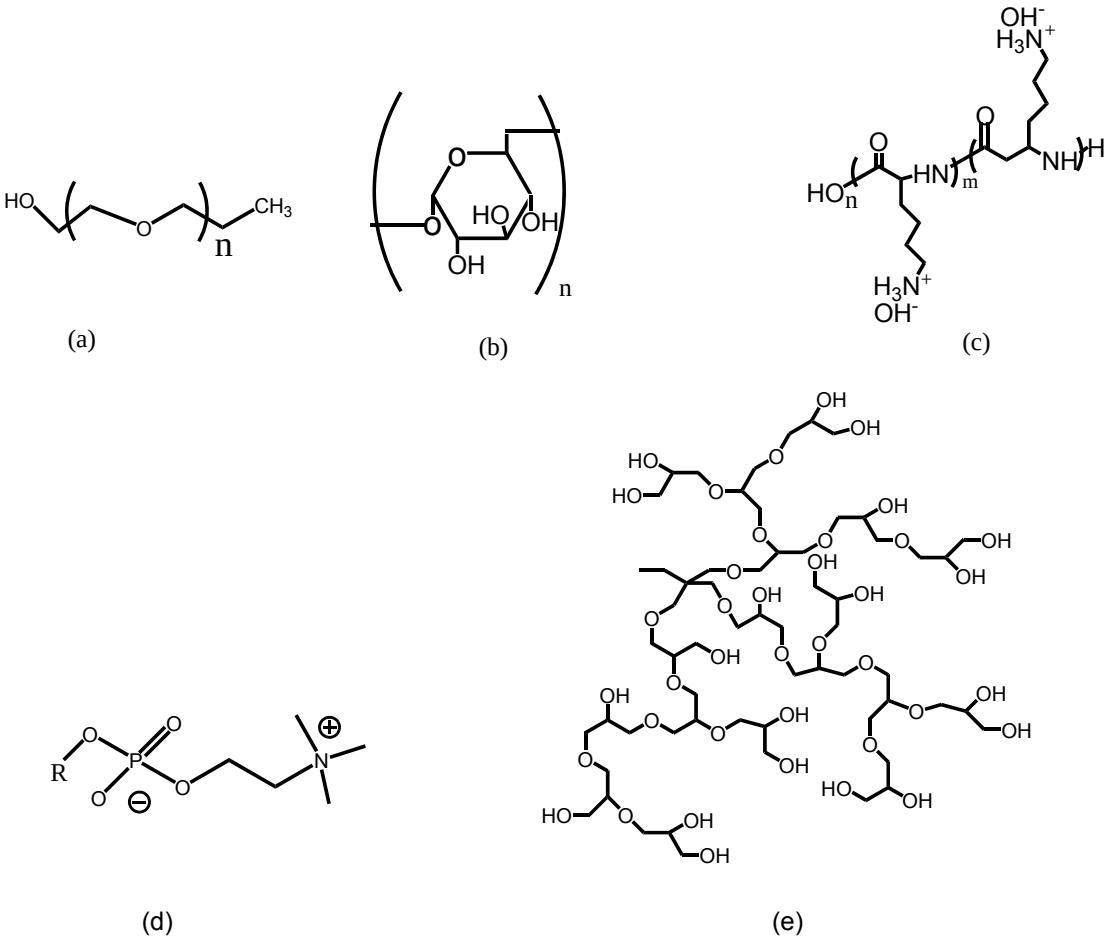

Figure 5.1 Structures of the antifouling materials (a) poly (ethylene glycol) (b) dextran (c) polyoxazolines (d) phosphorylcholine derivatives (a class of structures with zwitterionic groups) (e) hyperbranched polyglycerol.

Extensive research has been carried out in this field. A universal approach to induce antifouling characteristics is the prevention of the initial protein adsorption by surface modification with thin films of antifouling materials. The occurrence of PEG is a major step resulting from the discovery of strong resistance against protein adsorption since late 1980s.[3] Apart from

PEG-like materials, several types of antifouling materials, such as dextran derivatives,[4] polyoxazolines,[5] and polymers or oligomers with zwitterionic groups[6] (Figure 5.1), have been introduced. Although various kinds of antifouling materials have been developed, the mechanism of protein resistance of all above mentioned protein repellent surfaces has not yet been fully revealed and understood. None of the already reported mechanisms can explain the protein resistant behavior under all conditions. Since the PEG-like materials are the most commonly used materials for this area, the unusual behavior of PEG is an area of research for the past two decades and many researchers have proposed several theories based on PEG-like materials. To date, two mutually complementary points are addressed according to the study of PEG-like materials from the literatures.[7] One is well-explained by "steric repulsion": confinement of PEG chains due to protein molecules approaching the surface results in a free energy increase because of dehydration and conformational entropy decrease. On the other hand, protein resistance of self-assembled oligo(ethylene glycol) monolayer appears to be related to the ability of the ether groups constituting the SAMs to coordinated water in their interior and on their surface. This enhanced water binding aptitude leads to an overall increase of the protein resistance.[8] So far, from the series of systematic study, several factors inducing the non specific protein adsorption have been concluded such as, Van der Waals forces, electrostatic interactions, steric forces, pH, and isoelectric points.[9] Furthermore, several criteria have been revealed to design an antifouling coating. For example, it was proposed that the presence of hydrogen bond accepters, an overall neutral charge, and the hydrophilicity of the material surface are important properties for ensuring resistance to protein adsorption.[10] However, these factors are not adapted in all systems.

Furthermore, PEG-like materials also have some drawbacks including thermal instability and sensitivity toward oxidation especially under

physiological conditions.[11] Therefore, it is critical to search for the alternative materials with high stability. One alternative is the hyperbranched polyglycerol. [12] Haag et al. have demonstrated that surfaces coated with hyperbranched polyglycerols possess the ability to resist non specific protein adsorption.[13] Due to its dendritic architecture, high end-group functionality, thermal stability and a fully biocompatible [14] polyether scaffold, hyperbranched polyglycerol is currently used for various biomedical purposes.[15] Recently, Haag et al. further studied the protein resistance on glycerol dendron surfaces and oligoglycerol derivatized surfaces.[10, 16]

In general, strategies for fabrication of antifouling materials on the substrates can be classified into two categories: "grafting from" [17] or "grafting to".[18] "Grafting from" means to start a polymerization on the surface and grow the chains from the surface into the solution. "Grafting to" is realized via self assembly to fabricate the functional layer on the substrate. There are several limitations regarding these two strategies: the "grafting from" technique requires a high grafting ratio and the "grafting to" method requires special substrates, such as silver and gold substrates, which can hardly be adapted to biomaterials in the physiological environment.[19] In order to minimize the aforementioned disadvantages and optimize the experimental results, Schaaf et al. have developed a kind of antifouling film constituted of both charged groups and antifouling groups (zwitterionic groups) which was fabricated on the underlying precursor polyelectrolyte multilayer films via electrostatic interaction.[8(a),19(b)]

Based on these preliminary studies of various antifouling surfaces, we fabricated the anionic hbPG single layers and cationic hbPG/anionic hbPG bilayers with charges instead of neutral hyperbranched polyglycerol thin films and studied the antifouling property of these films. The anionic hbPG single layers and cationic hbPG/anionic hbPG bilayers fabricated by electrostatic interaction can adsorb on various kinds of underlying oppositely

charged surfaces under biological conditions. The factors affecting the antifouling properties were determined through systematically carrying out the protein adsorption on the anionic hbPG single layers and cationic hbPG/anionic hbPG bilayers with SPR.

5.2 Experimental Section

Materials and Substrates

Hyperbranched polyglycerol (hbPG) was synthesized by the procedure which has been previously reported in our group.[10] Anionic hbPGs were prepared according to the previous published paper.[20] The structure is shown in Chapter 4. Three different molecular weights of anionic $hbPG_m(COO^-H^+)_n$, where m is the degree of polymerization (DP_n) plus three, and n is the conversion of –OH groups into –COOH groups. They are $hbPG_{42}(COO^-H^+)_{28}$, $hbPG_{90}(COO^-H^+)_{52}$ and $hbPG_{433}(COO^-H^+)_{288}$, respectively. Bovine serum albumin and fibrinogen were purchased from Sigma-Aldrich (Germany) and used without further purification. Other chemicals mentioned in this chapter were all purchased from Sigma-Aldrich (Germany).

Synthesis of Cationic Hyperbranched Polyglycerol (cationic hbPG)

hbPG-Br (Mw: 3000, DPn: 39): hbPG (3 g, 0.042 mol) and triphenylphosphine (15 g , 0.06 mol) were dissolved in dry dimethylformamide (DMF) (60 ml) and cooled to 0 ^oC. 9 g (0.05 mol) N-bromosuccinimide (NBS) was carefully added in small portions, and the reaction mixture was stirred at room temperature for 12 h. DMF was removed under reduced pressure at 40 ^oC for 5 days. The residue was dialyzed by employing a 1200 cut-off membrane, and evacuated to afford compound hbPG-Br as a brown paste. The reaction yield is 21%.

^1H-NMR (300MHz, CD_3OD):

δ=0.94 ppm (br, s, C***H***$_3$CH$_2$C(CH$_2$O)$_3$-hbPG-Br, 3H), δ=1.46 ppm (br, s, CH$_3$C***H***$_2$C(CH$_2$O)$_3$-hbPG-Br, 2H), δ=2.98 ppm (br, s, hbPG-C***H***$_2$-Br, 2H), δ=3.64-3.95 ppm (br, m, hbPG backbone), δ= 4.19-4.46 ppm (br, m, hbPG-C***H***-Br, H).

hbPG-N$^+$(CH$_3$)$_3$Br$^-$ (cationic hbPG): hbPG-Br (1.1 g, 0.07 mmol) was dissolved in distilled tetrahydrofuran (THF) (200mL) at room temperature and the solution was cooled to -10 ^{o}C. Condensed trimethylamine (TMA) (20 ml) was dropwise added and the solution was stirred for 24 h while gradually warming to room temperature. Finally, the solvents were removed under reduced pressure as a slight brown paste (yield: 31%). Nitrogen content from elemental analysis: 3.75% N. Conversion of -N$^+$(CH$_3$)$_3$Br$^-$ is 23.4%.

^{1}H NMR (300 MHz, D$_2$O):

δ=0.87 ppm [br, s, C***H***$_3$CH$_2$C(CH$_2$O)$_3$-hbPG-N$^+$(CH$_3$)$_3$Br$^-$, 3H], δ=2.56-2.94 ppm [br, m, -N$^+$(C***H***$_3$***)***$_3$Br$^-$, 9H], δ=3.22-3.33 ppm [br, m, hbPG-C***H***$_2$-N$^+$(CH$_3$)$_3$Br$^-$, 2H] , δ= 3.51-3.97 ppm [br, m, hbPG backbone], δ= 4.22-4.40 ppm [br, m, hbPG-C***H***-N$^+$(CH$_3$)$_3$Br$^-$, H].

Preparation of SAMs on Gold Substrates and hbPG Layers

The freshly evaporated gold substrates were prepared prior to use by immersion the gold substrate into the 1 mM 3-MPA or cysteamine solution for 12 h. Then substrates were rinsed for 1 min with ethanol, and dried under a stream of argon. The gold substrate with modified SAM was mounted on the sample holder. Solutions of anionic hbPG and cationic hbPG were prepared in phosphate buffer solution (PBS) (pH=7.4) at a concentration of 1 mg/mL. The anionic hbPGs with different molecular weights were directly fabricated onto the underlying cysteamine SAM. Cationic hbPG/anionic hbPG bilayers were achieved by the following process. The cationic hbPG layer was fabricated on the underlying 3-MPA SAM, and then anionic hbPG

layer was adsorbed on the cationic hbPG layer by electrostatic interaction.

Protein Adsorption on the Anionic hbPG Monolayers and Cationic hbPG/ Anionic hbPG Bilayers

BSA and fibrinogen (2 mg/mL, pH= 7.4 in PBS solution) were freshly prepared prior to use. The protein solution was added on the prepared anionic hbPG single layers or cationic hbPG/anionic hbPG bilayers. The protein adsorption process was in situ measured and recorded by SPR. After the adsorption reached equilibrium, the surface was rinsed with the PBS buffer. The flow rate used for all experiments was kept at 14.2 μL/s.

The SPR spectrum was recorded before and after protein adsorption in order to determine the thickness of adsorbed layer. The refractive index for BSA and fibrinogen used here are 1.45 and 1.39, respectively.[21] The experimental results for protein adsorption in terms of surface density were calculated using de Feijter's equation:[22]

$$M = d_A \frac{n_A - n_{sol}}{d_n / d_c} \qquad \textbf{Equation 5.1}$$

Where d_A is the thickness of the adsorbed layer and dn/dc is the refractive index increment of the molecules. n_A and n_{sol} are the refractive indices of the adsorbed layer and cover media, respectively. For proteins, the dn/dc is equal to 0.182g/cm^3.[21(a)]

Surface Plasmon Resonance Spectroscopy (SPR)

The principle of SPR for the characterization of thin films has already been introduced in details in Chapter 3.

AFM Measurement

AFM images were taken on air-dried multilayer films with a Veeco Dimension 3100 setup in tapping mode. Image processing was obtained using the Nanoscope 5.12r5 software.

5.3 Results and Discussion

In general, when the single layer of polyelectrolyte is adsorbed on the surface, the surface coverage is low, resulting in a remaining influence from the underlying surface or substrate. Therefore, deposition a bilayer from the oppositely charged polyelectrolytes is necessary to minimize the influence. In this chapter, we employed the counter pairs of hyperbranched polyglycerols to build up cationic hbPG /anionic hbPG bilayers. On the other hand, the capacity to resist the non specific protein adsorption on the hyperbranched polyglycerol bilayer coatings can be compared with the anionic hbPG single layer films.

5.3.1 Synthesis of the Cationic Hyperbranched Polyglycerol

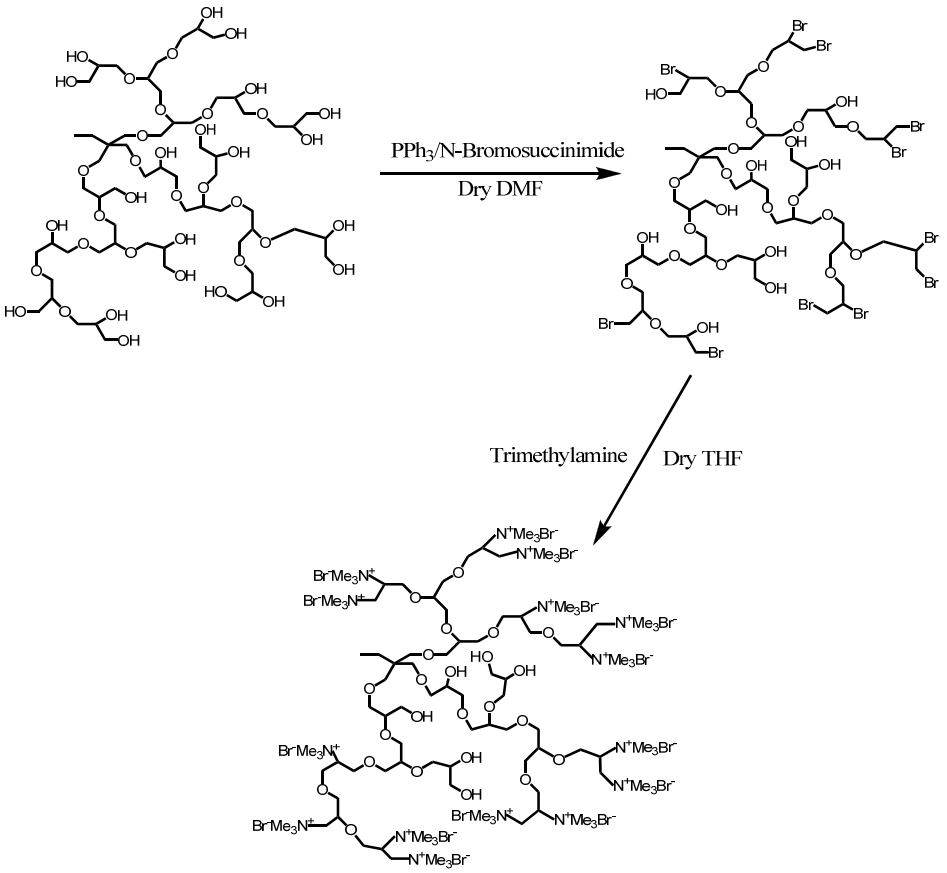

Figure 5.2 Schematic illustration of synthesis steps for the cationic hyperbranched polyglycerol from hyperbranched polyglycerol.

Figure 5.2 shows the general synthesis procedure for the cationic hyperbranched polyglycerol. The synthesis of the cationic hyperbranched polyglycerol was performed in two steps. Firstly, the hydroxyl groups are transformed into bromide. In close analogy to the synthesis method,[23] hyperbranced polyglycerol was treated with N-bromo-succinimide (NBS) and triphenylphosphine at room temperature to obtain hbPG-Br.

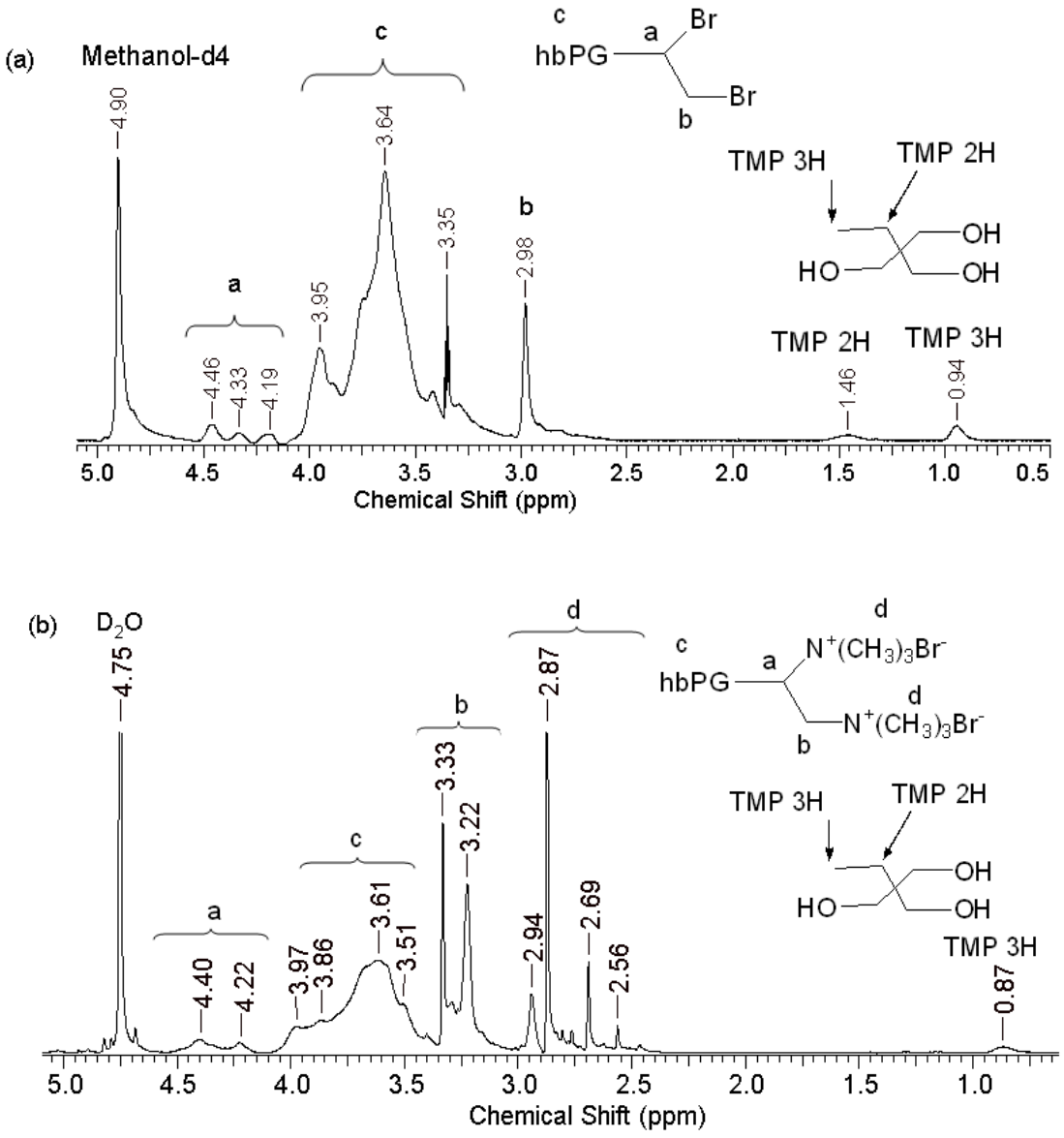

Figure 5.3 ^{1}H-NMR spectra of the hbPG-Br and hbPG-$N^{+}(CH_3)_3Br^{-}$.

^{1}H-NMR (Figure 5.3 (a)) supports the formation of hbPG-Br. Resonances at 0.94 ppm and 1.46 ppm are due to protons from the methyl group, and the methylene group of the initiator-core TMP (1,1,1-tris(hydroxymethylpropane). Signals between 3.64 ppm and 3.95 ppm are assigned to the protons from the backbone of hbPG. After the modification, the protons next to the newly achieved bromide groups are visible. The signal at 2.98 ppm is due to protons from the methylene groups next to the bromide. Resonances between 4.19 and 4.46 ppm are due to protons from the methane groups next to the bromide.

hbPG-Br was treated with trimethyl amine in dry THF. The moderate quaternary ammonium content (23%) could be achieved by elemental analysis. ^{1}H-NMR (Figure 5.3 (b)) represents the formation of hbPG-$N^+(CH_3)_3Br^-$. Resonances at 0.87 ppm is due to the protons from methyl groups of the initiator-core TMP (1,1,1-tris(hydroxymethylpropane). The signals between 2.56 ppm and 2.94 ppm are assigned to the protons from the quaternary ammonium. Resonances from 3.51 ppm to 3.97 ppm are due to the protons from the hbPG backbone. Resonances between 3.22 and 3.33 ppm are due to the protons from methylene groups next to the new modified quaternary ammonium groups. Signals from 4.22 to 4.4 ppm are assigned to methine groups next to the quaternary ammonium groups. The quaternary ammonium content is low. However, the modified positively charged hbPG can adsorb on the SAM monolayer with negative charges and the negatively charged hbPG can also adsorb on the positively charged hbPG through electrostatic interaction. These film deposition processes will be discussed below.

5.3.2 Characterization of Anionic hbPG Single Layers and Cationic hbPG/Anionic hbPG Bilayers

The aim of this chapter was to investigate how antifouling surfaces can

be obtained by the deposition of one or a small number of charged hyperbranched polyglycerols layers onto the SAMs and to study whether the negative charges from the anionic hbPG molecules affect the protein resistance. Materials used for fabrication of antifouling surfaces were hyperbranched polyglycerols with opposite charges including anionic hbPG molecules with three different molecular weights and one molecular weight of cationic hbPG. The cationic hbPG molecule was used to fabricate hbPG bilayers with the anionic hbPG by electrostatic interaction.

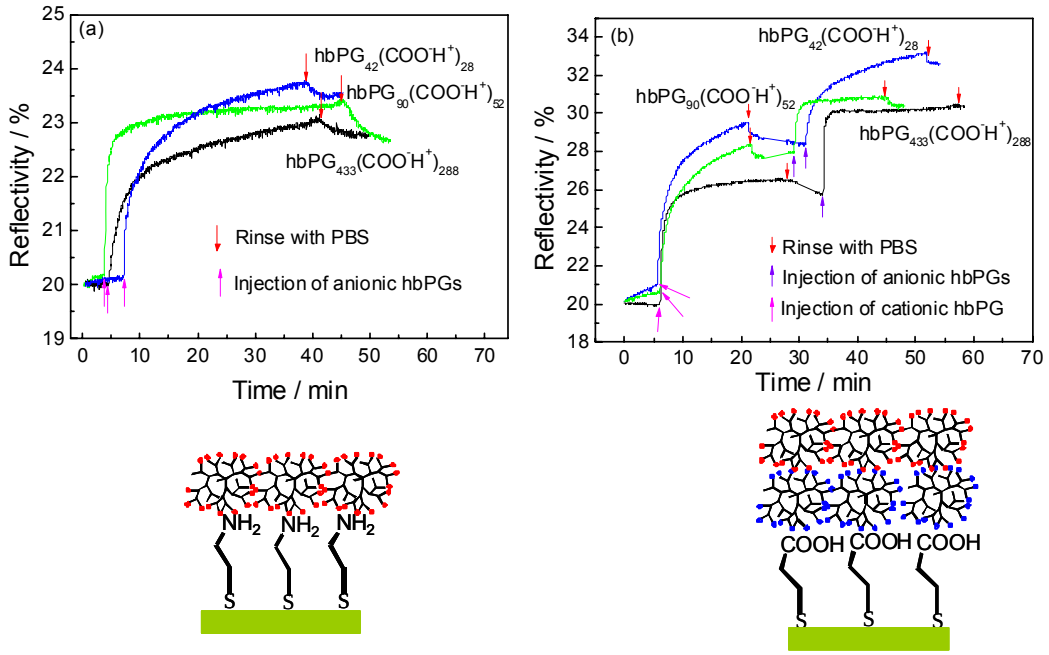

Figure 5.4 (a) Kinetic measurements of anionic hbPGs adsorption on the cysteamine SAMs. (b) Kinetic measurements of the cationic hbPG adsorption on the 3-MPA SAMs and then the anionic hbPGs adsorption on the cationic hbPG surfaces.

The antifouling films including anionic hbPG single layers and cationic hbPG/anionic hbPG bilayers deposited on 3-MPA or cysteamine precursor self-assembled monolayers were investigated by SPR. The SPR technique is extremely sensitive to the density of adsorbed molecules and the corresponding thickness of the adsorbed film. The anionic hbPGs with

different molecular weights adsorbed on cysteamine SAMs as the anionic hbPG single layers were shown in Figure 5.4(a). Far from saturation, during the early stages of this process, the rate of anionic hbPG molecules adsorption were essentially first-order in terms of anionic hbPG concentration above the cysteamine SAM surfaces, similar to Langmuir-type adsorption. Then the refractivity of the adsorbed anionic hbPG layers leveled off. The anionic hbPG layers were stable without significant desorption of anionic hbPGs upon rinsing with PBS buffer. Film thicknesses of anionic hbPG single layers are presented in Table 5.1. Thicknesses of anionic hbPGs monolayers are very thin and about 2 nm. The thinnest film with among these three single anionic hbPG layers is from $hbPG_{433}(COO^-H^+)_{288}$ with the highest molecular weight. This is unexpected. This may be attributed to the more extended structure from the high molecular weight with long branches as a result of thinner film thickness.

Table 5.1 Summary of the optical film thicknesses from the anionic hbPG single layers and cationic hbPG/anionic hbPG bilayers determined by SPR measurements. SPR results were reproducible within ±10%.

Antifouling layer	Film thickness (nm)
$hbPG_{42}(COO^-H^+)_{28}$ monolayer	2.2
$hbPG_{90}(COO^-H^+)_{52}$ monolayer	2.0
$hbPG_{433}(COO^-H^+)_{288}$ monolayer	1.8
$hbPG_{42}(COO^-H^+)_{28}$ bilayer	3.1
$hbPG_{90}(COO^-H^+)_{52}$ bilayer	3
$hbPG_{433}(COO^-H^+)_{288}$ bilayer	2.2

Similarly, the cationic hbPG/anionic hbPG bilayers (Figure 5.4(b)) were fabricated as detailed below. First, cationic hbPG layers were deposited on 3-MPA SAMs. Then, the anionic hbPG layers were fabricated on the cationic hbPG surfaces. The deposition of cationic hbPG layers and anionic hbPG layers were stable upon rinsing with PBS buffer. It is worth noting that the increase of reflectivity with the cationic layer deposition is different among these three layers, because it is hard to control the self assembled process to make all the self-assembled monolayers with the same surface coverage and film thickness. On the other hand, the adsorbed film thickness is not only simply achieved from the change of reflectivity, but also in terms of other factors, for example the refractive index of the medium. Therefore, film thicknesses of the cationic hbPG/anionic hbPG bilayers were simulated and shown in Table 5.1. The thinnest film was obtained from the cationic hbPG/anionic hbPG bilayers, in which the anionic hbPG with the highest molecular weight was present. This result is identical with that from anionic hbPG single layers.

5.3.3 Protein Adsorption on Anionic hbPG Single Layers and Cationic hbPG/Anionic hbPG bilayers

The anionic hbPG single layers and cationic hbPG/anionic hbPG bilayers were characterized by SPR. Hence, the ability of the anionic hbPG single layers and cationic hbPG/anionic hbPG bilayers to resist the non specific protein adsorption was discussed. Previously, the neutral hbPG with disulfide-functionalities has been studied and showed significant antifouling properties due to its highly flexible aliphatic polyether, hydrophilic surface groups, and a highly branched architecture.[13] However, the preparation of self-assembled monolayers depends on the novel metal layers (gold or silver) which are normally not adapted to the biosystems.[19(b)] In this chapter, layers adsorbed on the anionic hbPG single layers and cationic hbPG/anionic hbPG

bilayers with charges instead of the self-assembled monolayers. Conversely, they were deposited on the underlying self-assembled monolayers (3-MPA and cysteamine) by electrostatic interaction. There are two main reasons for employing these self -assembled monolayers as the precursor layer for the prepared anionic or cationic hbPG/anionic hbPG layers. Self-assembled monolayers are the most commonly used layers that covalently bind with the gold layers. Second, the 3-MPA and cysteamine self- assembled monolayers can provide charged surfaces for further adsorption of materials with opposite charges by electrostatic interaction. Except for the SAMs as the precursor layers, the polyelectrolyte multilayer films can also be employed.[19b] It was reported that the charge from the polyelectrolyte and thus of the surface has an influence, with a positive charge leading to stronger adsorption than a negative charge.[8a] It should be noted that the top layers for the protein adsorption employed in this chapter were the anionic hbPG layers with negative charges. The cationic hbPG layers with positive charges have not been used.

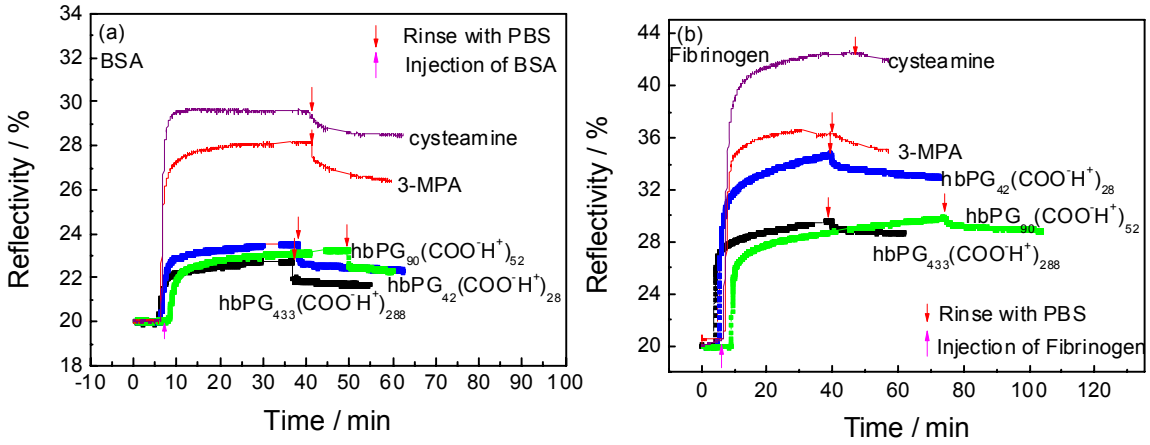

Figure 5.5 (a) Kinetic measurements of BSA adsorption on anionic hbPG single layers. (b) Kinetic measurements of fibrinogen adsorption on anionic hbPG single layers.

Two proteins are selected for the detection of non specific protein adsorption. BSA is chosen because it is the most abundant protein in blood with a characteristic size of about 3×3×8 nm^3.[8(a)] The second one is fibrinogen which is present in relatively large quantities in the blood with size of 6×9×45 nm^3 and is known to adsorb strongly on most surfaces.[8(a)] Several factors affecting the non specific protein adsorption were analyzed and the ability of protein resistant was evaluated. The adsorption of BSA and fibrinogen on the anionic hbPG monolayers was shown in Figure 5.5. The prepared anionic hbPG monolayers were brought in contact with BSA and fibrinogen solutions and the kinetic processes of protein adsorption were recorded by SPR. In contrast to the protein adsorption on the anionic hbPG monolayers, the proteins (BSA and fibrinogen) adsorption on the underlying SAMs of 3-MPA and cysteamine was also carried out and shown in Figure 5.5. BSA and fibrinogen adsorption on the SAMs of 3-MPA and cysteamine lead to higher reflectivity increase than that on the anionic hbPG single layers. Further rinsing the protein adsorption surfaces by PBS buffer, the SAMs of 3-MPA and cysteamine were not able to prevent non specific protein completely. It should be stressed that a decrease of BSA and fibrinogen adsorption on the anionic hbPG single layers deposited with an increasing molecular weight of the anionic hbPGs was found. The thicknesses of anionic hbPG monolayers measured from above are similar and about 2 nm. It means that the surface coverage of these films is similar. Therefore, the higher molecular weight of anionic hbPG molecules in the unit area can provide more aliphatic ether groups than lower molecular weight of anionic hbPG molecules. The protein adsorption in terms of surface density calculated using de Feijter's equation is shown in Figure 5.6. The surface density of BSA on the 3-MPA and cysteamine self -assembled monolayers are about 1.4 ng/mm^{-2} and 1.5 ng/mm^{-2}, respectively. In contrast, the surface density of BSA on the anionic hbPG single layers is lower and about 0.6

ng/mm^{-2}. From the above results, it can be concluded that the non specific protein adsorption could be reduced on the anionic hbPG single layers compared with the protein adsorption on the 3-MPA and cysteamine SAMs. However, these layers can not prevent non specific protein adsorption completely. This might be due to the thin film thickness of anionic hbPG single layers resulting in the lower surface coverage and the non specific protein adsorption can be affected from the underlying SAMs.

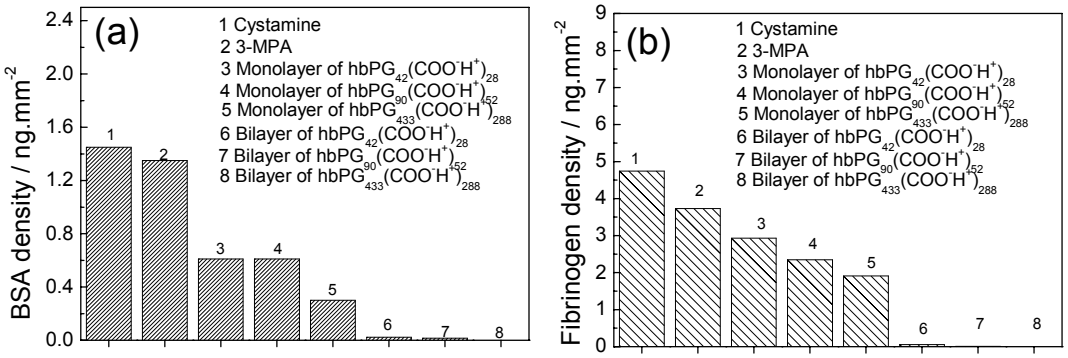

Figure 5.6 Comparison of BSA and fibrinogen adsorption on various layers including SAMs, anionic hbPG single layers and cationic hbPG/anionic hbPG bilayers.

In order to further reduce the non specific protein adsorption, even larger distances from the underlying SAMs was achieved through the fabrication the cationic hbPG/anionic hbPG bilayers via electrostatic interaction. The cationic hbPG molecule was used with one molecular weight and anionic hbPG molecules were employed with three molecular weights. The prepared cationic hbPG/anionic hbPG bilayers were brought in contact with BSA and fibrinogen solutions and the kinetic process of protein adsorption was recorded by SPR (Figure 5.7). The BSA and fibrinogen adsorption on the cationic hbPG/anionic hbPG bilayers made the reflectivity increase in a small range. When further rinsing the protein adsorption surfaces by PBS buffer, the proteins were removed and the reflectivity almost

went back to the initial level. Figure 5.6 presents the surface densities of BSA and fibrinogen adsorbed on the cationic hbPG/anionic hbPG bilayers. Surface densities of BSA and fibrinogen adsorbed on the cationic hbPG/anionic hbPG bilayers are even lower than that on the anionic hbPG single layers. These results demonstrate that the cationic hbPG/anionic hbPG bilayers can more effectively prevent the non specific protein adsorption compared to the anionic hbPG single layers.

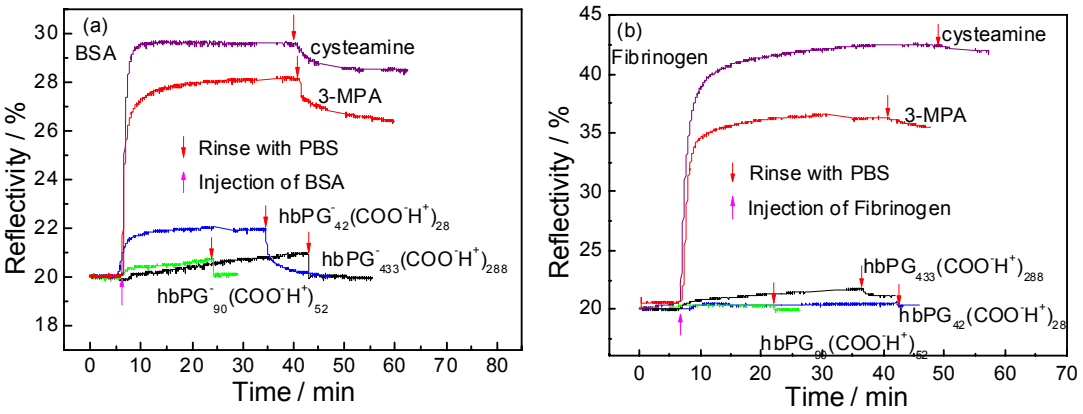

Figure 5.7 (a) Kinetic measurements of BSA adsorption on the cationic hbPG/ anionic hbPG bilayers. (b) Kinetic measurements of fibrinogen adsorption on the cationic hbPG/ anionic hbPG bilayers.

5.4 Conclusion

The present work describes the design of anionic hbPG single layers and cationic hbPG/anionic hbPG bilayers, which are able to reduce or totally prevent the non specific protein adsorption. The anionic hbPG single layers and cationic hbPG/anionic hbPG bilayers with varying molecular weights were fabricated on the underlying charged SAM surfaces through the electrostatic interaction. The deposition of anionic hbPG single layers and cationic hbPG/anionic hbPG bilayers was in-situ measured by SPR. The ability to prevent non specific protein adsorption was evaluated by SPR and the factors to affect the antifouling properties were discussed and identified.

On the one hand, the molecular weight of anionic hbPGs has an influence, with elevated molecular weights leading to the apparent resistant of non specific protein adsorption than the lower molecular weight. The higher molecular weight of anionic hbPG can provide more antifouling groups in unit area for the fabrication of the layers. The second important parameter is the charge of hbPGs. In general, protein adsorption decreases with decreasing absolute charges. However, it is not necessary to have zero charge in order to obtain protein resistant surfaces.[24] Because most of the protein with negative charges could adsorb on the positively charged surface, protein adsorption on the cationic hbPG layer was not detected in this work. All the protein adsorption was carried out on the anionic hbPG single layers and cationic hbPG/anionic hbPG bilayers with negative charges on the outermost surfaces and they can resist or reduce the non specific protein adsorption. The last parameter is the film thickness of hbPG layers. The cationic hbPG/anionic hbPG bilayers have an improved ability to prevent the non specific protein adsorption than anionic hbPG single layers. Because the film thicknesses of cationic hbPG/anionic hbPG bilayers are higher than for anionic hbPG single layers, the larger distance from the underlying charged surfaces could eliminate the non specific protein adsorption originating from the underlying charged SAM surfaces. This work provides a simple strategy to design the adsorption of anionic hbPGs single layers and cationic hbPG/anionic hbPG bilayers on the underlying oppositely charged surfaces which is adapted to biological systems and not limited to the specific substrates (Au or silver layers).

5.5 Reference

1 (a) Zhu, H.; Snyder, M. *Curr. Opin. Chem. Biol.* **2003**, *7*, 55. (b) Sharma, S.; Jonhnson, R.W.; Desai, T. A. *Biosens. Bioelectron.* **2004**, *20,* 227. (c) Evans, M.;

Sewter, C.; Hill, E. *Assay Drug DeV. Technol.* **2003,** *1*, 199. (d) Jenke, M. G.; Schreiter, C.; Kim, G. M.; Vogel, H.; Brugger, J. *Microfluid. Nanofluid.* **2007**, *3,* 189. (e) Marie, R.; Schmid, S.; Johansson, A.; Ejsing, L. E.; Nordstrom, M.; Hafliger, D.; Christensen, C. B. V.; Boisen, A.; Dufva, M. *Biosens. Bioelectron.* **2006,** *21*, 1327. (f) Noble, P. F.; Cayre, O. J.; Alargova, R. G.; Velev, O. D.; Paunov, V. N. *J. Am. Chem. Soc.* **2004**, *126*, 8092. (g) Xu, B. J.; Jin, Q. H.; Zhao, J. L. *Sens. Actuators, A* **2007**, *135*, 292. (h) Chang-Yen, D. A.; Gale, B. K. *Lab Chip* **2003,** *3*, 297. (i) Cheng, M. C.; Gadre, A. P.; Garra, J. A.; Nijdam, A. J.; Luo, C.; Schneider, T. W.; White, R. C.; Currie, J. F.; Paranjape, M. J. *Vac. Sci. Technol. A* **2004,** *22,* 837.

2 Li, L.; Chen, S.; Zheng, J.; Ratner, B.; Jiang, S. *J. Phys. Chem. B* **2005,** *109,* 2934.

3 (a) Lee, J. H.; Lee, H. B.; Andrade, J. D.; *Prog. Polym. Sci.* **1995,** *20*, 1043. (b) Jeon, S. I.; Lee,J. H.; Andrade, J. D. ; de Gennes, P. J. *J. Colloid Interface Sci.,* **1991,** *142,* 149. (c) Kenausis, G. L.; Vorös, J.; Elbert, D. L.; Huang, N.; Hofer, R.; Ruiz-Taylor, L.; Textor, M.; Hubbell, J. A.; Spencer, N. D. *J. Phys. Chem. B* **2000,** *104*, 3298. (d) Dalsin, J. L.; Lin, L.; Tosatti, S.; Vorös, J.; Textor, J.; Messersmith P. B. *Langmuir,* **2005,** *21,* 640.

4 (a) Frazier, R. A.; Matthijs, G.; Davies, M. C.; Roberts, C. J.; Schacht, E.; Tendler, S. J. B. *Biomaterials* **2000,** *21,* 957. (b) Salzman, E.; Merrill, E.; Binder, A.; Wolf, C. F. W.; Ashford, T. P.; Austen, W. G. J. *Biomed. Mater. Res.* **1969,** *3,* 69. (c) De Sousa Delgado, A.; Leonard, M.; Dellacherie, E. *Langmuir* **2001,** *17,* 4386.

5 Konradi, R.; Pidhatika, B.; Muehlebach, A.; Textor, M. *Langmuir* **2008,** *24,* 613.

6 Holmlin, R. E.; Haag, R.; Chabinyc, M. L.; Ismagilov, R. F.; Cohen, A. E.; Terfort, A.; Rampi, M. A.; Whitesides, G. M. *J. Am. Chem. Soc.* **2001,** *123,* 5075.

7 Morra, M. J. Biomater. *Sci., Polym. Ed.* **2000,** *11,* 547.

8 (a) Reisch, A.; Voegel, J. C.; Gonthier, E.; Decher, G.; Senger, B. Schaaf, P.; Mésini, P. J.; *Langmuir* **2009,** *25,* 3610. (b) Herrwerth, S. ; Eck, W. ; Reinhardt, S. ; Grunze, M. *J. Am. Chem. Soc.* **2003,** *125,* 9359.

9 Frazier, R. A.; Matthijs, G.; Davies, M. C.; Roberts, C. J.; Schacht, E.; Tendler, S. J. B. *Biomaterials* **2000**, *21*, 957.

10 Wyszogrodzka, M.; Haag, R. *Biomacromolecules* **2009,** *10,* 1043.

11 (a) Herold, D. A.; Keil, K.; Bruns, D. E. *Biochem. Pharmacol.* **1989,** *38,* 73. (b) Talarico, T.; Swank, A.; Privalle, C. *Biochem. Biophys. Res. Commun.* **1998,** *250,* 354.

12 (a)Sunder, A.; Mulhaupt, R.; Haag, R.; Frey, H. *Macromolecules* **2000**, *33*, 253. (b) Haag, R., Stumbe J., Sunder, A., Frey H., Hebel. A. *Macromolecules* **2000,** *33,* 8158.

13 Siegers, C.; Biesalski, M.; Haag, R. *Chem. Eur. J.* **2004**, *10*, 2831.

14 Kainthan, R. K.; Janzen, J.; Levin, E.; Devine, D. V.; Brooks, D. E. *Macromolecules* **2006**, *7,* 703.

15 (a) Türk, H.; Haag, R.; Alban, S. *Bioconjugate Chem.* **2004,** *15,* 162. (b) Kainthan, R. K.; Mugabe, C.; Burt, H.; Brooks, D. E. *Biomacromolecules* **2008,** *9,* 886. (c) Oudshoorn, M. H. M.; Penterman, R.; Rissmann, R.; Bouwstra, J. A.; Broer, D. J.; Hennink, W. E. *Langmuir* **2007,** 23, 11819.

16 Wyszogrodzka, M.; Haag, R. *Langmuir* **2009,** *25,* 5703.

17 Moro, T.; Takatori, Y.; Ishihara, K.; Konno, T.; Takigawa, Y.; Matsushita, T.; Chung, U. I.; Nakamura, K.; Kawaguchi, H. *Nat. Mater.* **2004,** *3,* 829.

18 (a) Ostuni, E.; Chapman, R. G.; Holmlin, R. E.; Takayama, S.; Whiteside, G. M. *Langmuir* **2001,** *17,* 5605. (b) S. Herrwerth, W. Eck, S. Reinhardt and M. Grunze, *J. Am. Chem. Soc.* 2003, *125*, 9359.

19 (a) Feng, W.; Zhu, S.; Ishihara, K.; Brash, J. L. *Langmuir* **2005,** *21,* 5980. (b) Reisch, A.; Hemmerlé, J.; Voegel, J.-C.; Gonthier, E.; Decher, G.;

Benkirane-Jessel, N.; Chassepot, A.; Mertz, D.; Lavalle, P.; Mésini, P.; Schaaf, P. *J. Mater. Chem.* **2008,** *18,* 4242.

20 (a) Tziveleka, L.; Kontoyianni, C.; Sideratou, Z.; Tsiourvas, D.; Paleo, C. M. *Macromol. Biosci.* **2006,** *6,* 161. (b) Yu, Y. M.; Wilms, D.; Kemmer-Jonas, U.; Caminad, A. M.; Majoral, J. P.; Frey, H. *In preparation.*

21 (a) Zhang, Z.; Menges, B.; Timmons, R. B.; Knoll, W.; Förch, R. *Langmuir* **2003,** *19,* 4765. (b) Voros, J. *Biophys. J.* **2004,** *87*, 553.

22 de Feijter, J. A.; Benjamins, J.; Veer, F. A. *Biopolymers* **1978**, *17*, 1759.

23 Pisula, W.; Kastler, M. Wasserfallen, D.; Pakula, T.; Müllen, K. *J. Am. Chem. Soc.* **2004**, 126, 8074.

24 Reisch, A.; Voegel, J.-C.; Gonthier, E.; Decher, G.; Senger, B.; Schaaf P.; Mésini, P. J. *Langmuir* **2009,** *25,* 3610.

Chapter 6

Detection of DNA Hybridization on Phosphorus Dendrimer Multilayer Films by Surface Plasmon Field Enhanced Fluorescence Spectroscopy

In this chapter, phosphorus dendrimers have been used to construct a highly sensitive and specific DNA sensor. The phosphorus dendrimers were assembled into a multilayer architecture on a gold substrate using a layer-by-layer (LbL) approach. The influence of the NaCl concentration on the multilayer film thickness was studied. By controlling the concentration of NaCl solution, the optimized optical thickness of single dendrimer layer was achieved. Amine terminated single strand DNA (ss-DNA) molecules were covalently immobilized on the dendrimer multilayers. The resulting system was able to selectively hybridize with complementary single strand target DNA and detected with SPFS. The limit of detection for target DNA hybridization was measured on various dendrimer multilayer platforms.

6.1 Introduction

Charged water soluble phosphorus containing dendrimers can be electrostatically assembled into different nanostructures (nanotubes and microcapsules) in a layer-by-layer (LbL) approach using curved templates (aluminum oxide[1] and colloidal particles[2]).[3] Apart from the multilayers achieved from the curved substrates, the phosphorus dendrimer multilayers on planar substrates as biosensor, nanofabrication, biomimics and tissue engineering[4] are also an interesting topic to be studied.

Biosensor is one of the most important applications of the multilayer films. Molecular recognition is central to biosensing. Since the first biosensor was developed by Updike and Hicks (1967), many biosensors have been

studied and developed.[5] As shown in Figure 6.1, a biosensor is defined as an analytical device which contains a biological recognition element immobilized on a solid surface and a transduction element which converts analyte binding events into a measurable signal.[6] Biological recognition can surpass any man-made device in sensitivity and specificity. This specificity permits very similar analytes to be distinguished from each other by their interaction with immobilized bio-molecule (antibodies, enzymes or nucleic acids).[7]

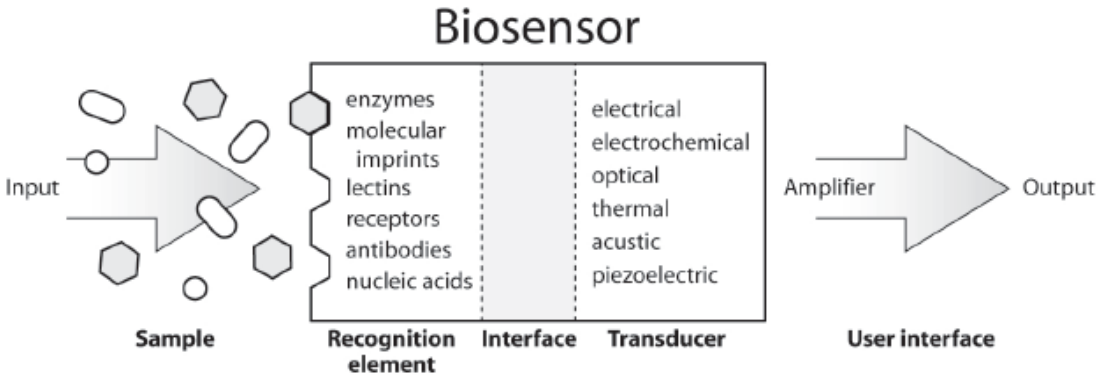

Figure 6.1 Configuration of a biosensor showing biorecognition, interface, and transduction elements.[5]

Three most frequently used surface-sensitive transduction devices are electrochemical, piezoelectric (acoustic) and optical detectors. The biosensor based on surface plasmon resonance spectroscopy technique (SPR) is one of the optical biosensors. In SPR technique, the evanescent light wave is used to excite the nearly free electron gas in a thin film (~50nm) of metal at the interface. The excitation of the resulting surface waves gives rise to a field enhancement compared to the intensity of the incident electromagnetic field.

Analytical methods incorporating fluorescence based detection are widely used in chemical as well as biochemical research due to the extraordinary sensitivity and the favorable time scale on which fluorescence

occurs. Recently surface plasmons were used as intermediate states between the incident light and the excited fluorophore in surface plasmon field enhanced fluorescence spectroscopy (SPFS).[8] Depending on the nature of the metal, the plasmon field provides the possibility to enhance the fluorescence signal up to a factor of 80. SPFS allows for probing the presence of fluorescent analytes with high sensitivity and simultaneously provides information about the sensor architecture.

An important issue in the design of a biosensor is the biochemical nature of the interfacial layer at the sensor surface, which allows specific biorecognition reactions in applications like protein chips[9] and DNA chips.[10] It was already shown that probe DNA could be immobilized on the modified substrates (e.g. gold, glass and silicon wafer) by various strategies, such as electrostatic interaction,[11] physical adsorption,[12] and covalent attachment.[13] However, most of the DNA microarrays seemed to lose their inherent activity and function in the aqueous phase when confined to a common two-dimensional (2-D) interfacial layer due to electrostatic perturbation between immobilized probes.[14]

In order to minimize these drawbacks, the lateral spacing between the immobilized biomolecules has been optimized.[15] Among various strategies used, Liebermann et al.[16] made use of the 2-D architecture of a mixed self-assembled monolayer (SAM) of a biotinylated thiol derivative and a short-chain hydroxy-terminated thiol assembled on Au substrates generating a binding matrix to detect DNA hybridization. The mixed SAM provides a reduced density of functional groups, which significantly avoids the electrostatic perturbation and shows better performance for the DNA microarray compared to the surface-active materials without the density control. However, they could not ensure regular spacing between the surface-immobilized DNAs, because statistics govern the lateral distribution and thiols can still move around on gold. In addition, similar molecules tend

to associate closely to form aggregates, [17] which can lead to a reduced activity for recognition of biomolecules.

To alleviate these drawbacks, the deposition of three-dimensional (3-D) architectures onto solid substrates as an alternative has received increasing attention.[18] Plasma polymer networks synthesized by plasma polymerization exhibit a 3-D structure, and reactive sites to an approximate depth of 40 nm were shown to participate in the DNA immobilization reaction.[19] Other 3-D polymer based systems[20] were also used in order to overcome the intrinsic limitations of 2-D platforms mentioned before. This included hyperbranched polymers,[21] polymer brushes,[22] hydrogels,[23, 24, 25, 26] and dendrimers.[27]

Considering their application for biosensors, dendrimers have shown significant improvements for the detection of DNA hybridization. Dendrimers could be used as linkers between the substrate and probe DNA[28] to elevate the surface coverage for the immobilization of probe DNA molecules. Benters et al. [29] reported that fourth generation PAMAM (polyamidoamine) dendrimers grafted onto glass slides afforded high surface homogeneity and good stability as DNA microarrays. Majoral et al.[30] described the use of neutral phosphorus dendrimers bearing aldehyde function deposited on glass slides as DNA microarrays which showed 2-fold higher sensitivity than other available DNA microarrays.

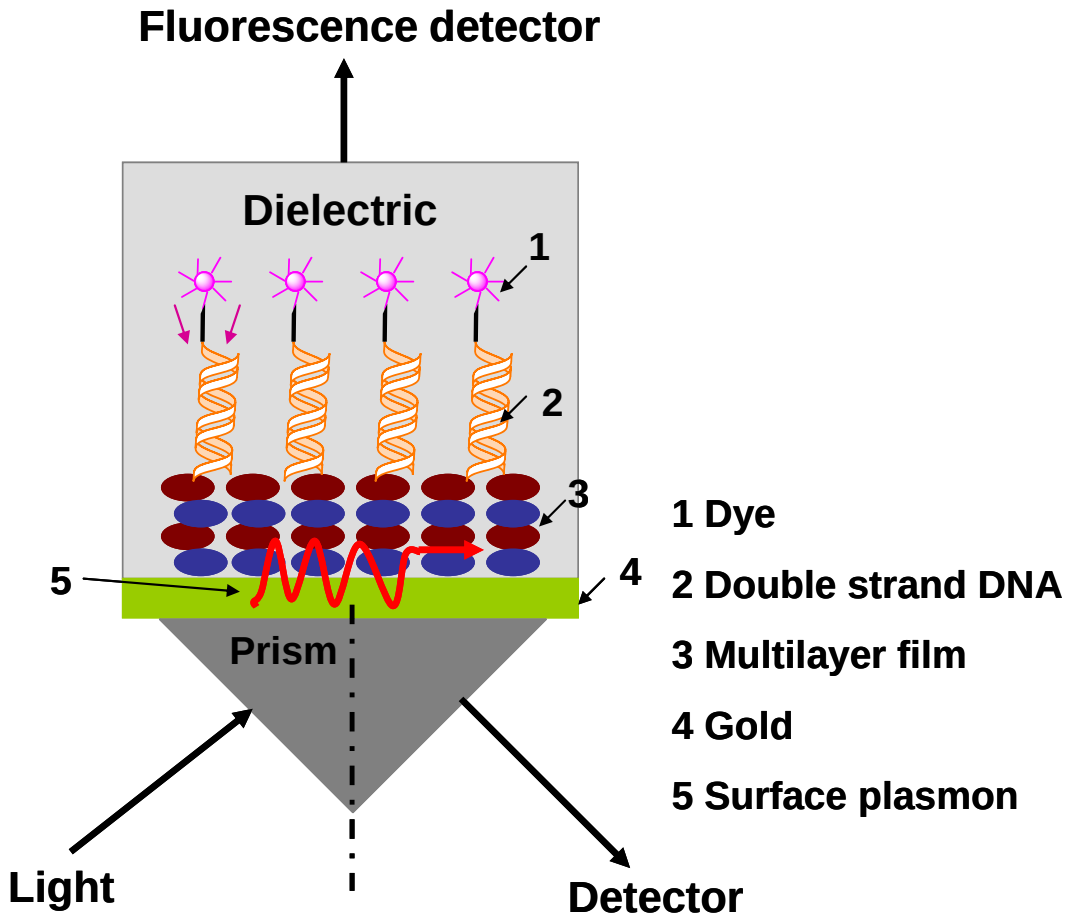

Figure 6.2 Schematic drawing of SPFS DNA biosensor.

In this work, we used SPFS to study the phosphorus dendrimer multilayer based DNA biosensor. The schematic illustration of the SPFS DNA biosensor was shown in Figure 6.2. Additionally, the influence of the presence of NaCl in solution was investigated and the conditions for multilayer construction were optimized. The multilayer growth and the immobilization of probe DNA molecules were detected by SPR. Furthermore, we employed SPFS to detect DNA hybridization processes on multilayer films. This is, to our knowledge, the first DNA hybridization process on phosphorus dendrimer multilayer surfaces detected by SPFS. Multilayers deposited by the LbL technique can not only be adsorbed on most of the commonly used substrates (gold, silicon wafer, glass, colloidal particles, etc.),

but make the solid substrate biocompatible.[9] Our group has used this sensitive technique to characterize the interactions of oligonucleotides and proteins on planar surface matrices, to detect free prostate-specific antigen and to analyze PCR product using a peptide nucleic acid (PNA) probe.[31] In our work, DNA hybridization was studied and the limit of detection for hybridization was evaluated on different numbers of dendrimer multilayer films.

6.2 Experimental Section

(1) Reagents and Chemicals

The synthesis of oppositely charged phosphorus dendrimers used here has been described in the papers published earlier.[32] The chemical structures of polycationic and polyanionic phosphorus dendrimers have been introduced in Chapter 4. Other chemicals were all purchased from Sigma-Aldrich (Germany) and used without further purification. The water used in all experiments was prepared in an ultra purification system and had a resistivity of 18.2 MΩcm.

All ss-DNA molecules were purchased from MWG Biotech, Ebersberg, Germany. The sequences chosen in this work were:

Probe DNA: 5′-NH_2-TTT TTT TTT TTT TTT TTT TTT TTT TTT TTT TGT ACA TCA CAA CTA-3′

Target DNA:

Complementary (MM0) 3′-ACA TGT AGT GTT GAT-Cy5-5′

One mismatch (MM1) 3′-ACA TGC AGT GTT GAT-Cy5-5′

Two mismatches (MM2) 3′-ACA TGC ACT GTT GAT-Cy5-5′

(2) Surface Modification

The substrates used throughout this work were LaSFN9 glass slides (Hellma Optik, Jena, Germany) coated with 50 nm gold by electrothermal evaporation (Edwards Auto 305). The gold surfaces were modified by a

self-assembled monolayer of 3-mercaptopropionic acid (3-MPA) (5×10^{-3} M in ethanol, at least 6 h immersion at room temperature), followed by rinsing with water. The first positively charged $G_4(NH^+Et_2Cl^-)_{96}$ layer was deposited on the MPA-modified substrate for 20 min, then the sample was thoroughly washed with water in order to remove excess of dendrimer. The first negatively charged $G_4(CH\text{-}COO^-Na^+)_{96}$ layer was deposited onto the first layer $G_4(NH^+Et_2Cl^-)_{96}$ in the same way. The deposition of the two oppositely charged dendrimers as a double layer was repeated until the desired number of bilayers was obtained. The terminal layer was always composed of negatively charged carboxyl groups which were activated by 1-ethyl-3-(3-dimethylaminopropyl) carbodiimide (EDC) and N-hydroxysuccinimide (NHS) for 30 min. The surface immobilization reaction is depicted in Figure 6.3. Ultimately, the probe DNA molecules with amino modified groups were covalently bound on the surface.

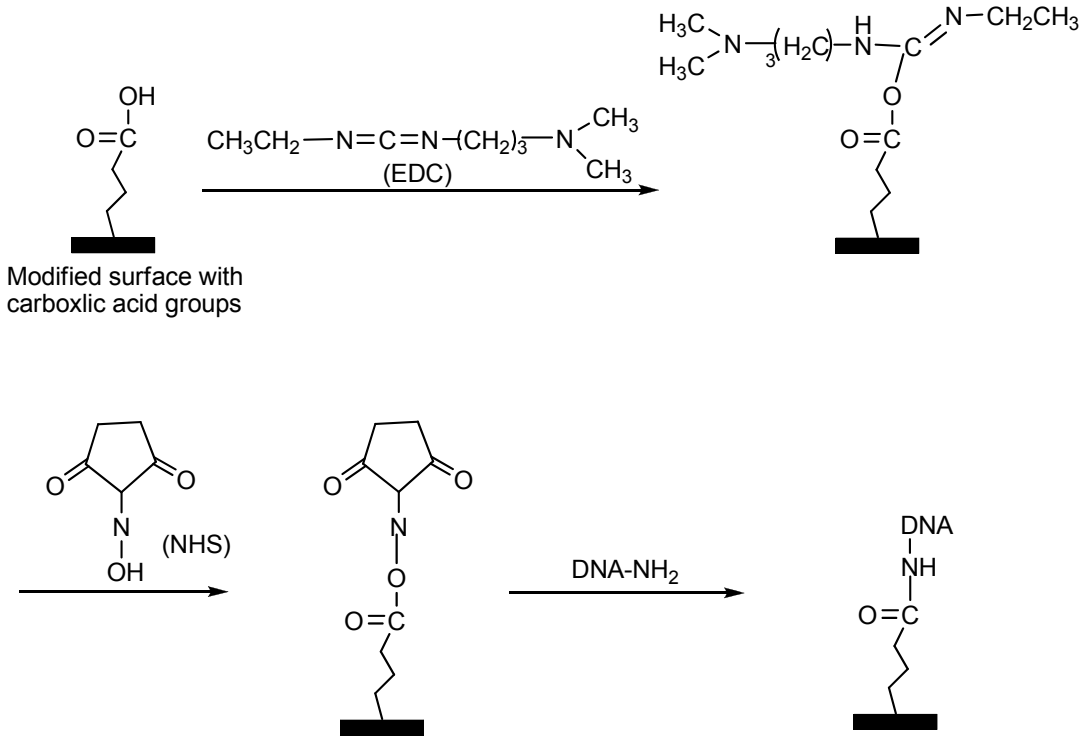

Figure 6.3 Schematic illustration the reaction of the activation of surface with carboxylic groups and immobilization of the DNA molecules with amine groups on the activation surface.

(4) Instruments

The tailor made SPR and SPR combined fluorescence (SPFS) setups were used for the LbL deposition and DNA immobilization processes in real-time. Their theory backgrounds were introduced in Chapter 3.

6.3 Results and Discussion

The approach to generate a biosensor matrix suitable for immobilizing amino-modified oligonucleotides and DNA hybridization is outlined in Figure 6.4.

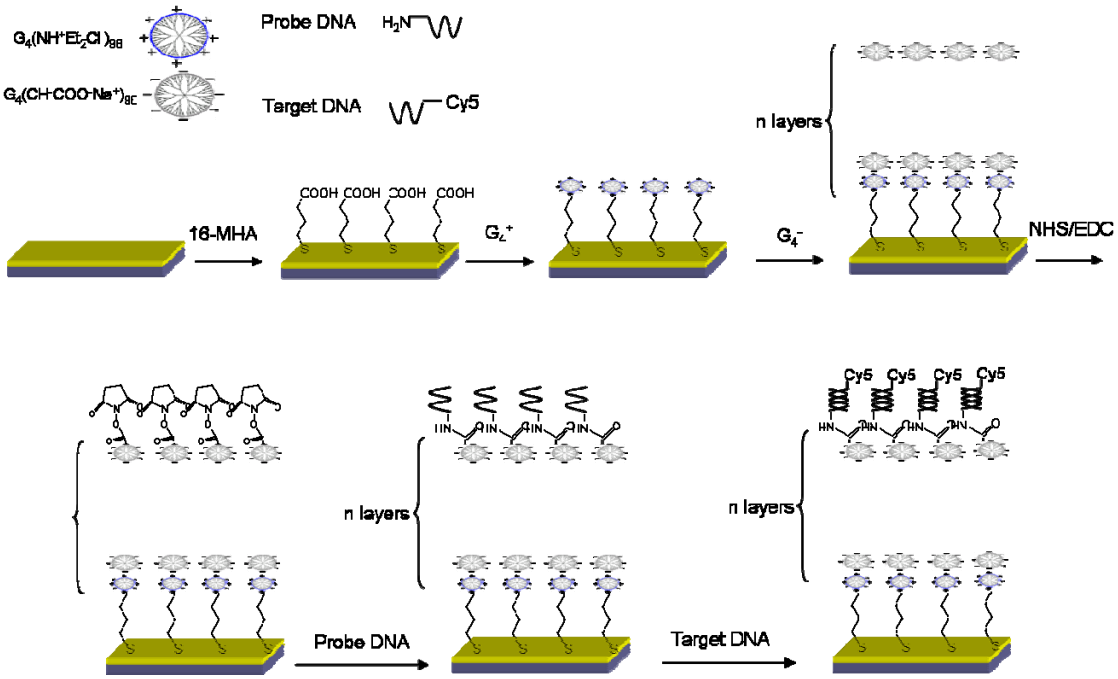

Figure 6.4 Schematic representation of the general procedure for probe DNA immobilization and hybridization. (a) Gold coated glass substrate. (b) 3-MPA modified gold substrate. (c) First $G_4(NH^+Et_2Cl^-)_{96}$ layer was deposited on the 3-MPA modified gold substrate. (d) $G_4(CH^-COO^-Na^+)_{96}$ layer was adsorbed on the first $G_4(NH^+Et_2Cl^-)_{96}$ layer and the n layers were fabricated using the same procedure. (e) The outermost layer with carboxyl groups was activated by NHS/EDC. (f) Probe DNA with amino groups was immobilized on the outermost layer. (g) DNA hybridization with target DNA was carried out on the probe DNA attached layer.

6.3.1 Phosphorus Dendrimer Multilayer Assembly in the Absence of NaCl

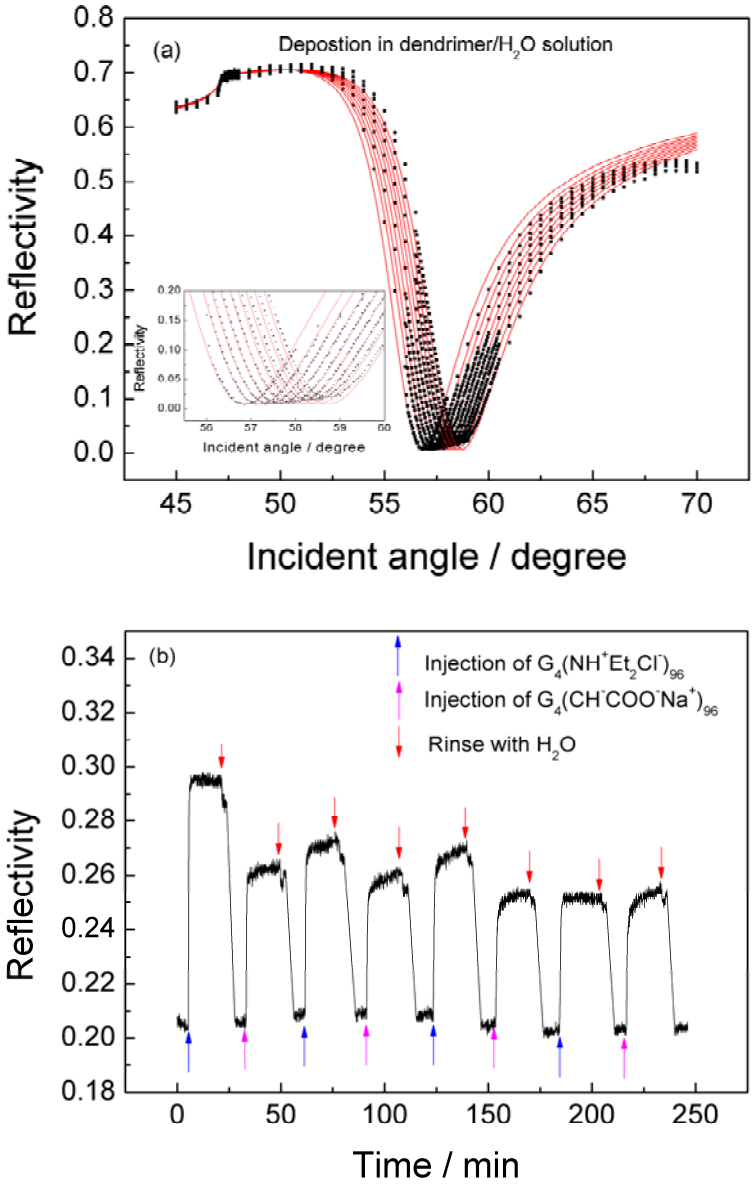

Figure 6.5 Scan mode (a) and kinetic mode (b) SPR spectroscopy showing the consecutive deposition of oppositely charged dendrimers up to 4 bilayers in H_2O. After each layer deposition, the incident angle was fixed at the position with reflectivity of 0.2 on the left of the scan curve to monitor the next layer deposition process in the kinetic mode.

Figure 6.5(a) shows the scan mode of consecutive deposition of $G_4(NH^+Et_2Cl^-)_{96}$ and $G_4(CH\text{-}COO\text{-}Na^+)_{96}$ in H_2O. A regular angular shift of the resonance angle with the number of layers is observed in Figure 6.5(a). The

resonance angular shifts from 56.8° to 58.7° after depositing 4 bilayers (zoom in curves from Figure 6.5(a)) and the resulting kinetic mode SPR curves are shown in Figure 6.5 (b). The incident angle after each layer deposition is fixed at the position (reflectivity at 0.2 on the left side of the angle scan curve) where the measured scan curve exhibits a linear slope. It shows that the addition of each layer leads to a regular increase of the resonance angle. The accumulated growth shift of resonance angle was converted to the geometrical film thickness by assuming a refractive index of 1.5[33] for dendrimers and the simulated thickness of each layer is about 1.1 nm. The film thickness is very thin compared with the size of the phosphorus dendrimer in solution.[30] However, the optical thickness measured by SPR is an optical thickness which is influenced by the factors such as refractive index and surface coverage or surface densities of the adsorbed molecules. The thinner dendrimer thickness might due to the low surface density or collapsed structure.

6.3.2 Effect of Concentration of NaCl on the Phosphorus Dendrimer Multilayer Thickness

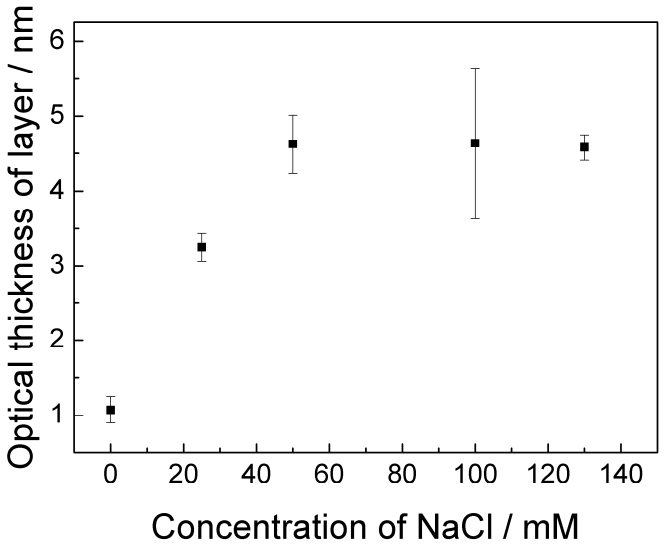

Figure 6.6 Dependence of the optical thickness of a dendrimer monolayer on the NaCl concentration.

The prepared multilayers can be employed as the platform for DNA biosensing. Hence, probe DNA molecules can be immobilized on the multilayers for DNA hybridization. In this work, because the SPFS was employed as the tool to detect DNA hybridization, the target DNA molecules need to be labeled with fluorescent dyes for the measurement. Gold slides are the fundamental substrates used for SPFS experiment. However, gold is a normal quencher for fluorescent dyes. In order to reduce the fluorescence losses due to the gold-induced quenching, a large distance (larger than 7 nm, Förster radii[9]) between the binding sites and gold surface is required. The strategy employed here is to add monovalent salt (e.g., sodium chloride). Adding NaCl to polymer solutions can promote the adsorption process and an increased thickness of polyelectrolyte multilayers can be expected.[34] In this work, NaCl was also used during the dendrimer multilayer deposition process. Here, film thickness was studied as a function of the NaCl concentration (Figure 6.6). The optical thickness of an average layer increased with concentration of NaCl. For NaCl concentration above 50 mM the optical thickness of dendrimer layer reaches a plateau value of 4.5 nm. The next experiments were all based on this optimized concentration of NaCl to fabricate dendrimer multilayers for the further study.

6.3.3 Phosphorus Dendrimer Multilayer Assembly in the Optimized Concentration of NaCl

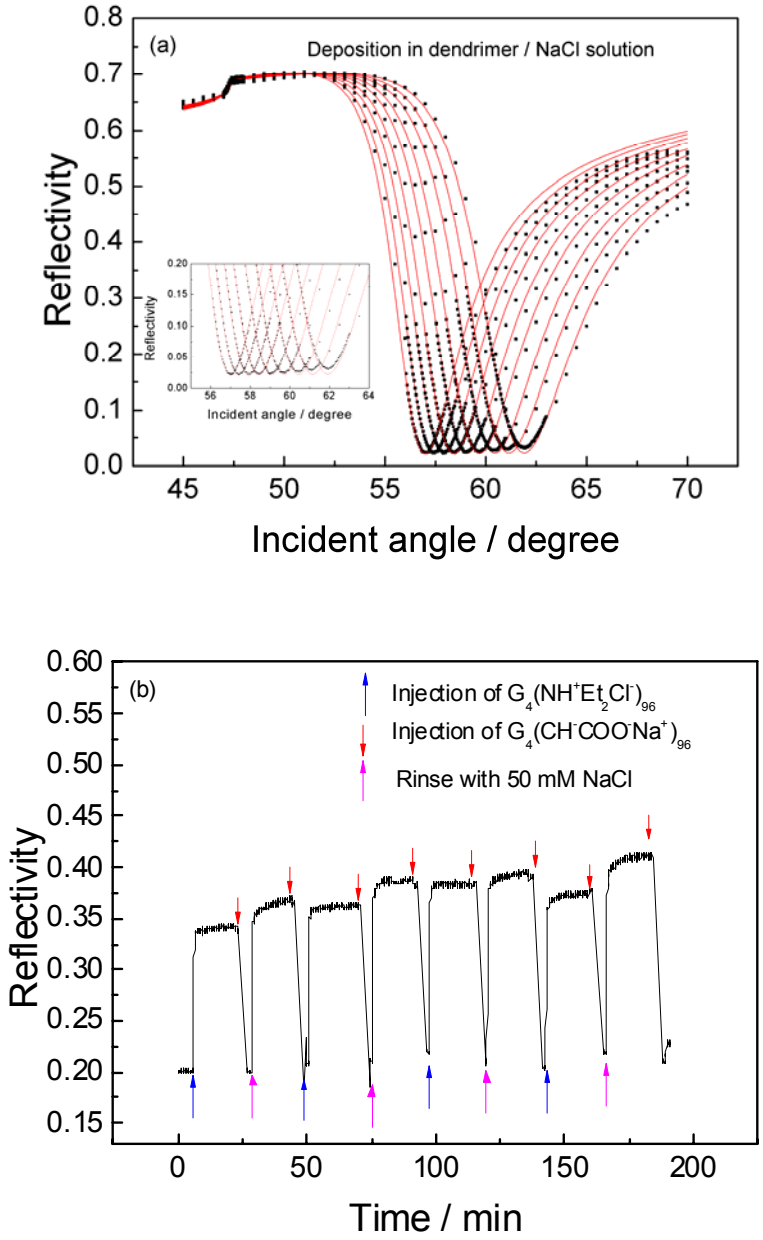

Figure 6.7 Scan mode (a) and kinetic mode (b) SPR spectroscopy showing the consecutive deposition of oppositely charged dendrimers up to 4 bilayers in 50mM NaCl solution. After each layer deposition, the incident angle was fixed at the position with reflectivity of 0.2 (on the left).

The stepwise formation of dendrimer multilayer exhibited a regular shift of resonance angle from 56.9 °- 61.9° by depositing 4 bilayers in 50 mM NaCl

solution, as demonstrated by scan mode SPR (Figure 6.7 (a)). The simulated thickness of each layer is about 4.5 nm. The alternating deposition of dendrimer multilayer was monitored by the kinetic mode SPR, as shown in Figure 6.7 (b). Compared with the dendrimer deposition in the absence of NaCl, a larger reflectivity increase was obtained in the presence of NaCl from the curve of the kinetic mode SPR. These results suggest that the deposition in the presence of NaCl can increase the optical thickness of dendrimer layer because salt could screen the electrostatic charges resulting in a more compact dendrimer structure. Furthermore, it results in a higher density of dendrimer molecule in the deposited monolayer with a concomitantly higher thickness. Figure 6.8 shows the linear growth of both optical film thicknesses in the absence and presence of NaCl as a function of the number of layers.

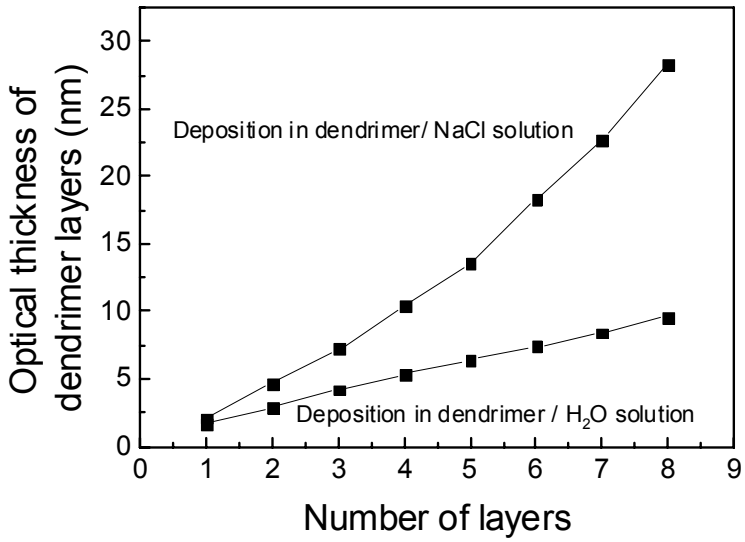

Figure 6.8 Optical thicknesses versus the number of bilayers deposited in the absence and presence of NaCl.

6.3.4 Effect of the Number of Multilayers on the Binding Capacity of Probe DNA Molecules

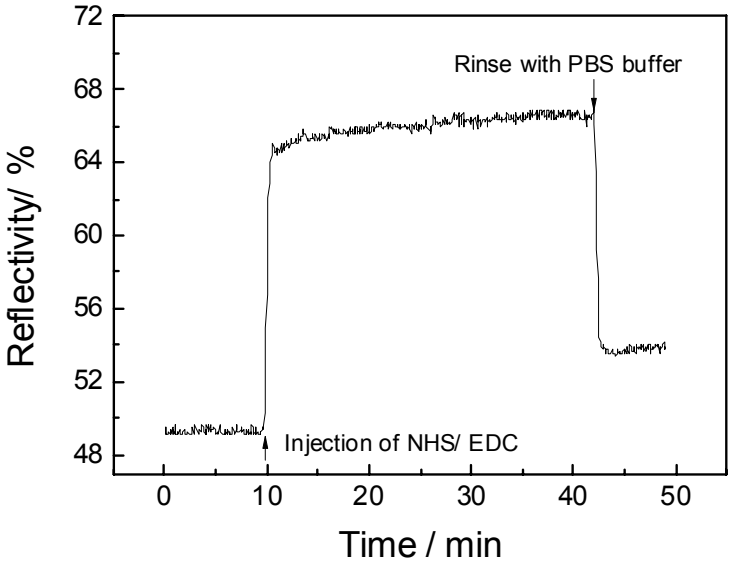

Figure 6.9 SPR kinetic measurement showing the activation with NHS/ EDC on the topmost layer surface with carboxylic acid groups from the phosphorus dendrimer multilayer surface.

The topmost layer from the multilayer is the negatively charged layer of $G_4(CH\text{-}COO\text{-}Na^+)_{96}$ with carboxylic acid groups. In order to covalently bind probe DNA modified with amino groups, a cross-linking method was employed that uses NHS/ EDC[35] to activate the carboxylic acid groups. In the case of 1 bilayer of phosphorus dendrimers at 50 mM NaCl, for example, Figure 6.9 shows the SPR kinetic measurement of the process of NHS/EDC activation on the surface. Since the immobilization and hybridization of DNA molecules are carried out in the physiological condition which is kept at pH=7.4 buffer solution, the PBS buffer at pH=7.4 is used below. Firstly, the PBS buffer was introduced into the quartz flow cell to stabilize the multilayer surface. Then the freshly prepared mixture of NHS/EDC solution was injected into the flow cell, and was circulated using a peristaltic pump for 30 min. After that the PBS buffer was injected again to the flow cell to remove

the excess NHS and EDC molecules. Clearly, the activation process is working as indicated by an increase in reflectivity as shown in Figure 6.9.

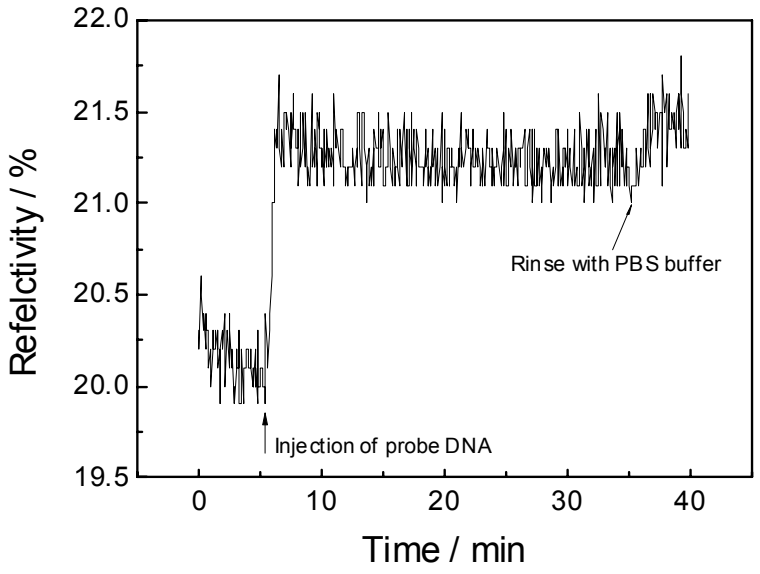

Figure 6.10 SPR kinetic mode of probe DNA adsorption on the NHS/EDC activated multilayer surface.

After the topmost layer was activated by NHS/EDC, the probe DNA molecules with 45-mer (a NH_2 group at its 5′-end for covalent binding to the dendrimer multilayer surfaces) was injected into the flow cell and circulated using a peristaltic pump for 30 min (Figure 6.10). The probe DNA molecules could bind to the activated surface resulting in a reflectivity increase (Figure 6.10). After that, the probe DNA coated surface was rinsed with PBS buffer to remove the non-covalent binding probe DNA molecules.

In order to study the influence of the dendrimer multilayer thickness on the probe DNA binding capacity, DNA immobilization on dendrimer multilayers with different numbers of layers was carried out by applying a 45-mer oligonucleotide from PBS with a concentration of 1 μM. The probe DNA adsorption was followed in real time by SPR measurements in the kinetic mode. In order to calculate the thickness of the immobilized DNA

layer from an angular scan, a refractivity index of n = 1.375 is used for the DNA layer.[19] Figure 6.11 shows an increase of the DNA binding with an increasing number of bilayers. If the DNA molecules were immobilized on 1 dendrimer bilayer, the optical thickness of the DNA layer was around 1.2 nm. The DNA film thickness, which reflects the DNA binding capacity of the multilayers, increased from 1 bilayer to 5 bilayers to up to 9 nm of DNA and the DNA film thickness remained 9 nm above 5 bilayers. One possible explanation is that the surface is not fully or homogeneously covered which means that there are some defects (voids or nanopores) in the system. So the probe DNA molecules could not just be immobilized on the outer multilayer surface by covalent binding, but it might diffuse inside of the multilayer system.

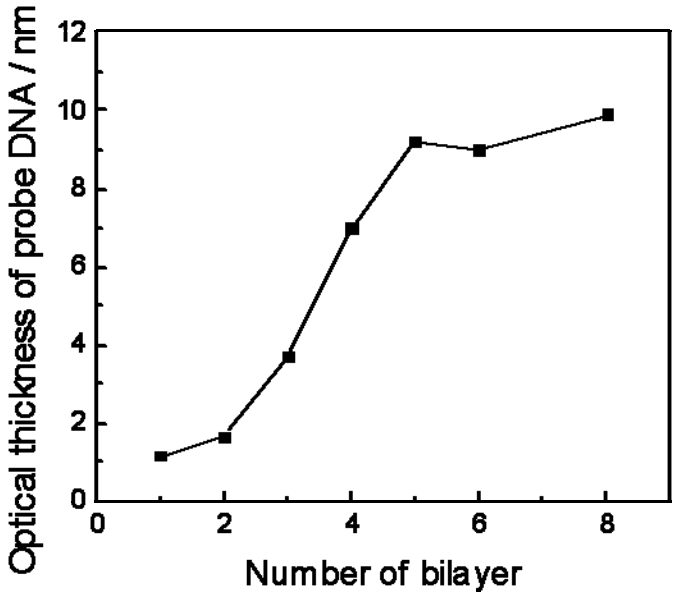

Figure 6.11 Relationship between the number of bilayers and optical thickness of probe DNA immobilization on the dendrimer multilayer surfaces.

6.3.5 DNA Hybridization on Phosphorus Dendrimer Multilayer Films

Using 1 bilayer deposited from a 50 mM NaCl solution as a model system, hybridization of target DNA was investigated by SPFS. Here, the thickness of 1 dendrimer bilayer with the thiol layer (3-MPA) is about 11 nm which is larger than Förster radii (5-7 nm).[9] Therefore, the effect of quenching from gold substrate on the labeled Cy5 dye can be neglected. Cy5 is a reactive water-soluble fluorescent dye of the cyanine dye family. It is usually synthesized with reactive groups on either one or both of the nitrogen side chains so that it can be chemically linked to either nucleic acids or protein molecules. Cy5 is excited maximally at 649 nm and emits maximally at 670 nm, in the far red part of the spectrum. The laser light used to excite surface plasmons on the gold surface is the red laser with 632.8 nm. Therefore, cy5 can be excited by the red laser light. Figure 6.12 shows the discrimination of probe DNA in recognizing target DNA by using three kinds of target DNA with different mismatches (MM0, MM1 and MM2). The nonspecific adsorption of target DNA molecules on the probe immobilized substrates includes not only the so called physical adhesion, but also other interactions such as electrostatic interation and hydrogen bonding. The presence of additional interaction sites would introduce competition of the binding to the surface probe, which is unexpected and leads to deviations from the expected response. Therefore, the investigation of the nonspecific adsorption is indispensable. Here, we select the target DNA with two mismatches (MM2) for the nonspecific detection. Upon exposing the surface with probe DNA to MM2 target DNA molecules, a small rise above the background was observed in the fluorescence intensity (Figure 6.12 region A). The rapid decrease of this fluorescence signal upon rinsing by buffer solution suggests that there is no significant nonspecific adsorption to the dendrimer/DNA surface.

The addition of one mismatch (MM1) in the target strand compared to the probe sequence showed a slow increase in the fluorescence intensity (Figure 6.12 in region B), indicating hybridization. Upon rinsing by PBS buffer, the dissociation of the MM1 target can be clearly observed and a single exponential (Langmuir model)[19] was fitted to the kinetic. The fully complementary target (MM0) hybridization (Figure 6.12 in region C) lead to an even larger increase in the fluorescence intensity, suggesting that hybridization had occurred and stable hybrids were formed within the dendrimer multilayers. Clearly, different DNA targets, i.e., MM0, MM1 and MM2, respectively, showed difference in their hybridization behavior to the surface attached probes. The present DNA sensor can successfully discriminate the DNA targets with one base pair mismatch.

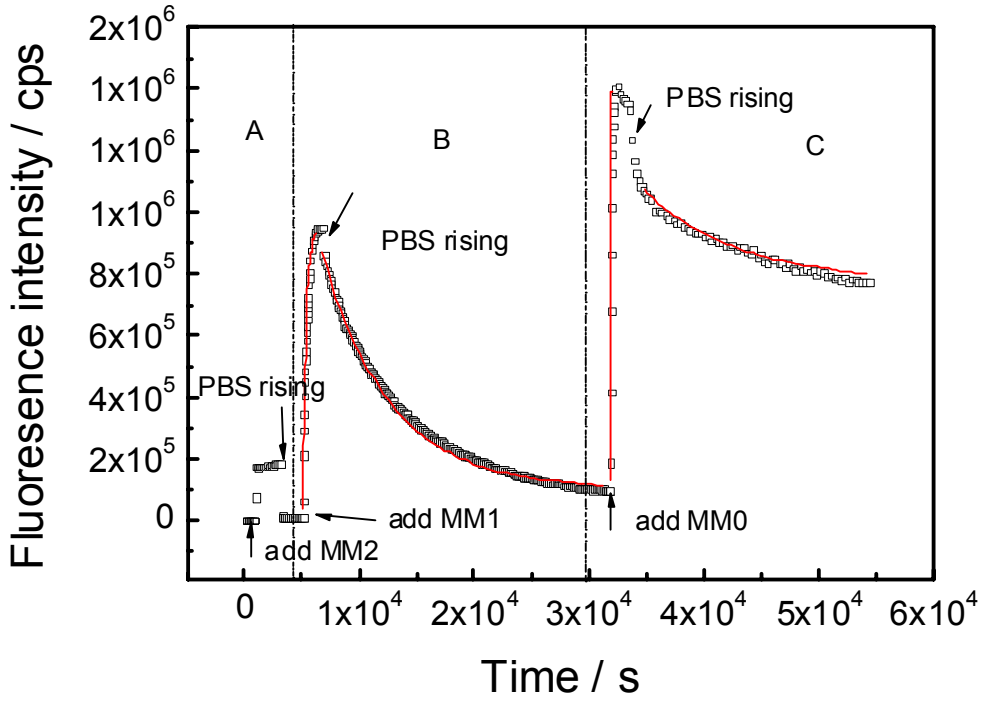

Figure 6.12 SPFS measurements of DNA hybridization reaction using the target DNA with different mismatches. The concentration of three types of target DNA is 50 mM. Region A, B and C are hybridization processes carried out with MM2, MM1 and MM0 target DNAs, respectively.

Kinetic information could be collected by fitting the SPFS data with a simple one-to-one interaction model. According to the Langmuir approach, the association process should follow:

$$I_{fl}(t) = I_{max}(1- \exp(-(k_{on}c_0 + k_{off})t)) \quad \textbf{Equation 6.1}$$

and the dissociation process should be described by

$$I_{fl}(t) = I_{max} \exp(-k_{off}t) \quad \textbf{Equation 6.2}$$

The red curves in Figure 6.12 show the fitting curves based on the above equations, giving the rate constants summarized in Table 6.1.Within the Langmuir model, the affinity constant K_A is given by:

$$K_A = k_{on} / k_{off} \quad \textbf{Equation 6.3}$$

It is apparent from the data outlined in Table 6.1 that K_A for MM0 is more than one order higher than that of MM1. This result is also in good agreement with previous work done in our group.[9]

Table 6.1 Summary of kinetic data, i.e. adsorption (hybridization) rate constant k_{on}, dissociation rate constant k_{off} and affinity constant $K_A = k_{on}/k_{off}$ for the reaction of the probe DNA to the target DNA (MM0 and MM1), immobilized at the dendrimer multilayer surfaces.

	k_{on} / $M^{-1}s^{-1}$	k_{off} / s^{-1}	K_A / M^{-1}
MM0	3×10^5	1.3×10^{-4}	2.5×10^9
MM1	3×10^4	1.7×10^{-4}	1.8×10^8

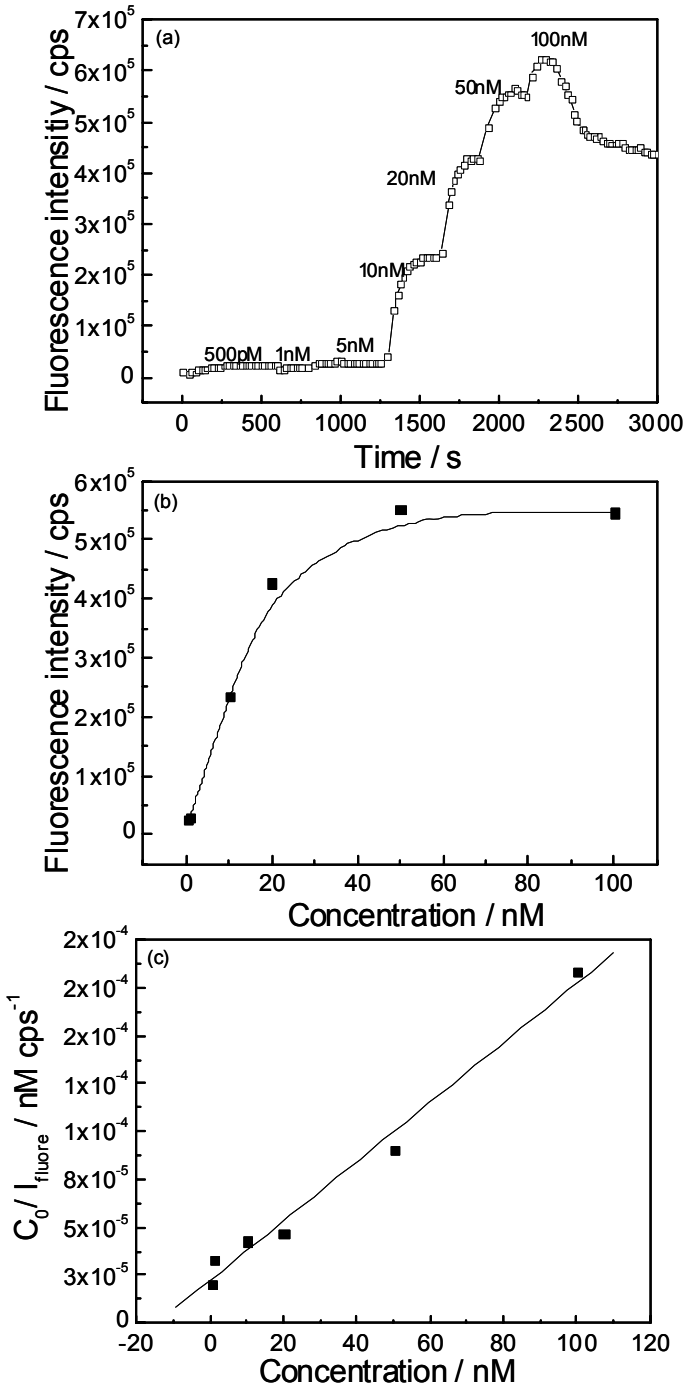

Figure 6.13 (a) Langmuir adsorption isotherm experiment of MM0 binding to probe DNA. (b) The fluorescence intensity increases and reaches an equilibrium level when the concentration c_0 of MM0 is increased. The higher the added concentration, the faster the fluorescence intensity increases. (c) The equilibrium fluorescence intensities (I_{fl}) as a function of the solution concentration c_0. Linear representation of the data given in (c), i.e. c_0/I_{fl} versus c_0 with a linear regression that yields K_A.

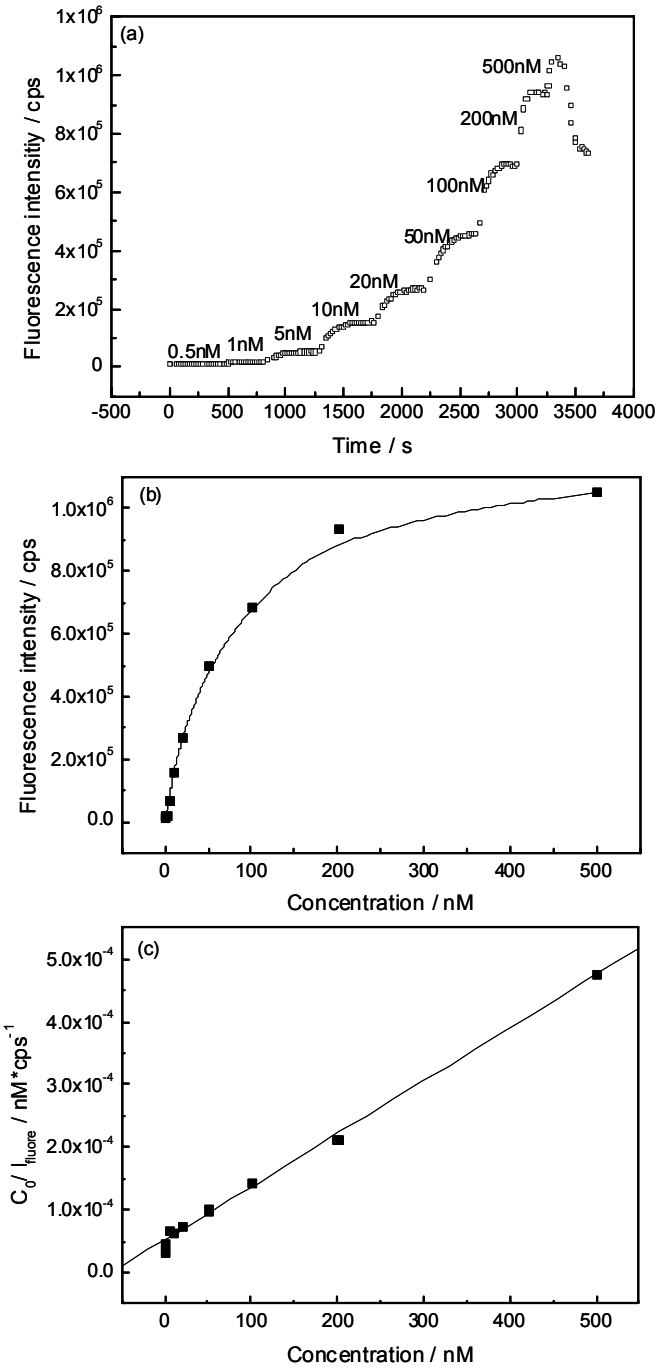

Figure 6.14 (a) The experiment of MM1 binding to probe DNA. (b) The fluorescence intensity increases and reaches an equilibrium level when the concentration c_0 of MM1 is increased. The higher the concentration is added, the faster the fluorescence intensity can increase. (c) The equilibrium fluorescence intensities (I_{fl}) as a function of the solution concentration c_0. Linear representation of the data given in (c), i.e. c_0/I_{fl} versus c_0 with a linear regression that yields K_A.

Further support for affinity constants of K_A (MM0 and MM1) come from the measurements of the Langmuir isotherm, which are presented in Figure 6.13 and Figure 6.14, respectively. By stepwise increasing the concentration of MM0 and MM1, the new equilibrium coverage is reached equivalent to new stable fluorescence intensities. As predicted by the equation for the adsorption (hybridization),[36] the time needed to reach the new equilibrium coverage gets shorter as the solution concentration c_0 is increased. If these equilibrium intensities are plotted as a function of c_0 (Figure 6.13 (a) and Figure 6.14 (a)), the Langmuir adsorption isotherm can be obtained. A plot of c_0/I_{fl} (the flurescence intensity at equilibrium) as a function of c_0 (Figure 6.13 (b) and Figure 6.14 (b)) yields a straight line from which the affinity constant K_A ($K_A = K_{on}/K_{off}$) can be deduced. This plot together with a linear regression is shown in Figure 6.13 (c) and Figure 6.14 (c), giving $K_A = 6.9\times10^8$ M^{-1} for MM0 and $K_A = 1.6 \times10^7$ M^{-1} for MM1. The DNA hybridization with complementary target DNA (MM0) and dissociation can be described by a simple Langmuir model ($K_A=2.5\times10^9$ M^{-1}) and Langmuir adsorption isotherm ($K_A = 6.9\times10^8$ M^{-1}). For DNA hybridization with one mismatch target probe DNA (MM1), K_A obtained from the simple Langmuir model ($K_A = 1.6\times10^7$ M^{-1}) and Langmuir adsorption isotherm ($K_A = 1.8\times10^8$ M^{-1}). Although the K_A obtained from a simple Langmuir model and Langmuir adsorption isotherm are slightly different, the DNA hybridization and diassociation with complementary or one mismatch target DNA can be distinguished by both strategies.

6.3.6 Comparison of Sensitivity of Surfaces with Different Numbers of Dendrimer Multilayers

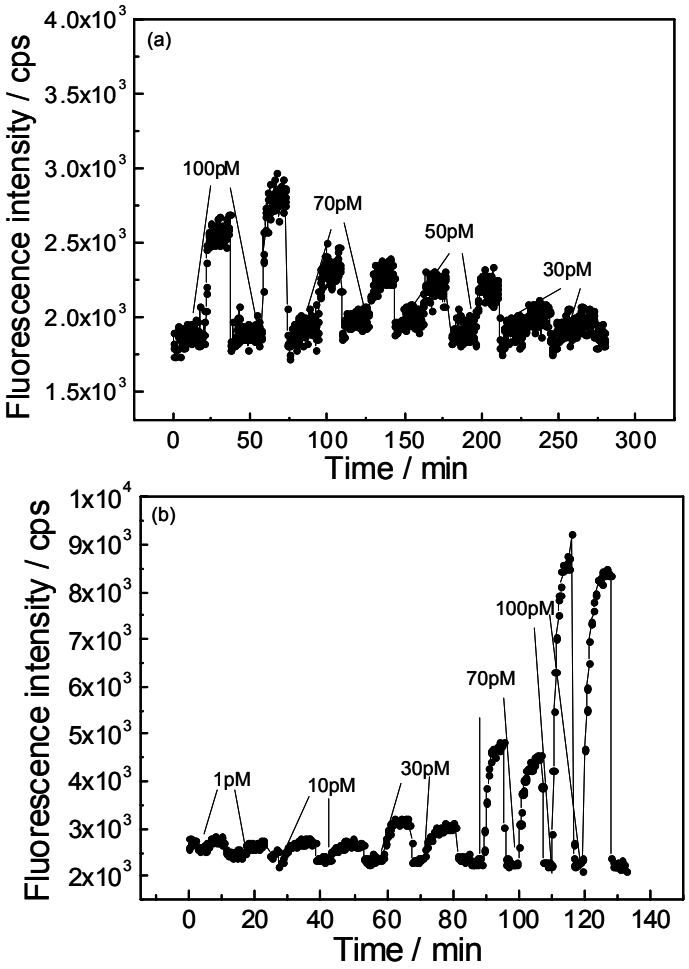

Figure 6.15 Hybridization of target MM0 to the DNA surfaces based on 1bilayer (a) and 4 bilayers (b) multilayer respectively in the presence of sodium chloride during the deposition.

The experiments reported above have already indicated that a surface with dendrimers has a high immobilization capacity for probe DNA, which increases with the thickness of dendrimer films. Moreover, it has excellent accessibility for the targets to hybridize with the probe strands. To further investigate this property and to determine a detection limit of the

fluorescence signal, we performed the hybridization analysis on 1 bilayer and 4 bilayers deposited in the presence of NaCl, respectively. Figure 6.15 (a) shows the target DNA hybridization process on 1 bilayer dendrimer surface binding with an amino-modified oligomer. The multilayer surface with immobilized probe DNA molecules was hybridized to fully complementary oligonucleotide target (MM0) solutions with increasing concentration from 30 pM to 100 pM. If a 30 pM solution of MM0 was added, there was no obvious increase in the fluorescence intensity signal. However, a 50 pM solution was sufficient to generate a clear increase in the fluorescence intensity.

For the concentration analysis by SPFS to detect the limit of detection, we operated under mass-transport limited binding conditions in the association phase. Usually, at a relatively low analyte bulk concentration, the initial binding is under mass-transport control. The binding rate is constant and not related to the interaction affinity. The slope of binding is proportional to the analyte concentration.

The possibility to re-use DNA arrays could be an advantage in transcriptomic studies, as it allows reproducibility of experiments on the same technical support. It also reduces the cost, while improving accuracy of the genomic data.[30] Therefore, we investigated the re-usability of the DNA arrays generated from phosphorus dendrimer multilayer surfaces. Under some conditions such as high temperatures, chemicals such as urea and alkali, the two strands of DNA can break apart. This is called DNA denaturation. Here, we selected diluted NaOH solution to make DNA denaturate and recover the single probe DNA molecules on surfaces. At each injection of the target DNA solution, the target DNA was allowed to interact for certain period of time and was followed by rinsing the surface with a 10 mM NaOH solution for about 1 min. The probe surface demonstrated good robustness, surviving repetitive regeneration for at least 10 cycles. In the low

target concentration region, the initial hybridization process was controlled by the diffusion of the target DNA from the bulk to the surface, thus showing a linear signal increase with time.

Using the same method, adding 30 pM of target DNA solution increased the fluorescence intensity signal on 4 bilayers of dendrimer multilayer surface (Figure 6.15 (b)). From the comparison of the results from the two dendrimer multilayer surfaces, detection sensitivity on 4 bilayers is close to that on the 1 bilayer and the detection sensitivities are in the same order of magnitude as the results from the neutral phosphorus dendrimer (1 pM).[25] It seems that the hybridization reaction occurred only on the outermost layer.

6.4 Conclusion

In this work, we have shown that LbL deposition of dendrimer multilayers on gold substrates in the presence of NaCl. The mutilayer coatings can be used as active platforms for biomolecule immobilization because of their tunable film thickness and high molecular loading capabilities. At the optimized concentration of NaCl, dendrimer multilayers with different number of layers were fabricated. An increase in the covalent loading of probe DNA with the number of dendrimer layers was observed. This phenomenon is attributed to the diffusion of probe DNA, namely probe DNA could both immobilize on the top surface and penetrate into the multilayer system. The limit of detection of DNA hybridization was determined to be 50 pM and 30 pM on 1 bilayer and 4 bilayer films, respectively, which are in the same order of magnitude as the results from the neutral dendrimer (1 pM).[30] The experimental results demonstrate that the multilayers based on phosphorus dendrimer deposited in the presence of NaCl constitute an attractive and simple platform for the immobilization of biomolecules with high densities and a sensitive DNA microarray for the detection of DNA hybridization. This study also introduces LbL technique as

an alternative strategy to build up the dendrimer multilayers which could be fabricated onto various substrates and templates.

6.5 References

1 (a) Cai, Z.; Martin, C. R. *J. Am. Chem. Soc.* **1989,** *111,* 4138. (b) Liang, W.; Martin, C. R. *J. Am. Chem. Soc.* **1990,** *112,* 9666.

2 (a) Quinn, J. F.; Caruso, F. *Langmuir* **2004,** *20,* 20. (b) Quinn, J. F.; Caruso, F. *Macromolecules* **2005,** *38,* 3414. (c) Jaber, J. A.; Schlenoff, J. B. *Macromolecules* **2005,** *38,* 1300.

3 (a) Kim, D. H.; Karan, P.; Göring, P. ; Leclaire, J.; Caminade, A. M.; Majoral, J. P.; Gösele, U.; Steinhart, M.; Knoll, W . *Small* **2005,** *1,* 99. (b) Feng, C. L. ; Zhong, X. H.; Steinhart, M.; Caminade, A. M.; Majoral, J. P.; Knoll, W. *Small* **2008,** *4,* 566. (c) Feng, C. L. ; Zhong, X. H.; Steinhart, M.; Caminade, A. M.; Majoral, J. P.; Knoll, W. *Adv. Mater.* **2007,** *19,* 1933. (d) Kim, B. S.; Lebedeva, O. V.; Kim, D. H.; Caminade, A. M.; Majoral, J. P.; Knoll, W.; Vinogradova, O. I. *Langmuir* **2005,** *21,* 7200.

4 (a) Decher, G.; Schlenoff, J. B. (Eds.) *Multilayer Thin Films, Sequential Assembly of Nanocomposite Materials,* Wiley-VCH, Weinheim, Germany, **2003.** (b) Shi, X.; Shen, M.; Möhwald, H. *Prog. Polym. Sci.* **2004,** *29,* 987. (c) Hammond, P. T. *Adv. Mater.* **2004,** *16,* 1271. (c) Jiang, C.; Tsukruk, V. V. *Adv. Mater.* **2006,** *18,* 829. (d) Tang, Z.; Wang, Y.; Podsiadlo, P.; Kotov, N. A. *Adv. Mater.* **2006,** *18,* 3203.

5 Chambers,J. P.; Arulanandam, B. P.; Matta, L. L. ; Weis, A. ; and Valdes, J. J. *Curr. Issues Mol. Biol.* **2008,** *10,* 1.

6 Caruso, A. F. C. a. F. *Biosensors: recent advances Reports on Progress in Physics 1997,* **60,** 1397.

7 (a) Turner; A. P.; Karube;, I.; Wilson, G. S., *Biosensors: Fundamentals and applications Oxford University Press*, New York: **1987**. (b) Lowe, C. R. *Biosensors* **1985,** 1, 3.

8 (a)Liebermann, T.; Knoll, W. *Colloids and Surfaces A* **2000,** *171,* 115. (b) Neumann, T.; Johansson, M. L.; Kambhampati, D.; Knoll, W., *Advanced Functional Materials* **2002,** *12,* 575. (c) Kwon, S. H.; Hong, B. J.; Park, H. Y.; Knoll, W.; Park, J. W. *Journal of Colloid and Interface Science* **2007,** *308,* 325.

9 MacBeath, G.; Schreiber, S. L. *Science* **2000,** *289,* 1760.

10 Mark, S. S.; Sandhyarani, N.; Zhu, C.; Campagnolo, C.; Batt, C. A. *Langmuir* **2004,** *20,* 6808.

11 (a) Conzone, S. D.; Pantanot, C. G. *Mater. Today* **2004,** *7,* 20. (b) Lemeshko, S. V.; Powdrill,T.; Belosludtsev, Y. Y.; Hogan, M. *Nucleic Acids Res.* **2001,** *29,* 3051. (c) Belosludtsev, Y.; Iverson, B.; Lemeshko, S.; Eggers, R.; Wiese, R.; Lee, S.; Powdrill, T.; Hogan, M. *Anal. Biochem.* **2001,** *292,* 250.

12 De La Escosura-Muniz, A.; Gonzalez-Garcia, M. B.; Costa-Garcia, A. *Biosens. Bioelectron.* **2007,** *22,* 1048.

13 (a) Pividori, M. I.; Merkoci, A.; Alegret, S. *Biosens. Bioelectron.* **2000,** *15,* 291. (b) Ligaj, M.; Jasnowska, J.; Musial, W. G.; Filipiak, M. *Electrochim. Acta* **2006**, *51,* 5193. (c) Dharuman, V.; Nebling, E.; Grunwald, T.; Albers, J.; Blohm, L.; Elsholz, B.; Wörl, R.; Hintsche, R. *Biosens. Bioelectron.* **2006,** *22,* 744. (d) Walsh, M. K.; Wang, X.; Weimer, B. C. *J. Biochem. Biophys. Methods* **2001,** *47,* 221. (e) Wrobel, N.; Deininger, W.; Hegemann, P.; Mirsky, V. M. *Colloids Surf. B* **2003,** *32,* 157.

14 (a) Southern, E.; Mir, K.; Shchepinov, M. *Nat. Gene.* **1999,** *21,* 5. (b) Angenendt, P.; Glökler, J.; Murphy, D.; Lehrach, H.; Cahill, D. J. *Anal. Biochem.* **2002,** *309,* 253.

15 (a) Prime, K. L.; Whitesides, G. M. *Science 1991, 252,* 1164. (b) Prime, K. L.; Whitesides, G. M. *J. Am. Chem. Soc.* **1993,** *115,* 10714. (c) Chapman, R.G.;

Ostuni, E.; Liang, M. N.; Meluleni, G.; Kim, E.; Yan, L.; Pier, G.; Warren, H. S.; Whitesides, G. M. *Langmuir* **2001,** *17,* 1225. (d) Holmlin, R. E.; Chen, X.; Chapman, R.; Takayama, S.; Whitesides, G. M. *Langmuir* **2001,** *17,* 2841. (e) Luk, Y.; Kato, M.; Mrksich, M. *Langmuir* **2000,** *16,* 9604.

16 Liebermann, T.; Knoll, W.; Sluka, P; Herrmann, R. *Colloids Surf. A* **2000,** *169,* 337.

17 Kwon, S.; Hong, B.; Park, H; Knoll, W.; Park, J. *J. Colloid Interface Sci.* **2007,** *308,* 325.

18 (a) Delamarche, E.; Michel, B.; Biebyck, H. A.; Gerber, C. *Adv. Mater.* **1996,** *8,* 719. (b) Lang, P.; Mekhalif, Z.; Rat, B.; Gernier, F. J. *Electroanal. Chem.* **1998,** *441,* 83. (c) Huseman, M.; Morrisson, M.; Benoit, D.; Frommer, J.; Mate, C. M.; Hinsberg,W. D.; Hedrick, J. L.; Hawker, C. L. *J. Am. Chem. Soc.* **2000,** *122,* 1844.

19 (a) Zhang, Z.; Chen, Q.; Knoll, W.; Förch, R. *Macromolecules* **2003,** *36,* 7689. (b) Zhang, Z.; Knoll, W.; Förch, R. *Macromolecules* **2005,** *38,* 1271.

20 (a) Falconnet, D.; Koenig, A.; Assi, F.; Textor, M. *Adv. Funct. Mater.* **2004,** *14,* 749. (b) Feng, C.; Zhang, Z.; Förch, R; Knoll, W.; Vancso, G. J.; Schönherr, H. *Biomacromolecules* **2005,** *6,* 3243. (c) Feng, C.; Vancso, G. J.; Schönherr, H. *Adv. Funct. Mater.* **2006,** *16,* 1306.

21 Rowan, B.; Wheeler, M. A.; Crooks, R. M. *Langmuir* **2002,** *18,* 9914.

22 Pirri, G.; Chiari, M.; Damin, F., Meo, A. *Anal. Chem.* **2006,** *78,* 3118.

23 Timofeev, E.; Kochetkova, S. V.; Mirzabekov, A.; Florentiev, V. L. *Nucleic Acids Res.* **1996,** *24* , 3142.

24 Rehman, F. N.; Audeh, M.; Abrams, E. S.; Hammond, P. W.; Kenney, M.; Boles, T. C. *Nucleic Acids Res.* **1999,** *27,* 649.

25 Kumar, A.; Larsson, O.; Parodi, D.; Liang, Z. *Nucleic Acids Res.* **2000,** *28,* e71.

26 Kumar, A.; Liang, Z. *Nucleic Acids Res.* **2001,** *29,* e2.

27 (a) Niemeyer, C. M.; Blohm, D. *Angew. Chem., Int. Ed.* **1999,** *38,* 2865. (b) Schulze, A.; Downward, J. Nat. *Cell Biol.* **2001,** *3,* E190. (c) Benters, R.; Niemeyer, C. M.; Drutschmann, D.; Blohm, D.; Wöhrle, D. *Nucleic Acids Res.* **2002,** *30,* e10. (d) Pathak, S.; Singh, A. K.; McElhanon, J. R.; Dentinger, P. M. *Langmuir* **2004,** *20,* 6075. (e) Majoral, J. P.; Turrin, C. O.; Laurent, R.; Caminade, A. M. *Macromol. Symp* **2005,** *229,* 1. (f) Caminade, A. M.; Majoral, J. P. *Prog. Polym. Sci.* **2005,** *30,* 491.

28 Caminade, A. M.; Padié, C.; Laurent, R.; Maraval, A.; Majoral, J. P. *Sensors* **2006,** *6,* 901.

29 Benters, R.; Niemeyer, C. M.; Wöhrle, D. *Chem. Bio. Chem.* **2001,** *2,* 686.

30 (a) Leberre, V. L.; Trévisiol, E.; Dagkessamanskaia, A.; Sokol, S.; Caminade, A. M.; Majoral, J. P.; Meunier, B.; François, J. *Nucleic Acids Res.* **2003,** *31,* e88. (b) Trévisiol, E.; Leberre-Anton, V.; Leclaire, J.; Pratviel, G.; Caminade, A. M.; Majoral, J. P.; François, J.; Meunier, B. *New J. Chem.* **2003,** *27,* 1713.

31 (a) Yu, F.; Persson, B.; Löfas, S.; Knoll, W. *Anal. Chem.* **2004,** *76,* 6765. (b) Yao, D.; Yu, F.; Kim, J.; Scholz, J.; Nielsen, P. E.; Sinner, E.; Knoll, W. *Nucleic Acids Res.* **2004,** *32,* e177.

32 (a) Gallliot, C. ; Larré, C. ; Camminade, A. M. ; Majoral, J. P. *Science* **1997,** 277, 1981. (b) Loup, C.; Zanta, M. A.; Caminade, A. M.; Majoral, J. P.; Meunier, B. *Chem. Eur. J.* **1999,** *5,* 3644. (c) Boggiano, M. K.; Soler-Illia, G.; Rozes, L.; Sanchez, C.; Turrin, C.O. ; Caminade, A. M; Majoral, J. P. *Angew. Chem. Int. Ed.* **2000,** *39,* 4249. (d) Launay, N.; Caminade, A. M. ; Lahana, R. ; Majoral, J. P. *Angew. Chem., Int. Ed. Engl.* **1994,** *33,* 1589.

33 Kim, D. H.; Hernandez Lopez, J. L.; Liu, J.; Mihov, G.; Zhi, L.; Bauer, R. E.; Grebel Köhler, D.; Klapper, M.; Weil, T.; Müllen, K.; Mittler, S.; Knoll, W. *Macromol. Chem. Phys.* **2005,** *206,* 52.

34 Fery, A.; Schöler, B.; Cassagneau, T.; Caruso, F. *Langmuir* **2001**, *17,* 3779.

35 (a) Montalbetti, C. A. G. N.; Falque, V. *Tetrahedron* **2005**, *61,* 10827. (b) Olde Damink, L. H. H.; Dijkstra, P. J.; van Luyn, M. J. A.; van Wachem, P. B.; Nieuwenhuis, P.; Feijen, J. *Biomaterials* **1996,** *17,* 765.

36 Liebermann, W. Knoll, P. Sluka, R. Herrmann, *Coll. Surf. A* **2000,** *169,* , 337.

Chapter 7

Dendritic Star Polymer Multilayer Thin Films: Surface Morphology and DNA Hybridization Characteristics

This chapter describes the characterization of dendritic star polymers multilayer films and the application of multilayer films as DNA biosensors. The oppositely charged dendritic star polymers employed here are based on the dendritic polyphenylene core with arms possessing amino groups (positive charges) and carboxylic acid groups (negative charges). The as-assembled dendritic star polymer multilayer films were analyzed by atomic force microscopy (AFM) and exhibited distinct morphology changes upon post-treatment under different pH conditions. Kinetic binding of probe DNA molecules on the outermost negatively charged dendritic multilayer surface was studied by SPR as well. The binding capacities of probe DNA on the multilayer surfaces fabricated from the first-generation and the second-generation of dendritic star polymers were compared. DNA hybridization reaction on dendritic multilayer films was investigated by surface plasmon field enhanced fluorescence spectroscopy (SPFS).

7.1 Introduction

The layer by layer (LbL) assembly technique has been broadly employed as a versatile and convenient method in fabricating nanostructures with precise control of film structures and composition.[1] The LbL method is typically based on the alternate adsorption of oppositely charged polyelectrolytes. A wide variety of materials have been developed to construct building blocks for LbL assembly beyond linear polyelectrolytes, including polymeric micelles,[2] dendrimers,[3] biological macromolecules,[4] inorganic nanoparticles,[5] and carbon nanotubes.[6] As new materials are

introduced in the formation of multilayer films, it would be interesting to investigate the structural and morphology characteristics of multilayer films that contain materials with unusual architecture and functionalities compared to the conventional linear polyelectrolytes. The general results reported for linear polyelectrolyte systems may not be applicable to the systems of which the average size and shape of the macromolecules are unique. Star polymers have branched topology with a globular shape and multiple arms connected to a central core.[7] In comparison with their linear analogues, star polymers have different rheological and mechanical properties and possess an apparently higher degree of functionalities.[8] The construction of star polymers into multilayer thin films has been investigated by a few groups recently. For example, Chen et al. have reported a multilayer prepared based on poly(acrylic acid) (PAA) star polymers with an inorganic precursor core.[9] Recently, Connal et al. have shown the incorporation of cross linked PAA star polymers into LbL assembled polymeric multilayers and studied their pH responsive surface properties.[10] Similarly, Kim et al. reported all-star polymer multilayers (poly[2-(dimethylamino)ethyl methacrylate] (PDMAEMA) and poly(acrylic acid)) as pH responsive nanofilms.[8]

Dendritic star polymers possess the characters of both dendrimer and star polymer. Features of dendritic star polymers are similar to those of regular dendrimers, such as the presence of a central core, a precise number of branching points and terminal functions. Moreover, the dendritic star polymer also resembles the star polymer with multiple arms.[11] The combination of various structural conformations, dimensions and high densities of active functional groups makes dendritic star polymers unique candidates for a diverse range of applications, including surface engineering, novel responsive materials and drug delivery. The dendritic star polymers used in this chapter consist of a central rigid polyphenylene dendrimer core

and a flexible shell with six or twelve linear polymer arms containing carboxylic acid groups or amine groups, which provide a perfectly branched structure, and the availability of a defined number of functional groups at the surface.

In this chapter, we introduce the first example of ultrathin films exclusively based on the dendritic star polymers. The thickness and composition of these films can be precisely controlled. The primary aim of this work is to demonstrate the preparation of dendritic star polymers multilayers by means of electrostatic LbL assembly. Furthermore, we have discovered an unusually high tendency toward pH responsive morphological rearrangements in the dendritic star/star multilayer films due to the changes in ionization of the polyelectrolytes from the arms and the distinctive geometry of star polymers. Finally, the dendritic star polymer multilalyers were employed as the platform for the immobilization and hybridization of DNA. These results were also compared with those of phosphorus dendrimer multilayer systems.

7.2 Experimental Section

Reagents and Chemicals

The first- and second-generation dendritic star polymers (DP_1^+, DP_1^-, and DP_2^-, Figure 7.1) with opposite charges were synthesized according to the previous published work.[12]

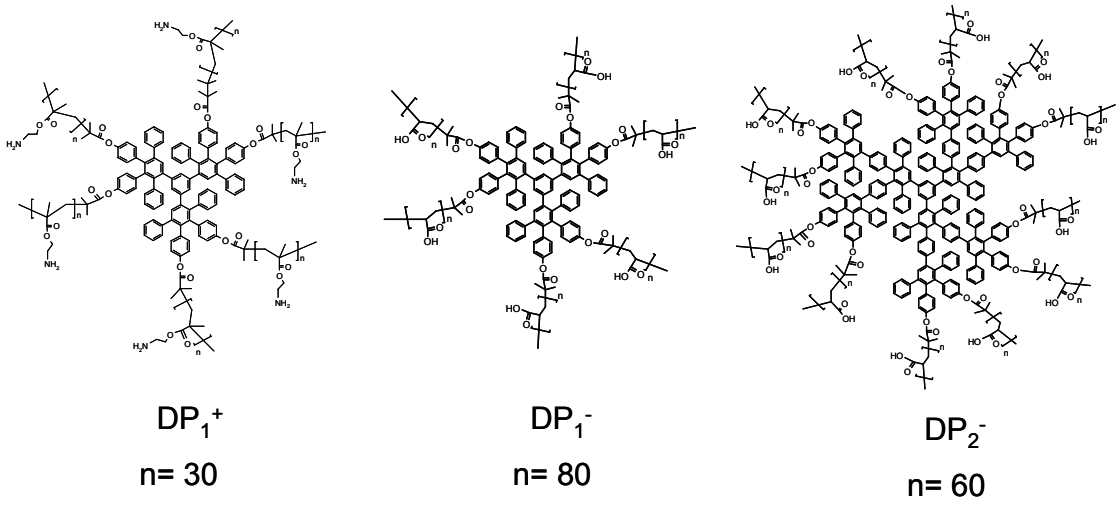

Figure 7.1 Structures of oppositely charged dendritic star polymers (DP_1^+, DP_1^-, and DP_2^-).

Other chemicals were all purchased from Sigma-Aldrich (Germany) and used without further purification. A MilliQ system was used to produce high purity water with a resistivity of 18.2 MΩcm.

The probe DNA was purchased from MWG Biotech, Ebersberg, Germany. The sequences chosen in this work were given as follows:

5′- NH_2-$(TTT)_{10}$ TGT ACA TCA CAA CTA-3′

The target DNA sequences for the hybridization reaction were listed below.

MM0 (complementary target): 3′-ACA TGT AGT GTT GAT-Cy5-5′;

MM1 (single base pair mismatch target): 3′-ACA TG<u>C</u> AGT GTT GAT-Cy5-5′;

MM2 (two base pair mismatches target): 3′-ACA TG<u>C</u> A<u>C</u>T GTT GAT-Cy5-5′.

Stock solutions of probe DNA in phosphate buffer at pH 7.4 with a concentration of 1 $\times 10^{-5}$ M were prepared and used throughout this work. Target MM0, MM1 and MM2 solutions with concentrations of 1×10^{-7} M were prepared for the Langmuir isotherm adsorption discussed below.

Surface Modification

The substrates used in this work were $LaSFN_9$ optical glass slides (Hellma Optik, Jena, Germany) coated with approximately 50nm gold by the use of thermal evaporation. The gold surfaces were functionalized by a self-assembled monolayer of 3-mercaptopropionic acid (3-MPA) (5×10^{-3} M in ethanol, at least 6 h immersion at room temperature). The first positively charged DP_1^+ layer was deposited on the MPA-modified substrate for 20 min and then the surface was thoroughly washed with water in order to remove excess DP_1^+. The substrate was then exposed into the DP_1^- or DP_2^- dendritic star polymer solution for 20 min, followed by the same rinsing protocol as before. The deposition of the oppositely charged dendritic star polymers as a double layer was repeated until the desired number of bilayers. The outermost layer was DP_1^- or DP_2^- containing negatively charged carboxyl groups which were activated by 1-ethyl-3-(3-dimethylaminopropyl) carbodiimide (EDC) and N-hydroxysuccinimide (NHS) for further covalently binding probe DNA molecules.

Instruments

(1) Spin Coating

The solutions of DP_1^+ and DP_2^+ in methonal at a concentration of 0.001 mg/mL were spin-coated at 3000 rpm on freshly cleaved mica for 60 s. Samples were visualized with AFM immediately after preparation.

(2) Potentiometric Titration

Potentiometric titrations were conducted by the use of a Mettler Toledo MP225 pH meter. Aqueous solutions of dendritic star polymers were prepared in 0.025 mg/mL and titrated with a 0.1 M NaOH. The pH values were plotted as a function of activity coefficient $\alpha = C_b / C_{AA}$, where C_b is the

concentration of NaOH added to the solution and C_{AA} is the concentration of acrylic acid groups in solution.

(3) Atomic Force Microscopy

Atomic force microscopy (AFM) images of air dried multilayer films on gold substrates were captured by a Veeco Dimension 3100CL setup in tapping mode. Image processing was obtained using the Nanoscope 5.12r5 software. Silicon tips with a radius of < 10nm, spring constant of $\sim$40N/m, and resonance frequency of $\sim$300 kHz were used.

(4)SPR and SPFS

The principles of SPR and SPFS have been described in Chapter 3.

7.3 Results and Discussion

7.3.1 Characterization of the Single Dendritic Star Polymer Molecules by AFM

In order to understand the fundamental characters and properties including the size and shape of the dendritic star polymers, dendritic star polymer molecules of DP_1^- and DP_2^- were characterized by AFM. In addition, AFM imaging of such molecules on surfaces also provides information concerning properties, e.g., their molecular rigidity as judged by their shape on the surface. Establishing the morphology of these dendritic star polymers is helpful not only to confirm their structure, but also to indicate potential applications. Atomic force microscopy is suitable to investigate such dendritic structures since the AFM can provide atomic level resolution, simple sample preparation, and fast image acquisition. The capability of imaging at the molecular level allows the surface profile of each molecule to be obtained, from which the molecular volume of individual molecules can be calculated.[13]

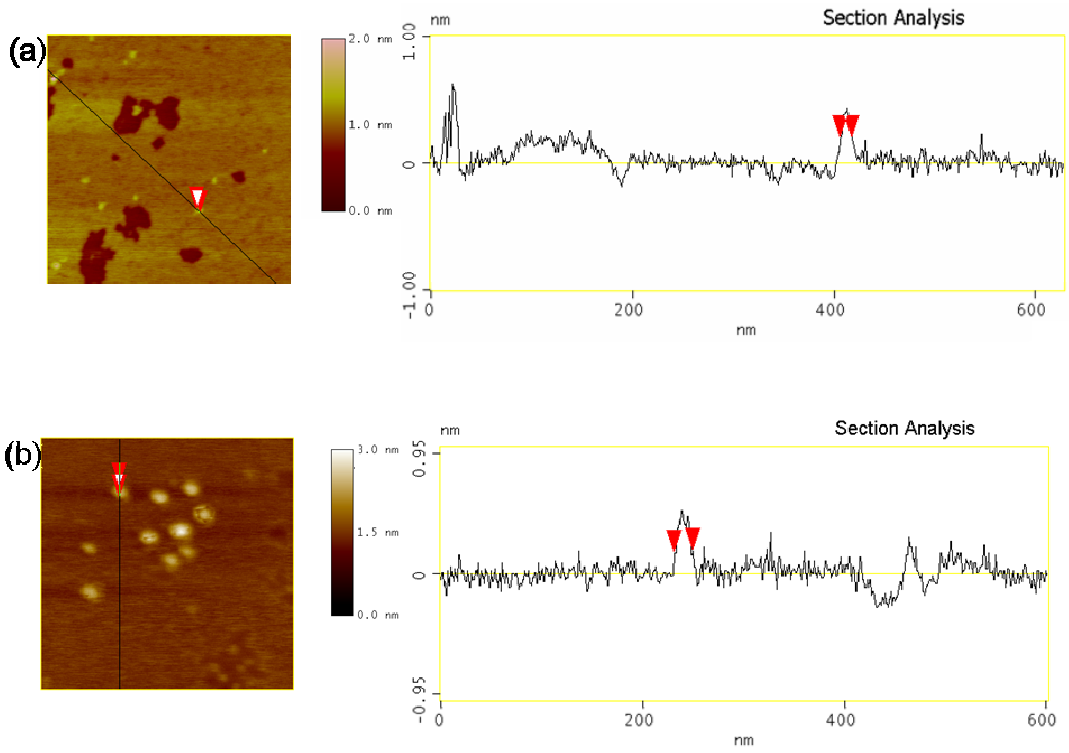

Figure 7.2 (a) AFM image (500 nm × 500 nm) of individual DP_1- molecules on mica, spin-coated at a concentration of 0.001 mg/mL in methanol. The section analysis shows the topology profile across the center of an individual DP_1- molecule presented in topology. (b) AFM image (500 nm × 500 nm) of individual DP_2- molecules on mica, spin-coated at a concentration of 0.001 mg/mL in methanol. The section analysis shows the topology profile across the center of an individual DP_2- molecule presented in topology.

Figure 7.2(a) shows the tapping mode AFM images of dendritic star polymers (DP_1-) by spin-coating the 0.001 mg/mL solution in methanol on a freshly cleaved mica surface. Many randomly separated globular spots can be observed, which appear to be substantially uniform in size, i.e., they are essentially monodisperse. The average height of the spot is 0.35±0.06 nm. The height of the dendritic star polymer of the DP_2- can also be measured from Figure 7.2 (b) to be 0.90±0.21 nm. The heights and diameters of two generation of dendritic star polymers are summarized below in Table 7.1. However, the diameters of DP_1- and DP_2- are fairly larger, which are 12.54±0.73 nm and 23.76±2.76 nm respectively, compared with the height of

molecules. This could be explained by the fact that the flexible polymer shells are flattened on the mica surface in a result of large diameters. On the contrary, the height of the dendritic star polymers is mainly due to the rigid core of molecules.

Table 7.1 Molecular size of the dendritic star polymers of DP_1^- and DP_2^-.

	DP_1^-	DP_2^-
Diameter (d)/nm	12.54±0.73	23.76±2.76
Height (h)/nm	0.35±0.06	0.90±0.21

7.3.2 Determination of pKa of Negatively Charged Dendritic Star Polymers

Since the shells of the dendritic star polymers are composed of linear polymers with weak acid or base groups, it is necessary to know the pKa values of their solutions before the fabrication of multilayers. Potentiometric titrations were carried out to determine the pKa of two generations of negative charged dendritic star polymers. Both DP_1^- and DP_2^- solutions were purified by ultra filtration before titration measurements. The pH dependence on the degree of ionization or the activity coefficient is depicted in Figure 7.3. The measured pKa of DP_1^- and DP_2^- are 5.4 and 5.8, respectively. The shape of the potentiometric curves does not change significantly with the increasing number of carboxylic acid groups. However, such an increase results in a shift of the titration curves to higher pH values and thus to higher apparent values of pKa=5.8 for DP_2^-, which is used as the pH at α=0.5. Since the number of carboxylic acid groups in the second-generation of DP_2^- is larger than that of the first-generation of DP_1^-, the carboxylic acid groups in DP_2^- are packed in close proximity and high densities. These properties result in a higher osmotic pressure inside the DP_2^- molecules and a higher pKa value compared to other linear polyelectrolytes.[14]

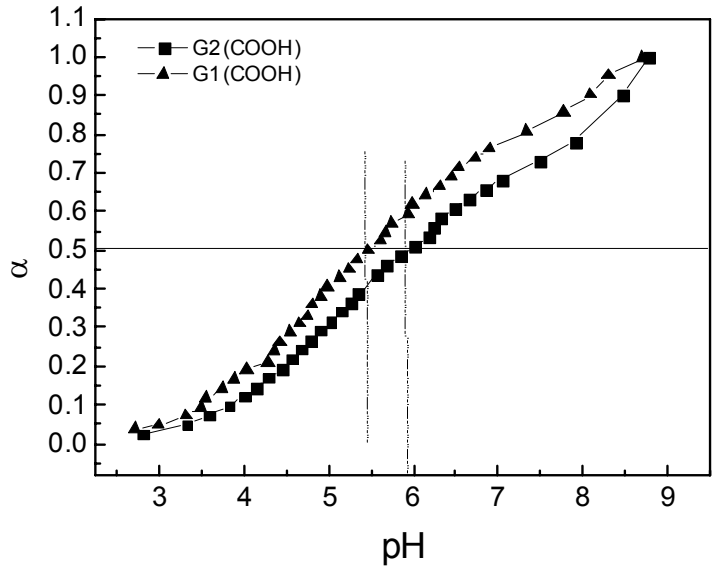

Figure 7.3 Potentiometric titration curves for negatively charged dendritic star polymers of DP_1^- and DP_2^- with carboxylic acid groups.

7.3.3 Characterization of Dendritic Star Polymer Multilayers by SPR

The dendritic star polymers outlined in this chapter afford the features of both dendrimer and polyelectrolytes with high functionalities. Therefore, these dendritic star polymers can be used as building blocks to prepare a new class of functional multilayer films. The fabrication of multilayers composed of all dendritic units, DP_1^+/DP_1^- and DP_1^+/DP_2^-, was investigated. In order to study the dendritic star polymer films affected by the different generation with negative charges, the positively charged first-generation dendritic star polymer DP_1^+ was employed in all the cases. pH values of negatively charged dendritic star polymers of DP_1^- and DP_2^- were adjusted at 6.5 to make the carboxylic acid groups fully ionized. The positively charged DP_1^+ solutions were prepared in water and the pH value of the solutions was kept at 6 without further pH adjustment. The first functionalized layer was the 3-MPA self-assembled monolayer on the gold surface providing negatively charged surface on which the first DP_1^+ layer was adsorbed. The consecutive alternating deposition steps were in-situ monitored by SPR and

the resulting kinetic mode curve was shown in Figure 7.4(a). Firstly, the 3-MPA gold substrate was immersed in water for 5 min and the reflectivity was kept at 20%. It can be clearly observed that the adsorption of DP_1^+ on the 3-MPA gold coated surface in the first step with reflectivity increase. In the same way, DP_1^- or DP_2^- was adsorbed on the DP_1^+ layer. After each layer deposition, the sample substrate was carefully rinsed with water in order to remove the physically adsorbed dendritic star polymers which could lead to a small reflectivity decrease. It is clearly observed that the addition of each layer leads to a regular increase of the reflectivity. Meanwhile, the angle scan curves shown in Figure 7.4(b) and Figure 7.4(c) also confirm the formation of each layer with regular resonance angle shift. The accumulated shift of resonance angle is converted into the geometrical film thickness by assuming a refractive index of 1.5 for all deposited dendritic star polymers.[15] The results are plotted in Figure 7.4(d) for multilayers of DP_1^+/DP_1^- and DP_1^+ / DP_2^-, respectively. Both curves show the nonlinear increase in film thickness at early stage (from the first layer to the fourth layer). Further increasing the deposition layers, the growth of multilayers is linear. Compared with the first-generation of dendritic multilayer (DP_1^+/DP_1^-), the film thickness from DP_1^+/DP_2^- is slightly larger which could be attributed to the larger size of the second generation of the dendritic core (DP_2^-).[19]

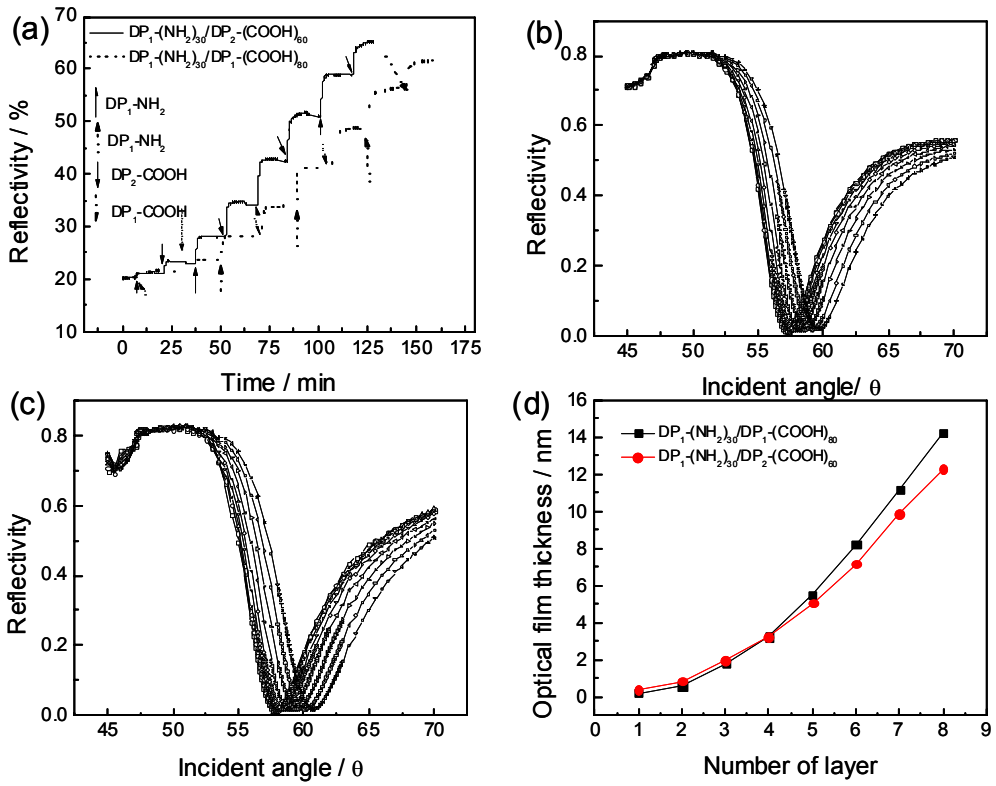

Figure 7.4 (a) Kinetic scans of reflectivity as a function of time during build up DP_1^+/DP_1^- and DP_1^+/DP_2^- multilayers with construction of 4 bilayers. (b) and (c) Angle scans of reflectivity as a function of incident angle from the multilayer of DP_1^+/DP_1^- and DP_1^+/DP_2^-, respectively. (d) Optical multilayer film thickness vs. number of layer for DP_1^+/DP_1^- and DP_1^+/DP_2^- multilayers, respectively.

7.3.4 Surface Morphology of pH Responsive Dendritic Star Polymer Multilayer Surfaces

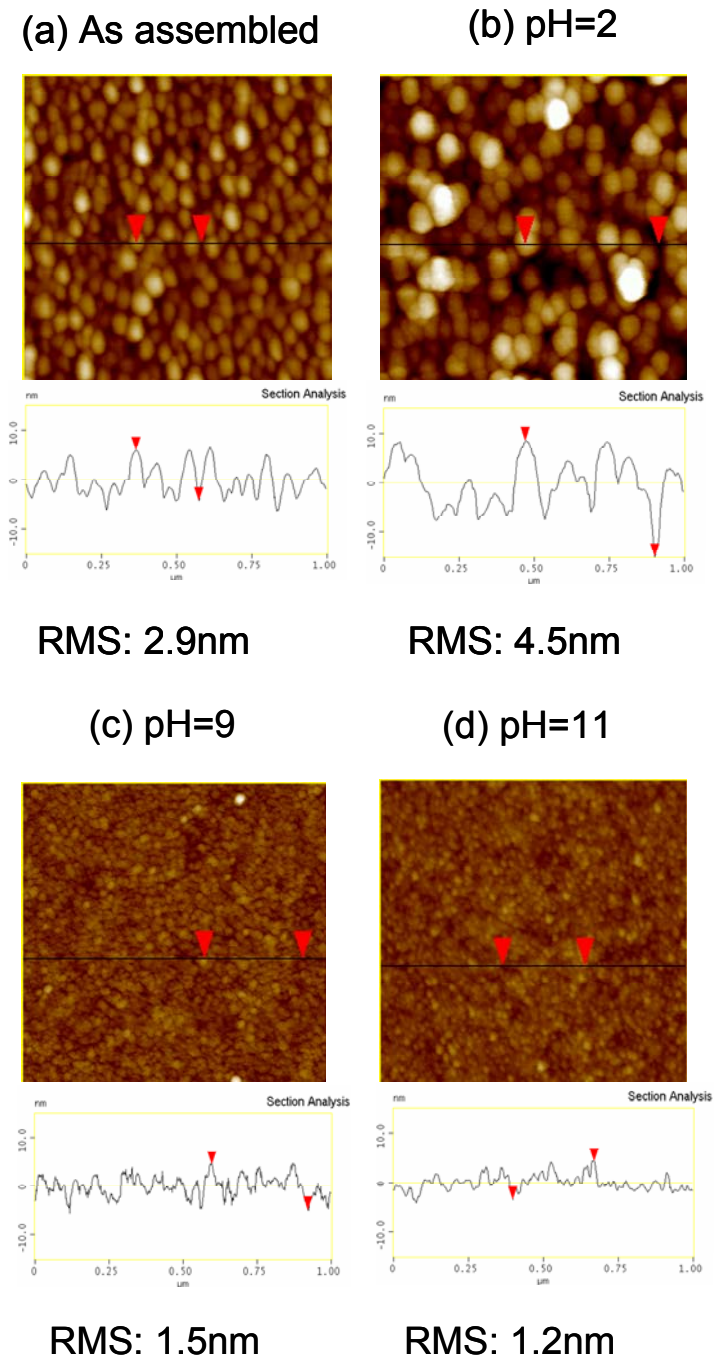

Figure 7.5 AFM images of $(DP_1^+/DP_2^-)_4$ dendritic star polymer multilayer films assembled from a DP_1^+ solution (pH at 6) and DP_2^- (pH at 6.5) before (a) and after 5 min exposure to pH 2(b), pH 9 (c) or pH 11(d) aqueous solutions.

All the dendritic star polymer multilayer films were further characterized by AFM to probe the pH dependent surface morphology. In this case, multilayer films assembled with DP_1^+ adsorbed at pH=6 and DP_2^- adsorbed at pH=6.5 were examined. Rubner and coworkers reported that multilayer films deposited from the linear polyacrylic acid (PAA) and linear polyallylamine are sensitive to pH adjustment.[16] Furthermore, the star polyacrylic acid (PAA) and star polyallylamine possessing the pH responsive properties are demonstrated by Caruso and coworkers recently.[17] An 8-layer dendritic star polymer multilayer film was firstly prepared on 3-MPA-coated gold substrate. The outermost film is the negatively charged dendritic star polymer (DP_2^-) (Figure 7.5(a)). The surface roughness measured from AFM is about 2.9 nm and there is no apparent island formed on the surface from this image. The dendritic star multilayer film was further exposed to a pH=2 (Figure 7.5(b)), pH= 9 (Figure 7.5(c)), or pH= 11 (Figure 7.5 (d)) aqueous solution for 5 min. The pH=2 treated multilayer film (Figure 7.5(b)) shows an apparently different surface morphology compared to the assembled film (Figure 7.5(a)) and the surface roughness is about 4.5 nm. The surfaces of the multilayer films immersed in aqueous solution at pH=9 and pH=11 are smoother than the multilayer film at pH=2 and the prefabricated multilayer film. It suggests that the ionization and protonation of the carboxylic acid groups can change the morphology of the multilayer surfaces. The carboxylic acid groups from the assembled multilayer surface treated at pH=2 are fully protonated due to the pH value is adjusted below its pKa value. Therefore, the surface roughness is higher than the prefabricated multilayer surface as a result of the highly coiled conformation. On the contrary, the surface morphology of multilayer film at high pH is smoother which is attributed to the more extended conformation of linear poly(acrylic acid).

7.3.5 DNA Immobilization on the Dendritic Star Multilayer Surfaces

Suitable functionalized surfaces for the DNA immobilization and DNA hybridization to develop the DNA biosensors are the challenge for the scientists since there are limitations for the commonly employed substrates including weak chemical resistance against organic solvents, mechanical instability and high intrinsic fluorescence properties. Taking these requirements into account, an ideal support should have an excellent surface chemistry allowing covalent binding of DNA with assurance that this attachment is stable and a high binding capacity obtained by increasing the number of reactive sites to which the probes can be covalently bound.[18] Furthermore, probes should not be spread on the support, as this could induce problems of accessibility during the hybridization step. To try to fulfill this requirement, dendrimers with the three-dimensional structure have been used for this application to design the new platforms for DNA immobilization and hybridization. One work described the use of prefabricated PAMAM dendrimer for the manufacture of biochips. [19] Although this technique possibly provides the best quality for DNA chips in terms of spots homogeneity, high sensitivity, low background and possible reutilization, the chemical procedure to functionalize glass slides is time consuming and leads to low thermal stability of the PAMAM dendrimers. Majoral's group employed their home developed phosphours dendrimers to fabricate the DNA chips. It improves the disadvantages from the PAMAM dendrimers and the limit of detection upon the DNA hybridization is higher compared to the DNA chips produced by other methods.[18] Based on the phosphorus dendrimers with charges instead of neutral phosphorus dendrimers, we deposited the phosphorus dendrimers multilayers as the platforms for the DNA immobilization and hybridization. The kinetic process of DNA hybridization was investigated and the limit of detection was detected. The results showed that the surfaces based on the phosphorus

dendrimer multilayers were stable and the limit of detection upon DNA hybridization can reach the same order of magnitude as the neutral phosphorus dendrimer surfaces which have been discussed in Chapter 6.

In this section, the multilayers fabricated based on the dendritic star polymers as the platforms for the DNA immobilization and hybridization will be investigated and the DNA hybridization behavior as well as the limit of detection upon DNA hybridization are compared with the system of phosphorus dendrimers. One of the advantages of the dendritic star polymer multilayer is that the multilayers are homogenous and well covered not only at multilayers deposited from more bilayers, but also at bilayers with less numbers (Figure 7.6). This is in contrast to the traditional LbL growth of linear polyelectrolytes where the early stages of the deposition involve nucleation of island-like growth sites.[20] Therefore, we could employ 3 bilayers of dendritic star polymer as platforms to study the behavior of DNA immobilization/hybridization and omit the tedious process to fabricate more bilalyers. The film thickness of the 3 bilayers together with the SAM is about 9 nm larger than the Förster radii (5-7 nm).[21]

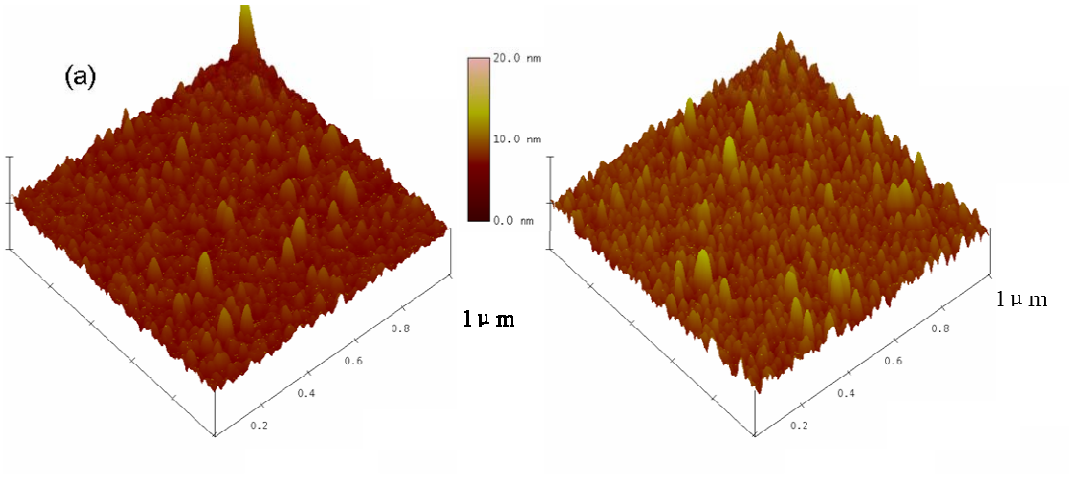

Figure 7.6 Surface morphology of 3 bilayers deposited from dendritic star polymers ((a) DP_1^+/DP_1^- and (b) DP_1^+/DP_2^-).

In the initial step, the multilayer surface with carboxylic acid groups need to be activated and then can make the probe DNA molecules with amine groups immobilize on the surface. A typical method involves EDC and NHS in aqueous condition as a carboxyl activating agent for the coupling of primary amines to yield amide bonds. This coupling reaction is controlled by the amount of the EDC/NHS ratio.[22] The pH of the solvent for the coupling reaction should be higher than the pKa values which are 5.4 and 5.8 for DP_1^- and DP_2^-, respectively. This is because the carboxylate anions otherwise exhibit a higher coupling rate than that exhibited by the carboxyl groups.[22(c)] EDC and NHS as a mole ratio of 1:5 were freshly prepared into the aqueous solution with the pH adjusted at 6 which is higher than their pKa values to make the carboxyl groups ionized into carboxylate groups. The activation step could be in-situ monitored by SPR. Figure 7.7 shows the activation process by NHS/EDC aqueous solutions on the 3 bilayers of DP_1^+/DP_1^- and DP_1^+/DP_2^-. The fabricated-3bilayers of DP_1^+/DP_1^- and DP_1^+/DP_2^- were rinsed with water at pH=6 for 5 min. Then the NHS/EDC aqueous solution was added upon the topmost of surface and the reflectivity was increased rapidly in the beginning and leveled off in a short time. After around 35 min, the activated surfaces were rinsed with water to remove the unreacted EDC/NHS solution from the surface as a result of reflectivity decreasing. However, it is still higher than the original data which confirms that there are new amide groups formed from the activation reaction.

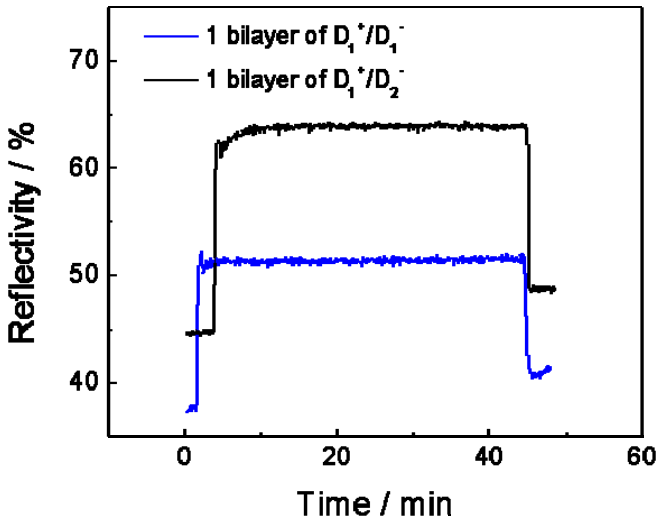

Figure 7.7 Activation steps of 3 bilayers of DP_1^+/DP_1^- and DP_1^+/DP_2^- by adding of NHS and EDC in aqueous solution at pH 6.

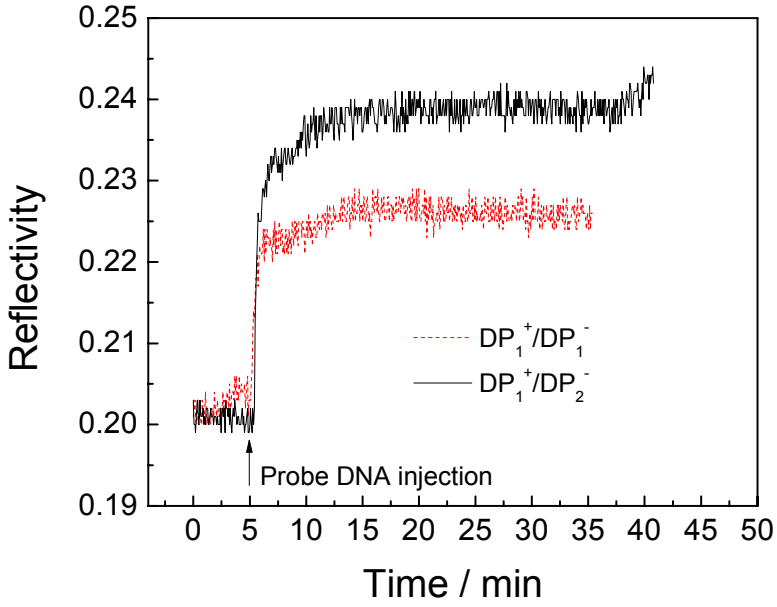

Figure 7.8 Kinetic scans of reflectivity of DNA immobilization as a function of time.

Figure 7.8 shows the kinetic immobilization of DNA on the 3 bilayers of DP_1^+/DP_1^- and DP_1^+/DP_2^-. The kinetic immobilization of probe DNA clearly shows that DNA has been covalently bonded on the surface and there is no

DNA obviously removed by the PBS buffer rinsing. The optical thickness of immobilized DNA is obtained by converting the resonance angle shift. Improved binding capacity is observed from DP_1^+/DP_2^- with the optical thickness of 3.2 nm compared to DP_1^+/DP_1^- with 2.6 nm of the film thickness, indicating the more reactive sites available from the second-generation of DP_2^-. There are more carboxylic acid groups in the second-generation of DP_2^- composing twelve branches of linear polyacrylic acid. In contrast, there are six branches of linear polyacrylic acid in the first-generation of DP_1^-.

7.3.6 DNA Hybridization

Kinetic study of DNA hybridization could deepen our understanding of the effect of DNA immobilized-surfaces on the DNA hybridization rate constants. However, the common DNA microarray detected by the fluorescence microscopy is not adequate for this purpose. Surface plasmon field enhanced fluorescence spectroscopy (SPFS) is a combination of SPR and fluorescence, which has been used for the detection of DNA hybridization reactions. SPFS measurements for the hybridization reactions were carried out on DP_1^+/ DP_1^- surface with covalently bonded probe DNA molecules by adding the three target DNA molecules (MM2, MM1 and MM0) (Figure 7.9(a)). With a decreasing number of mismatches, from MM2, MM1 to MM0, the maximum fluorescence intensity increased, indicating the improved hybridization quality between probe and target DNA molecules. Upon passing the MM2 target with two mismatches over the immobilized probes, a slight fluorescence increase above the background is observed. Subsequently a rapid fluorescence decrease upon rinsing by PBS buffer suggests only unspecific binding of the target. A different behavior is found from the MM1 experiment. The fluorescence intensity increases to a maximum value after addition of the labeled one mismatch target DNA molecules. Then the hybridization surface is rinsed by the pure PBS buffer solution, the

fluorescence signal gradually decreases until the intensity goes back to the original level. Furthermore, upon the addition of the MM0 solution, the fluorescence intensity rises rapidly and reaches a stable constant value. Rinsing with PBS buffer leads to a slow decrease in fluorescence intensity with time. The hybridization reactions on the DP_1^+/ DP_2^- surface (Figure 7.9(b)) shows the similar hybridization behavior with MM2, MM1 and MM0 compared with the reactions on DP_1^+/ DP_1^- surface. For MM1 and MM0, the kinetic information can be fitted by a simple Langmuir model.[23]

According to the fitting equations[24] for the time dependence of the fluorescence change (Figure 7.9), the hybridization rate constants are summarized in Table 7.2. Hybridization of MM0 and MM1 target probe DNA molecules show that, the association rate (k_{on}) decreases and the dissociation rate (k_{off}) increases with increasing the mismatch. The k_{on} and k_{off} values from DP_1^+/DP_1^- and DP_1^+/DP_2^- are in the same order of magnitude. This indicates that the amount of carboxylic acid groups from the surfaces fabricated from different generation of dendritic star polymers does not affect the kinetics of DNA hybridization reaction very much. Compared to the affinity data from the 1 bilayer of phosphorus dendrimer (in chapter 6), the affinity data from the dendritic star polymer surfaces are slightly lower. This can be explained from their molecular structures. Both phosphorus dendrimers and dendritic star polymers have the hydrophobic backbone and hydrophilic surface. However, the degrees of polarity between them are different. The phosphorus dendrimer used in Chapter 6 is the 4th generation with 76 carboxylic acid groups. In dendritic star polymers, the 1st generation contains 6 branches of linear polyacrylic acid with 80 repeating units and totally possesses of 480 carboxylic acid groups. For the 2nd generation of dendritic star polymer, it is constituted with 12 branches of linear polyacrylic acid with 60 repeating units and contains 720 carboxylic acid groups. Therefore, the dendritic star polymer might be more hydrophilic than

phosphorus dendrimers. Meanwhile, the polarity of the prefabricated both multilayer surfaces was measured by contact angle (in Figure 7.10). In the same experimental condition, the contact angles measured on 1 phosphorus dendrimer bilayer (at 50 mM NaCl) surface, 3 bilayers of DP_1^+/ DP_1^- surface, and 3 bilayers of DP_1^+/ DP_2^- are 57.6±0.6°, 47.7±0.5°, and 36.1±0.5°, respectively. These results further confirm that the phosphorus dendrimer multilayer surface is more hydrophobic than dendritic star polymer surfaces. DP_1^+/ DP_1^- multilayer surface is more hydrophobic than DP_1^+/ DP_2^- surface. The sugar-phosphate backbone is the major structural component of the DNA molecule and is composed of phosphate deoxyribose with negative charges. There is stronger repelling force between the DNA molecules and molecules containing more negative charges. Hence, from Table 7.2, for MM0, the k_{on} from the dendritic star polymer surface is lower than that from phosphorus dendrimer. Because the behavior of the k_{off} is not affected from the underlying surface, the k_{off} values from dendritic star polymer surface and phosphorus dendrimer surface are similar.

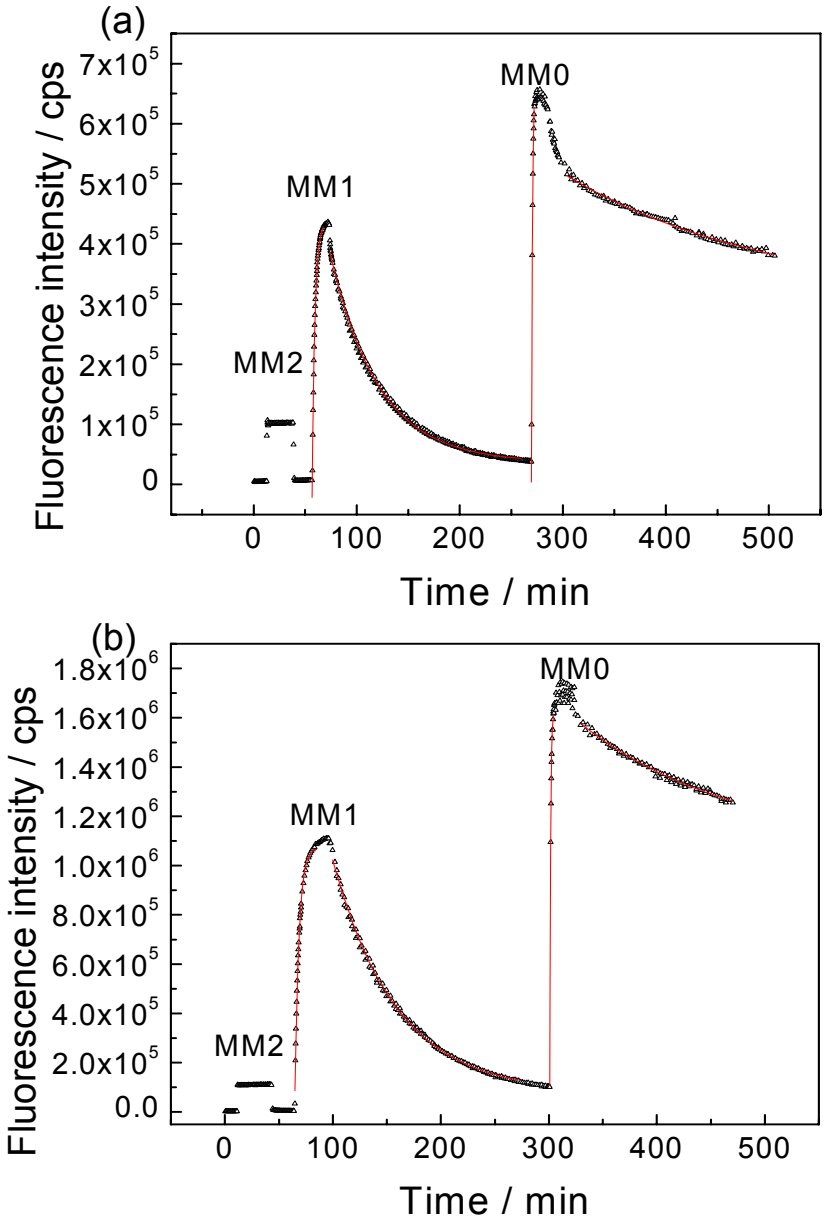

Figure 7.9 SPFS kinetic measurements for hybridization (association and dissociation) processes between the probe DNA and three different target DNA molecules: MM0, MM1 and MM2 on the surfaces of DP_1^+/ DP_1^- (a) and DP_1^+/ DP_2^- (b). The solid lines are theoretical calculations based on a simple Langmuir association/dissociation model.

Figure 7.10 Contact angle measurements of (a) 1 phosphorus dendrimer bilayer (at 50 mM NaCl) surface, (b) 3 bilayers of DP_1^+/ DP_1^- surface, and (c) 3 bilayers of DP_1^+/ DP_2^- at room temperature.

Table 7.2 Summary of the kinetic constants for the hybridization process of MM1 and MM0 from 3 bilayers of the DP_1^+/ DP_1^-, DP_1^+/ DP_2^- and 1 bilayer of G_4^+/G_4^- .

	DP_1^+/ DP_1^-		DP_1^+/ DP_2^-		G_4^+/G_4^-	
	MM1	MM0	MM1	MM0	MM1	MM0
$k_{on}/M^{-1}\,s^{-1}$	2.4×10^4	8.1×10^3	3.0×10^4	5.9×10^3	3.0×10^4	3×10^5
k_{off}/s^{-1}	8.4×10^{-5}	3.6×10^{-4}	1.2×10^{-4}	2.8×10^{-4}	1.7×10^{-4}	1.3×10^{-4}
k_A/M^{-1}	2.8×10^8	2.3×10^7	2.5×10^8	2.1×10^7	1.8×10^8	2.5×10^9

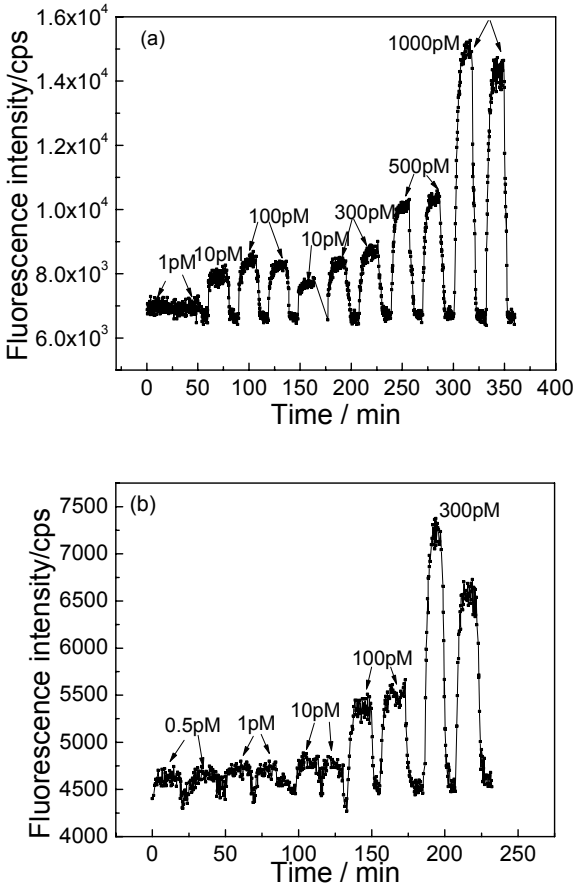

Figure 7.11 Hybridization of target MM0 to the DNA surfaces based on 3 bilayers of DP_1^+/ DP_1^- (a) and DP_1^+/ DP_2^- (b), respectively.

To further determine a limit-detection of the fluorescence signal, we performed the hybridization analysis on 3 bilayers of DP_1^+/DP_1^- and DP_1^+/DP_2^-, respectively. Figure 7.11 (a) shows the target DNA hybridization process on the 3 bilayers of DP_1^+/DP_1^- binding with an amino-modified probe DNA molecules, which was hybridized to fully complementary oligonucleotide target (MM0) solutions with increasing concentrations, from 1 pM to 1000 pM. If a 1 pM solution of MM0 was added, there was no obvious increase in the fluorescence intensity signal. However, a 10 pM solution was sufficient to generate a clear increase in the fluorescence intensity. Each injection of the target DNA solution was a certain period of time for the interaction and a surface regeneration step through rinsing the

surface with a 10 mM NaOH solution for 1 min. The probe surface demonstrated good robustness, sustaining repetitive regeneration for at least 10 cycles. In the low target concentration region, the initial hybridization process seems to be controlled by the diffusion of the target DNA from the bulk to the surface, thus showing a linear signal increase with time. Using the same method, adding a 10 pM of target DNA solution could obviously increase the fluorescence intensity signal on the 3 bilyers of DP_1^+/ DP_2^- surface (Figure 7.11 (b)). Compared with the results on the two dendritic star polymer multilayer surfaces, the detection of sensitivity on DP_1^+/ DP_2^- is the same as that on DP_1^+/ DP_1^-. The limit of detection from the 3 bilayers of dendritic star polymer is in the same order of magnitude as and slightly higher than the results from the 1 bilayer surface of phosphorus dendrimer (50 pM). [25] This might be due to the more reactive DNA immobilization groups for carrying out DNA hybridization. Because the branches of this dendritic star polymers are formed by the atomic transformation radical polymerization (ATRP) which can precisely control the reaction, the expect functionalities can be achieved. Therefore, the results show that this type of dendritic star polymers is a good alternative to design the bio-functional platforms as DNA biosensors.

7.4 Conclusion

The first- and second-generation of dendritic star polymer multilayers were successfully prepared on the SAM modified gold substrate and in situ characterized by SPR. These dendritic bilayers can be employed as stable platforms for DNA immobilization and hybridization. The platforms of dendritic star polymer multilayers not only improve probe DNA immobilization but also enable the successful hybridization of the surface covalently bonded probe DNA molecules with complementary target DNA molecules. DNA hybridization kinetics behaviors on the surfaces of DP_1^+/

DP_1^- and DP_1^+/ DP_2^- were compared and showed similar constant rates (k_{on}, k_{off} and k_A). Kinetic hybridization between the one mismatch and complementary targets can be distinguished. The limit-detection upon DNA hybridization from the dendritic star polymer bilayer surfaces is improved and higher than that from 1 bilayer surface from phosphorus dendrimer. The combination of improved DNA loading and distinguished DNA hybridization behaviors shows that this dendritic star polymer multilayer is a potential candidate for application in DNA biosensors.

7.5 References

1 (a) Decher, G. *Science* **1997**, *277*, 1232. (b) Decher, G.; Schlenoff, J. B. *Multilayer Thin Films*; Wily-VCH,New York, **2003**. (c) Hammond, P. T. *Adv. Mater.* **2004**, *16*, 321. (d) Tang, Z. Y.; Wang, Y.; Podsiadlo, P.; Kotov, N. A. *Adv. Mater.* **2006,** *18,* 3203.

2 Cho, J. H.; Hong, J. K.; Char, K.; Caruso, F. *J. Am. Chem. Soc.* **2006**, *128*, 9935.

3 Tsukruk, V. V. *Adv. Mater.* **1998**, *10*, 253.

4 Mamedov, A. A.; Kotov, N. A.; Prato, M.; Guldi, D. M.; Wicksted, J. P.; Hirsch, A. *Nat. Mater.* **2002**, *1*, 190.

5 Lee, D.; Rubner, M. F.; Cohen, R. E. *Nano Lett.* **2006**, *6*, 2305.

6 Khopade, A. J.; Caruso, F. *Nano Lett.* **2002**, *2*, 415.

7 Hadjichristidis, N.; Pitsikalis, M.; Pispas, S.; Iatrou, H. *Chem. Rev.* **2001**, *101*, 3747.

8 Kim, B. S.; Gao, H. F.; A. Argun, A.; Matyjaszewski, K.; T. Hammond, P. *Macromolecules,* **2009**, *42,* 368.

9 Yang, S.; Zhang, Y.; Wang, C.; Hong, S.; Xu, J.; Chen, Y. *Langmuir* **2006**, *22*, 338.

10 Conna, L. A. ; Li, Q ; Quinn, J. F. ; Tjipto, E. ; Caruso, F. ; Qiao, G. G.

Macromolecules **2008**, *41,* 2620.

11 Taton, D.; Feng, X. S.; Gnanou, Y. *New J. Chem.* **2007,** *31*, 1097.

12 (a) Yin, M. Z.; Ding, K.; Gropeanu, R. A.; Shen, J.; Berger, R.; Weil, T.; Müllen, K. *Biomacromolecules* **2008**, *9,* 3231. (b) Yin, M. Z.; Cheng, Y. J.; Liu, M. Y.; Gutmann, J. S.; Müllen, K. *Angew. Chem. Int. Ed.* **2008**, *47,* 8400.

13 (a) Kumaki, J.; Nishikawa, Y.; Hashimoto, T. *J. Am. Chem. Soc.* **1996,** *118,* 3321. (b) Prokhorova, S. A.; Sheiko, S. S.; Moller, M.; Ahn, C. H.; Percec, V. *Macromol. Rapid Commun.* **1998,** *19,* 359.

14 (a) Connal, L. A.; Li, Q.; Quinn, J. F.; Tjipto, E.; Caruso, F.; Qiao, G. G. *Macromolecules* **2008**, *41*, 2620. (b) Plamper, F. A.; Becker, H.; Lanzendorfer, M.; Patel, M.; Wittemann, A.; Ballauf, M.; Muller, A. H. E. *Macromol. Chem. Phys.* **2005**, *206*, 1813.

15 Kim, D. H.; Hernandez Lopez, J. L.; Liu, J.; Mihov, G.; Zhi, L.; Bauer, R. E.; Grebel Köhler, D.; Klapper, M.; Weil, T.; Müllen, K.; Mittler, S.; Knoll, W. *Macromol. Chem. Phys.* **2005,** *206,* 52.

16 Mendelsohn, J. D.; Barrett, C. J.; Chan, V. V.; Pal, A. J.; Mayes, A. M.; Rubner, M. F. *Langmuir* **2000**, *16*, 5017.

17 Connal, L.; Li, Q.; Quinn, J.; Tjipto, E. ; Caruso, F. ; Qiao, G. *Macromolecules,* **2008,** *41,* 2620.

18 Berre, V.; Trévisiol, E.; Dagkessamanskaia, A.; Sokol, S.; Caminade, A. M.; Majoral, J. P.; Meunier, B. ; François, J. *Nucleic Acids Research,* **2003,** *31,* e88.

19 (a) Benters, R.; Niemeyer, C. M.; Wohrle, D. *Chem. Biochem.* **2001,** *2,* 686. (b) Benters, R. ; Niemeyer, C. M. ; Drutschmann, D.; Blohm, D.; Wohrle, D. *Nucleic Acids Res.* **2002,** *30,* e10.

20 Kim, B. S.; Gao, H. F.; Argun, A. A.; Matyjaszewski, K.; Hammond, P. *Macromolecules* **2009**, *42,* 368.

21 De La Escosura-Muniz, A.; Gonzalez-Garcia, M. B.; Costa-Garcia, A.

Biosens. *Bioelectron.* **2007,** *22,* 1048.

22 (a) Olde Damink, L. H. H.; Dijkstra, P. J.; van Luyn, M. J. A.; van Wachem, P. B.; Nieuwenhuis, P.; Feijen, J. *Biomaterials* **1996,** *17,* 765. (b) Nam, K.; Kimura, T.; Kishida, A. *Biomaterials* **2007**, *28,* 1. (c) Nakajima, N.; Ikada, Y. *Bioconjugate Chem.* **1995,** *6,* 123.

23 Jensen, K.K.; Ørum, H.; Nielsen, P. E.; Norden, B. *Biochem.* **1997,** *36,* 5072.

24 Liebermann, T.; Knoll, W.; Sluka, P.; Herrmann, R. *Colloids and Surfaces A: Physicochem. Eng. Aspects* **2000,** *169,* 337.

25 Yu, Y. M.; Feng, C. L.; Caminade, A. M.; Majoral, J. P; Knoll, W. *Langmuir* **2009** on line.

Chapter 8

Summary

The focus of the present study was the development of functional multilayer films through electrostatic layer by layer (LbL) assembly of dendritic macromolecules and to investigate the fundamental properties of these multilalyered films. Various types of dendritic materials including hyperbranched polyglycerols (hbPGs) of rather narrow polydispersity, monodisperse phosphorus dendrimers as well as dendritic star polymers were employed to fabricate multilayer films, which were then characterized by a series of techniques such as SPR, SPFS, AFM and FTIR. Moreover, the hyperbranched polyglycerol layers were prepared as antifouling coatings to detect protein adsorption. In the final chapter, multilayers made of phosphorus dendrimers and the dendritic star polymers were used for the development of DNA biosensors.

Chapter 1 gives a short introduction about the thesis and in Chapter 2 a review of literature is given on dendritic macromolecules and the electrostatic assembly of polyelectrolytes. The basic types of dendritic macromolecules are briefly introduced. Following introductions on the general characteristics of polyelectrolytes are discussed. Chapter 3 introduces the employed techniques and their working mechanisms.

Chapter 4 deals with the synthesis of the anionic hyperbranched polyglycerols, the preparation of multilayers made of hbPG/phosphorus dendrimer as well as the influences of deposition conditions on multilayers. The anionic hbPGs with different molecular weight bearing carboxylic acid groups were obtained by succinate functionalization. The growth of multilayer films was in-situ monitored by SPR. The influence of assembly conditions, such as molecular weight, ionic strength and pH value of anionic hbPG solutions on the growth of multilayer thin films were systematically

investigated. The thicknesses of multilayer films increase with a decrease of molecular weight of anionic hbPGs. At first glimpse a puzzling result, however, we explain this tentatively by the higher number of charged carboxylic acid groups for high molecular weight of hbPG that induces a more extended structure on the surface. The multilayer films fabricated by low molecular weight hbPGs grow less regularly due to the less charged carboxylic acid groups providing the relative weaker electrostatic forces for the deposition. The thicknesses of multilayer films are reduced with increasing pH values and decreasing the concentration of NaCl from 0.025 M to 0.1 M. However, a further increase of the concentration of NaCl up to 0.5 M results in a drop of film thickness. Surface morphology of multilayers fabricated at various pH values was imaged by AFM. The observed changes of multilayer thickness and surface morphology could be interpreted with the aid of theories regarding the charge density and conformation of the anionic hbPG chains in solution. Finally, FTIR measurements further confirmed that structural changes of the multilayer films were induced by pH adjustments.

Besides the study of fundamental properties of hbPGs/phosphorus multilayer films, antifouling thin films derived from hbPG layers were developed in Chapter 5. The fabrication processes of hbPG single layers or bilayers were characterized by SPR. The adsorption of BSA and fibrinogen on a series of hbPG layers (hbPG single layers and hbPG bilayers) were measured and the ability to resist non specific protein adsorption was evaluated by SPR. The antifouling properties of hbPG layers were found to correlate with factors of the molecular weight of anionic hbPG and the film thickness. It was demonstrated that anionic hbPG single layer with highest molecular weight can reduce non specific protein adsorption more efficiently than single layer with lower molecular weight and all the hbPG bilayers possessed excellent property of antifouling. Therefore, these hbPG layers

fabricated by electrostatic interaction can act as good candidates for the development of antifouling coatings.

Phosphorus dendrimer multilayers were successfully prepared as the platforms to detect DNA immobilization and hybridization which were demonstrated in Chapter 6. Phosphorus dendrimer multilayers on gold substrates were fabricated by LbL technique and characterized by SPR. The effect of NaCl concentration on the multilayer film thickness was evaluated to obtain the optimized film thickness. Making use of the multilayer deposited at the optimized condition as a substrate, a high loading of DNA probes was achieved through covalent coupling of probe DNA with the as-formed multilayer films. The hybridization of target DNA with immobilized probe DNA was then carried out and studied by SPFS. The limit of detection upon hybridization was estimated on various dendrimer multilayer platforms. The minimum detection concentration for DNA hybridization can reach 30 pM on 4 bilayer surface which is in the same order of magnitude compared with other neutral phosphorus dendrimer systems. Furthermore, the LbL deposition of phosphorus dendrimer multilayers provided a mild and simple way to prepare platforms as DNA microarrays.

Based on the phosphorus dendrimer multilayer systems, Chapter 7 has employed dendritic star polymers which have more reactive groups than thatphosphorus dendrimers. This chapter described the preparation of multilayer films made of dendritic star polymers, which were also used as the platforms for the detection of DNA hybridization and compared with phosphorus dendrimer platforms. The as-assembled dendritic star polymer multilayer films exhibited such distinct morphology characteristics that they underwent extensive structural reorganization upon post-treatment under different pH conditions and could be detected by AFM. Kinetic binding of probe DNA molecules on the outmost negatively charged dendritic surface

was studied by SPR as well. The binding capacities of probe DNA on the multilayer surfaces fabricated from the first-generation and the second-generation of dendritic star polymers were compared. The improved binding capacity was achieved from the second-generation of dendritic star polymer multilayer films due to their more reactive groups. DNA hybridization reaction on dendritic multilayer films was investigated by SPFS. The similar hybridization behaviors were found on both multilayer surfaces. Meanwhile, the hybridization kinetic affinities were compared with that of phosphorus dendrimer multilayer surfaces and showed improved detection sensitivity than phosphorus dendrimer multilayer films.